

12-17-2009

# Modulation of Restriction Enzyme PvuII Activity by Metal ion Cofactors

Charulata Bhaskaran Prasannan

University of Missouri-St. Louis, charupras@gmail.com

Follow this and additional works at: <https://irl.umsl.edu/dissertation>



Part of the [Chemistry Commons](#)

---

## Recommended Citation

Prasannan, Charulata Bhaskaran, "Modulation of Restriction Enzyme PvuII Activity by Metal ion Cofactors" (2009). *Dissertations*. 497.

<https://irl.umsl.edu/dissertation/497>

This Dissertation is brought to you for free and open access by the UMSL Graduate Works at IRL @ UMSL. It has been accepted for inclusion in Dissertations by an authorized administrator of IRL @ UMSL. For more information, please contact [marvinh@umsl.edu](mailto:marvinh@umsl.edu).

# Modulation of Restriction Enzyme PvuII Activity by Metal ion Cofactors

by

Charulata Bhaskaran Prasannan

M.S, Chemistry, University of Missouri-Saint Louis, 2006

M.Sc, Physical Chemistry, University of Mumbai, 2002

B.Sc, Chemistry, University of Mumbai, 2000

A Dissertation

Submitted to the Graduate School of the

UNIVERSITY OF MISSOURI- ST. LOUIS

In partial fulfillment of the requirements for the degree

DOCTOR OF PHILOSOPHY

in

CHEMISTRY

with an emphasis in Biochemistry

December 2009

Advisory Committee

Dr. Cynthia M. Dupureur  
ChairPerson

Dr. Wesley R. Harris

Dr. Keith J. Stine

Dr. Wendy M. Olivas

## Abstract

Modulations of Restriction Enzyme-PvuII activity by metal ion cofactors

(December 2009)

Charulata B. Prasannan, M.Sc. University of Mumbai, India

Chair of Committee: Dr. C. M. Dupureur

Many nucleases require cofactors (usually  $Mg^{2+}$ ) for activity. Metal ions like  $Ca^{2+}$ ,  $Mn^{2+}$ ,  $Tb^{3+}$ ,  $Eu^{3+}$  etc., can bind at the active site and have varying effects on the enzymatic activity. In a crystal structure with DNA, two  $Ca^{2+}$  ions were bound to the active site of each PvuII monomer, and the metals share the ligands.  $Ca^{2+}$  ions promote DNA binding and not cleavage in many nucleases. We explored the role of  $Mg^{2+}$  and  $Ca^{2+}$  binding at the metal binding sites of PvuII to elucidate the role of each metal site.  $Ca^{2+}$  binding at the catalytic metal site would inhibit the cleavage activity, whereas its binding at the regulatory site can have varied effects. In EcoRV enzyme, it was seen that  $Ca^{2+}$  at the regulatory site increases the activity of the enzyme. We monitored the cleavage kinetics of PvuII in presence of mixed metals. The cleavage kinetics data for  $Ca^{2+}$  and  $Mg^{2+}$  set were modeled using parameters from previous studies on PvuII. Our global analysis on single turnover cleavage kinetics datasets show best fit to a model in which mixed metal species are formed and active. The cleavage rate constants for the mixed metal species ranged from 0.01-0.08  $sec^{-1}$ ,

which is similar to the rate when only one metal is bound. From earlier work in our lab,  $Tb^{3+}$  was shown to have a tight ( $2 \mu M$ ) binding site and a weak binding site in PvuII. The difference in affinity allows one site to be filled with  $Tb^{3+}$  and the other with another metal. Indirect  $Tb^{3+}$  luminescence spectroscopy of the  $Tb^{3+}$  bound to enzyme in presence of other metals indicates that  $Ca^{2+}$  and  $Mn^{2+}$  displace  $Tb^{3+}$  from the enzyme. This was observed by the decrease in the luminescence intensity of E- $Tb^{3+}$  complex with the addition of  $Ca^{2+}/Mn^{2+}$  ions. Under similar conditions, the addition of  $Mg^{2+}$  ions to the E- $Tb^{3+}$  complex results in an increase in the signal observed. This indicates the formation of the mixed species E- $Tb^{3+}$ - $Mg^{2+}$ . No enzymatic activity was detected for the enzyme with the addition of  $Mg^{2+}$  to the E- $Tb^{3+}$  complex, whereas with the addition of  $Mn^{2+}$  ions there was detectable activity. The observed activity with  $Mn^{2+}$  ion was due to the displacement of  $Tb^{3+}$  ions from the active site, forming the active  $EMn^{2+}Mn^{2+}$  species. Although the E- $Mg^{2+}$ - $Tb^{3+}$  species is catalytically inactive, it does bind the DNA as confirmed by fluorescence anisotropy using nonhydrolyzable phosphoramidate DNA.

To Acha, Amma, Aniyati, Deedi maman and Gouri mami.

## ACKNOWLEDGEMENTS

I would first like to thank my advisor Dr. Cynthia Dupureur who has guided me all along my PhD. There were times that I did not feel confident if I would ever be able to finish this work. I thank her for believing in me and guiding me forward each day to be able to finish my dissertation. I thank Dr. Wesley Harris for the suggestions on my project and for all the other times where he just made me feel so comfortable. I thank Dr. Keith Stine and Dr. Wendy Olivas for being in my committee and for the discussions and suggestions during my dissertation. I would also like to acknowledge Dr. Chung Wong and Dr. Michael Nichols who were my instructors for various courses for their support.

I thank my lab mates, Dr. Lori Bowen and Dr. Shabir Qureshi to help me adjust to the lab. I am extremely thankful to Dr. Grigorios Papadacos, Dr. Fuqian Xie, Supratik Dutta, and Binod Pandey for all the discussions that we had during the years of work, both science and fun.

I made wonderful friends during my years at UMSL, I thank Rashmi Sharma, Shaji Sadasivan, and Nilambari Pisat, for their unconditional support which gave me the strength to be happy so far away from home. I thank Geeta Paranjape, Florencia Lopez leban, Melanie Miller, Deepa Ajith, Maria Udan, Nikkilina Crouse, and Kenise Jefferson for all their help.

I thank my family; my parents, my sister, my uncles and my aunts who have always encouraged me and in spite of the distance have made me believe that they are just a phone call away.

Finally I thank Department of Chemistry and Biochemistry at UMSL for providing me the opportunity and financial support for graduate studies. I also thank NIH for funding.

## TABLE OF CONTENTS

	Page
ABSTRACT	ii
DEDICATION	iv
ACKNOWLEDGEMENTS	v
TABLE OF CONTENTS	vii
LIST OF FIGURES	ix
LIST OF TABLES	xii
LIST OF SCHEMES	xiii
I. INTRODUCTION	
Metals in Biological system	1
Mechanism of Phosphodiester bond hydrolysis	6
Studies on two metal ion mechanism	10
Mixed metal studies: A biochemical approach for mechanistic details	13
Association and dissociation rates: Metal exchange	18
Model system: Restriction Endonuclease	22
Introduction to PvuII Endonuclease	24
Global analysis of data	33
Overview of Dissertation	34
II. MATERIALS AND METHODS	
Enzyme preparation	36
Preparation of substrate	38
Metal salt stocks	40



Cleavage kinetics	41
Quench flow	41
Fluorescence spectroscopy	44
III. GLOBAL KINETIC ANALYSIS FOR MIXED METAL COMPLEXES OF PvuII.	
Introduction	46
Methods	50
Results	51
Conclusion	81
IV. METAL EXCHANGE: TO STUDY METAL BINDING TO PvuII.	
Introduction	86
Methods	89
Results	90
Conclusion	108
REFERENCES	109
APPENDIX	114
VITA	125

## LIST OF FIGURES

	Page
Figure 1.1. Concentration of metal ions present in the <i>E.coli</i> cell.	2
Figure 1.2. Structure of the Zinc finger domain of Transcription factor TfIIIA with Zinc metal and the EF domain of Calmodulin with Ca <sup>2+</sup> .	4
Figure 1.3. Depiction of the one metal ion mechanism in phosphodiester hydrolysis.	8
Figure 1.4. Two metal ion mechanism in phosphodiester bond hydrolysis.	9
Figure 1.5. Transition state structure of the three metal ion mechanism proposed for EcoRV.	11
Figure 1.6. Mechanism for the group I intron activity.	12
Figure 1.7. Two metal ion model of Endonuclease V.	16
Figure 1.8. Cleavage of cognate and non-cognate sequences by EcoRI and EcoRV enzymes under mixed metal conditions.	17
Figure 1.9 Indirect excitation of the lanthanides using the aromatic residues closer to the metal binding site.	21
Figure 1.10 Cartoon of the restriction modification system machinery.	23
Figure 1.11 Active site residues of PvuII endonuclease.	25
Figure 1.12. The crystal structure of PvuII endonuclease with the cognate DNA in presence of Ca <sup>2+</sup> ions.	26
Figure 2.1. An elution profile and SDS-PAGE gel from PvuII purification using heparin column.	39

Figure 2.2.	Cleavage kinetics polyacrylamide- urea gel and the corresponding progress curve.	42
Figure 2.3.	Quench flow Module for SFM 400.	43
Figure 3.1.	Two metal ion model of Endonuclease V.	49
Figure 3.2.	Script for a cleavage model written for Dynafit run.	52
Figure 3.3.	A snapshot during the program run of Dynafit.	53
Figure 3.4.	Plot of experimental $k_{\text{obs}}(\text{sec}^{-1})$ at varying $\text{Mg}^{2+}$ and $\text{Ca}^{2+}$ concentrations.	54
Figure 3.5.	Overlay plot of the experimental and fitted values for model 1a.	59
Figure 3.6.	Overlay plot of the experimental and fitted values for model 1b.	64
Figure 3.7.	Overlay plot of the experimental and fitted curves for models with mixed species.	67
Figure 3.8.	Overlay plot of the experimental and fitted $k_{\text{obs}}(\text{sec}^{-1})$ for models with mixed species.	69
Figure 3.9.	Concentration of mixed species from the simulations using model 1e.	71
Figure 3.10.	Contribution of species to product from the simulations using model 1e.	73
Figure 3.11.	Overlay plot of the experimental and fitted $k_{\text{obs}}(\text{sec}^{-1})$ for models with interconversion step.	78
Figure 3.12.	Overlay plot for the experimental and fitted $k_{\text{obs}}$ at $\text{Ca}^{2+}$ concentrations in mM for model with only one mixed species.	82

Figure 4.1.	Cartoon representation of a mixed metal enzyme complex.	88
Figure 4.2.	Luminescence intensity changes of E-Tb <sup>3+</sup> with metals, Mn <sup>2+</sup> , Ca <sup>2+</sup> and Mg <sup>2+</sup> .	92
Figure 4.3.	DNA binding for the Mixed metal complexes.	95
Figure 4.4.	Cleavage kinetics data of PvuII with Tb <sup>3+</sup> and Mg <sup>2+</sup> where Enzyme is preincubated with Tb <sup>3+</sup> .	96
Figure 4.5.	Cleavage kinetics data of PvuII with Tb <sup>3+</sup> and Mg <sup>2+</sup> without preincubation of enzyme with Tb <sup>3+</sup> .	98
Figure 4.6.	Cleavage activity of PvuII in presence of Mn <sup>2+</sup> and Tb <sup>3+</sup> .	99
Figure 4.7.	Exchange kinetics data with three different metal ions.	101
Figure 4.8.	Exchange kinetics to check reversibility of step $ETb^{3+} + Ca^{2+} \rightleftharpoons ECa^{2+} + Tb^{3+}$ .	102
Figure 4.9.	Experimental data (Ca <sup>2+</sup> and Tb <sup>3+</sup> ) fit with model from Scheme 4.1	105
Figure 4.10.	Experimental data (Ca <sup>2+</sup> and Tb <sup>3+</sup> ) fit with model from Scheme 4.2	107
Figure A1	Model with site specific species EM <sub>2</sub> and M <sub>2</sub> E	116
Figure A2	Fits using Model 1e with different set of parameters floated	118
Figure A3	Progress curve output from the simulation of parameter value K <sub>4</sub> (EC <sub>2</sub> M <sub>2</sub> formation).	120
Figure A4	The rate of cleavage (sec <sup>-1</sup> ) vs Mg <sup>2+</sup> concentration in mM at different Mg <sup>2+</sup> concentrations.	122
Figure A5	Fit with model 1e at higher Mg <sup>2+</sup> concentrations with and without Ca <sup>2+</sup>	124

## LIST OF TABLES

	Page
Table 3.1. List of parameters used in the models and their sources.	57
Table 3.2. Table shows the initial guess and the fitted values for the parameters obtained for model 1a and model 1b.	61
Table 3.3. Table shows the initial guess and the fitted values for the parameters obtained for model 1c, model 1d and model 1e.	68
Table 3.4. List of parameters changed in the models with interconversion.	76
Table 3.5. Table shows the initial guess for the parameters in Model 2c, 2d and 2e.	77
Table 3.6. Table shows the initial guess and the fitted values for the model where one mixed species is formed as shown in scheme 5.	83
Table 4.1. Ionic radii of metal ions used in the study at various coordination.	93

## LIST OF SCHEMES

	Page
Scheme 1.1 Kinetic models with and without interconversion step.	32
Scheme 3.1. Model 1a, mixed species not formed.	56
Scheme 3.2. Model 1b, mixed species formed and not active.	62
Scheme 3.3. Models with mixed species active.	66
Scheme 3.4. Models with mixed species active with interconversion.	74
Scheme 3.5. Model with one mixed species formed $EM_2C_2$ .	80
Scheme 4.1 Model for the exchange reaction using $Tb^{3+}$ and $Ca^{2+}$ .	104
Scheme 4.2 Model for the exchange reaction using $Tb^{3+}$ and $Ca^{2+}$ in Dynafit program.	104
Scheme A1 Model with the site specific species $M_2E$ and $EM_2$ .	115

## CHAPTER I

### INTRODUCTION

#### 1.1 Metals in Biological System:

Living organisms require 27 elements, 15 of which are metals. Some of them like potassium, magnesium, sodium, and calcium are used in major quantities, and others like manganese, iron, cobalt, copper, zinc, and molybdenum are used in minor quantities (Lippard and Berg, 1994). Elements like vanadium, chromium, tin, nickel, and aluminum are found as trace elements (Lippard and Berg, 1994). Metal ions are involved for the function of many proteins. A study showed the amount of metal ions present in the *E.coli* cells, and the summary of this study is shown in **Figure 1.1** (Outten and O'Halloran, 2001). Biologically, iron is the most important transition metal. Hemoglobin, which is an oxygen carrier in blood, and myoglobin, which stores oxygen in tissues, are two major iron proteins (Lippard and Berg, 1994). Tyrosinase, a protein involved in skin pigmentation, is a copper protein and carboxypeptidase involved in protein metabolism is a zinc protein (Lippard and Berg, 1994). Metal ions provide structural conformation to the protein and help with the specificity of its function. Some proteins require specific metal ions for their activity, and others work in the presence of similar metals. For these reasons, the size of the metal ions and their coordination sites are of interest. Alkaline earth metals like  $\text{Ca}^{2+}$  and  $\text{Mg}^{2+}$  are present in millimolar quantities in cells, which make it interesting to understand the process of specific metal binding of the proteins. Calcium and magnesium metals are involved in many processes, and proteins which bind them are an open area of study.

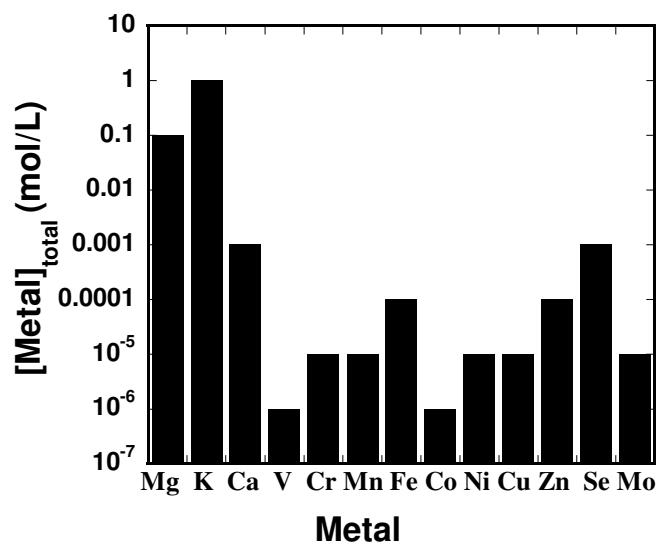


**Figure 1.1:** Concentration of metal ions present in the *E.coli* cell (Outten and O'Halloran, 2001). It is seen from this study that the alkaline earth metals  $K^+$ ,  $Mg^{2+}$  and  $Ca^{2+}$  are present in abundance in a cell. The protein that interacts with these metals should be very specific for the metal dependent function. Metal protein interactions are studied intensively to understand this specificity.



The tertiary structure of the protein allows or facilitates its interaction to macromolecules like DNA or RNA. The effect of metals on the structure and function of the proteins is an area which is not very well characterized for many proteins. Structural characteristics of many metalloproteins are studied by X-ray crystallography. X-ray analysis is most easily utilized for proteins where metal ions are tightly bound (Lippard and Berg, 1994). Some structural characteristics of metalloproteins analyzed by solution or crystal structure are shown below.

**a) Metalloproteins:**

The solution or crystal structures of proteins like zinc finger proteins and calmodulin have helped researchers understand their structure and function. Involvement of  $Zn^{2+}$  ions in nucleic acid binding and gene regulatory proteins such as the transcription factor TFIIIA created the need for the structure of these proteins. NMR structure provided details of the  $Zn^{2+}$  binding peptide sequences and the evidence that  $Zn^{2+}$ -finger proteins are folded in presence of the metal (**Figure 1.2**) (Frankel, et al., 1987). The  $Zn^{2+}$  ion binds to two cysteine and two histidine residues. The structure of the protein showed the presence of a hairpin turn, which contains cysteine residues followed by alpha helical structure (1TF3).

Another protein which requires metal ions for its structural stability and whose structural analysis is well characterized is calmodulin. Calmodulin is a calcium binding protein which has its role in signal transduction pathways.  $Ca^{2+}$  ion is involved in many cellular functions of cell differentiation, proliferation as well as apoptosis (Gifford, et al., 2007). The 'EF hand'  $Ca^{2+}$  binding motif has been studied to understand the

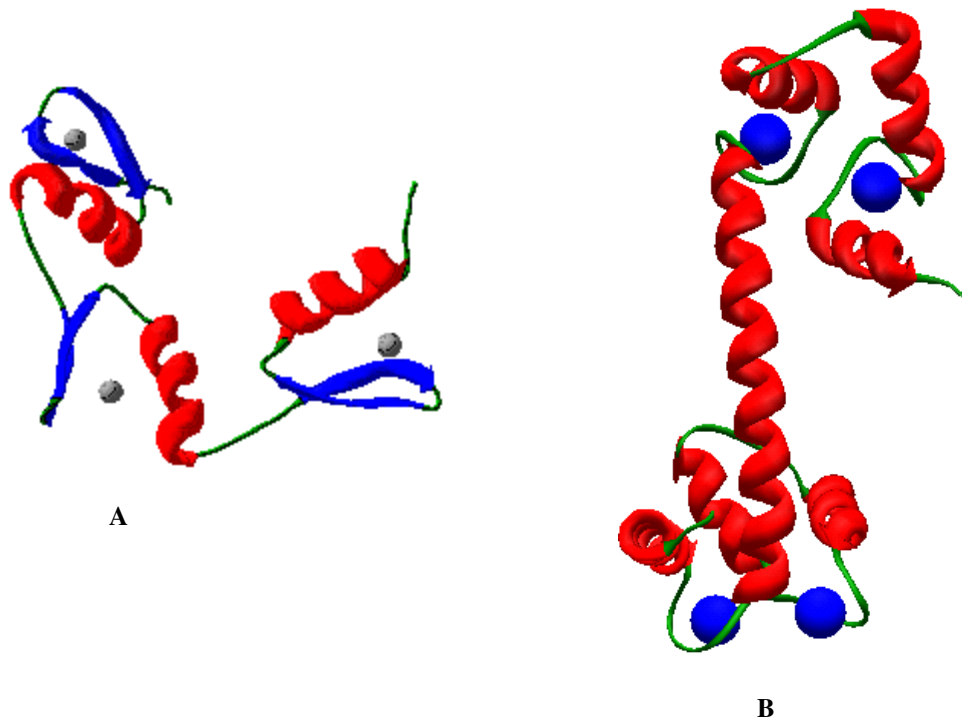


**Figure 1.2: Structure of the Zinc finger domain of the Transcription factor TFIID with Zinc metal and the EF domain of Calmodulin with  $\text{Ca}^{2+}$ .** A. NMR structure of the zinc finger domain shows the metal ions bound to the protein. (Pdb file 1TF3). B. Xray crystal structure of the calmodulin shows the metal ions bound to the protein. (Pdb file 1UP5). Figures were created using the pdb files in swiss pdb viewer.

functionality of a diverse family of calcium binding proteins (Gifford, et al., 2007). Calmodulin activates enzymes such as protein kinases and  $\text{Ca}^{2+}$  pumping ATPase (Lippard and Berg, 1994). Calmodulin is a monomeric protein which can bind four  $\text{Ca}^{2+}$  ions (**Figure 1.2**). The molecule has a dumbbell shape with alpha helix connecting the two domains (1UP5). The helix structure is stabilized by the presence of basic and acidic residues. It recognizes  $\text{Ca}^{2+}$  ions even at high intracellular  $\text{Mg}^{2+}$  concentrations. This specificity for  $\text{Ca}^{2+}$  is related to its higher coordination number of  $\text{Ca}^{2+}$  relative to  $\text{Mg}^{2+}$ . X-ray crystallography shows seven-coordinated  $\text{Ca}^{2+}$  ions using aspartate, asparagine, glutamate, carbonyl group, and water molecule as the ligands (Lippard and Berg, 1994). Although the bound metal ions are observed by crystal structure the biochemical analysis on the affinity of metal site, ligand requirement, and its activity are required (Corson, et al., 1983).

Biochemical investigation coupled with the theoretical approaches can provide mechanistic details about the role of metals in the activity of the protein/enzyme (Dupureur, 2008).

#### **b) Proteins with metal ion as cofactors:**

Study of the role of metal ions has always been interesting and challenging especially in very specific proteins or enzymes. For example, in  $\text{Mg}^{2+}$ -specific nucleases it has been difficult to study this cofactor role because of its lability and spectroscopic silence (Black and Cowan, 1997). Inert transition metal complexes with ammine or aquo ligands are used for the mechanistic studies of metallonucleases (Black and Cowan, 1997). Lanthanides, which are spectroscopically active metals, are also used to look at the role of metals in these enzymes (Bowen, et al., 2004). Most of these DNA binding

enzymes, which use metal as cofactors, use  $Mg^{2+}$  ions for the cleavage activity; however they can bind DNA in presence of other larger metals like  $Ca^{2+}$  and  $Ba^{2+}$ . One explanation for this observation is that the smaller metal ions like  $Mg^{2+}$  better stabilize the pentavalent transition state formed than the larger metal ions. Staphylococcal nuclease is an enzyme known to use  $Ca^{2+}$  ions for the hydrolysis of the phosphodiester bond (Cuatrecasas, et al., 1967). Many biochemical studies are done on enzymes like DNA polymerase I, Klenow fragment, transposases, ribozymes, endonucleases etc., to explain the metal ion mechanisms of the enzymatic process (Junop and Haniford, 1996; Lott, et al., 1998; Brautigam, et al., 1999; Doan, et al., 1999; Stahley, et al., 2007).

## **1.2. Mechanism of the phosphodiester bond hydrolysis:**

The general mechanism of the phosphodiester bond hydrolysis is comprised of three steps: the formation of the attacking nucleophile, the transition state formation and removal of the 3' hydroxyl group. In type II restriction endonucleases, PD...D/ExK motif present at the catalytic site are the residues involved in the phosphodiester cleavage (Pingoud, et al., 2005). These residues bind metal ions which assist the cleavage process. The number of metal ions required for the enzymes to do their work is still being explored. Different metal ion mechanisms are proposed for the variety of enzymes in the type II endonuclease system.

**One metal ion mechanism:** In crystal structures of EcoRI and BglII endonucleases, only one metal ion was bound at the active site (Lukas, et al., 2000; Grigorescu, et al., 2004). Biochemical studies on these proteins with modified substrates also indicate the involvement of one metal ion in the cleavage process. In a one metal ion

mechanism as seen in **Figure 1.3**, the metal ion stabilizes the transition state formed by the nucleophilic attack (Pingoud, et al., 2005). This mechanism is also called the substrate-assisted mechanism since the deprotonation of the water molecule, which acts as the nucleophile, is assisted by the phosphate group which is 3' to the phosphodiester bond that is broken.

**Two metal ion mechanism:** In this type of mechanism, metal ions are required for the transition state stabilization. Two metal ions are required for the hydrolysis reaction, one metal is involved in the formation of the nucleophile and another interacts with the 3' leaving group (Dupureur, 2008). Many different enzymes are known which feature two metal ions in their structures, e.g., BamHI, PvuII, BglII, DNA polymerase I-5'-3' exonuclease (Beese and Steitz, 1991; Newman, et al., 1998; Viadiu and Aggarwal, 1998; Horton and Cheng, 2000). Ideally metal ions should be approximately 4 Å apart to facilitate a two metal ion mechanism (Pingoud, et al., 2005). One of the metal ions lowers the  $pK_a$  of the neighboring water molecule which helps deprotonate the water molecule and form a nucleophile. The nucleophile generated attacks the phosphodiester bond and facilitates the hydrolysis reaction as shown in **Figure 1.4**. In type II endonucleases with PD...D/ExK motif at the active site, the generation of the nucleophile is debated over the role of the lysine residue, which is conserved in many type II endonucleases. Mutation of the active site lysine to alanine in enzyme PvuII diminishes its enzymatic activity (Nastri, et al., 1997). In the crystal structure of PvuII, the lysine residue was observed within hydrogen bond distance to the metal ligated water molecule (Horton and Cheng, 2000). Enzymes like BamHI and BglII contain glutamic acid and glutamine

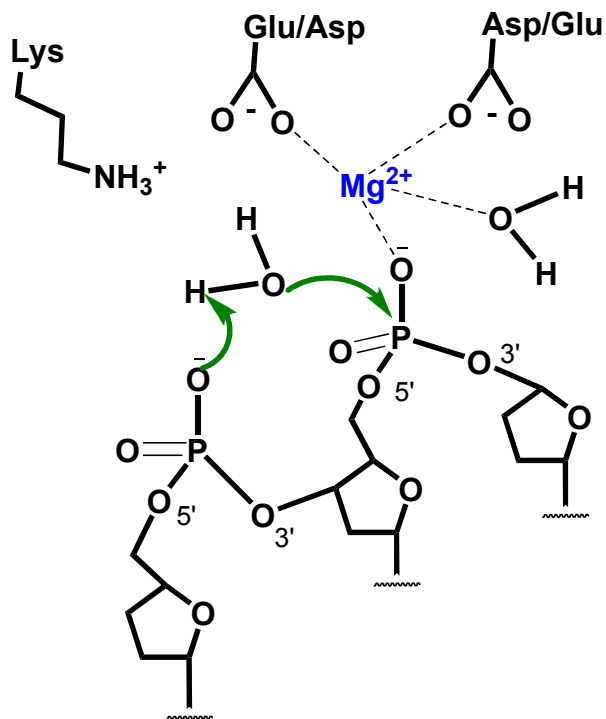


**Figure 1.3: Depiction of the one metal ion mechanism in phosphodiester hydrolysis:**

The transition state is stabilized by the metal ion. The 3' oxygen group from the DNA facilitates the nucleophile formation by deprotonation of the water molecule. Adapted from (Pingoud, et al., 2005).

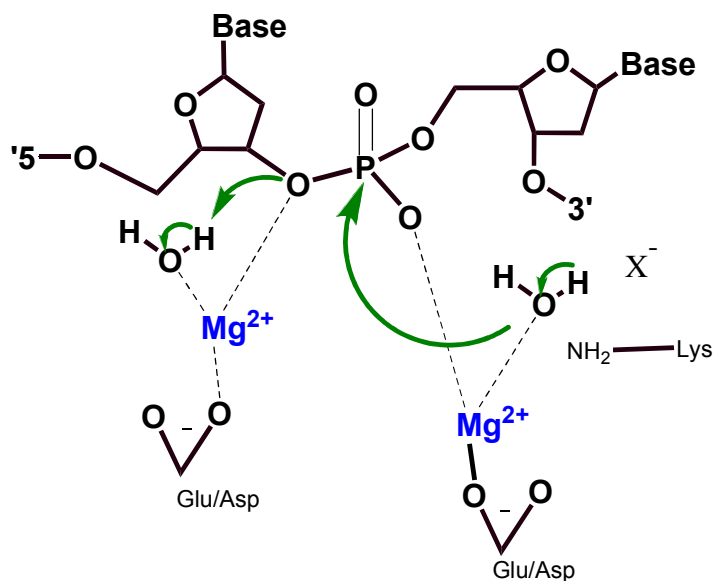


**Figure 1.4: Two metal ion mechanism in phosphodiester bond hydrolysis:** The pentavalent transition state is stabilized by two metal ions. They share the ligands of the active site and mediate phosphoryl transfer reactions (Horton and Cheng, 2000). BamHI and BglII, which also bind two metal ions, do not have the conserved lysine residue at their active site. This feature has led to questions about the role of lysine in the mechanism (Newman, et al., 1998; Viadiu and Aggarwal, 1998). Adapted from (Pingoud, et al., 2005).

residues, respectively, at their active site instead of the conserved lysine, which raises questions regarding the role of lysine in a two metal ion mechanism (Newman, et al., 1998; Viadiu and Aggarwal, 1998). Proteins with two metal ion mechanism are studied in detail below.

**Three metal ion mechanism:** This mechanism is not a widely accepted mechanism. Biochemical studies with EcoRV indicate three metal ion positions in the active site of this protein and therefore a three metal ion mechanism for the hydrolysis activity. In crystal structures of EcoRV, presence of three metal ions is not seen simultaneously. Metal ion at site I deprotonates the water molecule and thus formation of the nucleophile occurs as shown in **Figure 1.5**. The metal ion at site III stabilizes the transition state and then moves to site II. This metal ion then stabilizes the 3' leaving group by interacting with the water molecule (Pingoud, et al., 2005).

### 1.2.1 Studies on two metal ion mechanism:

The mechanism of catalysis by ribozymes has been investigated from the time that catalysis by RNA was proven (Zhou, et al., 1996). A general acid base mechanism and a specific mechanism with the metal ions are proposed for the ribozyme catalysis (Zhou, et al., 1996). In splicing process, group I introns are involved in the removal of introns and ligation of flanking exons (Steitz and Steitz, 1993). Both these steps in the splicing process with phosphoryl transfer reactions are shown in **Figure 1.6**. A two metal ion mechanism with  $Mg^{2+}$  is proposed for the phosphoryl transfer reaction of ribozymes (Steitz and Steitz, 1993). In the two metal ion mechanism proposed, the 3' OH group from the RNA chain works as the nucleophile in both steps. For the removal of introns, the 3' OH group from the guanosine activates the metal ion  $Mg_A^{2+}$  and the metal ion



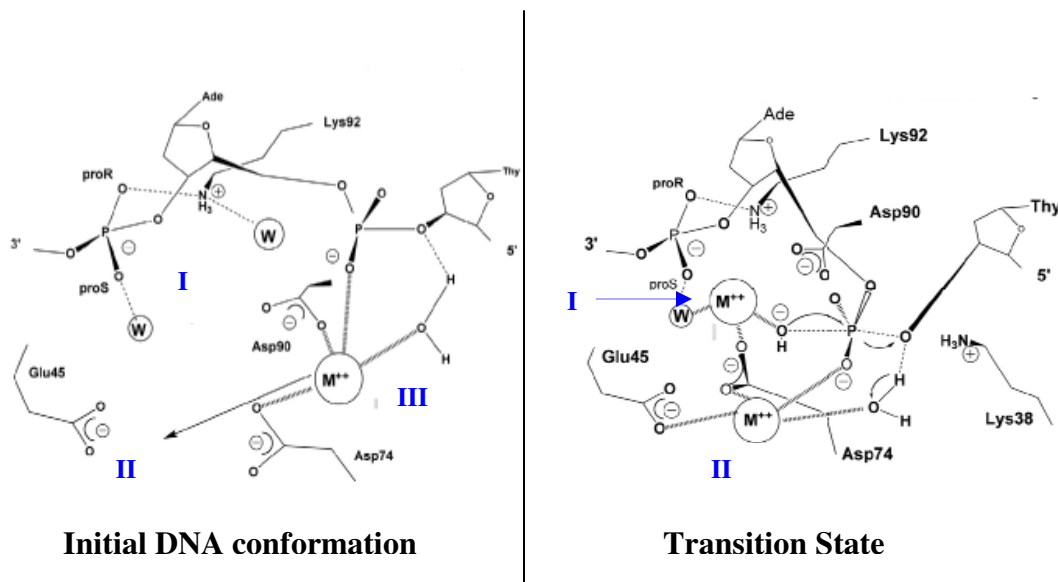


**Figure 1.5: Transition state structure of the three metal ion mechanism proposed for EcoRV:** A metal ion movement is proposed in this type of mechanism. There are three metal binding sites shown and they are involved in the catalytic process. The metal at site I facilitates the formation of the nucleophile, metal at site III stabilizes the transition state formation and that at site II interacts with the leaving group. In the initial complex site III is occupied by a metal ion, which moves to site II during transition state. Adapted from (Horton and Perona, 2004; Dupureur, 2008).

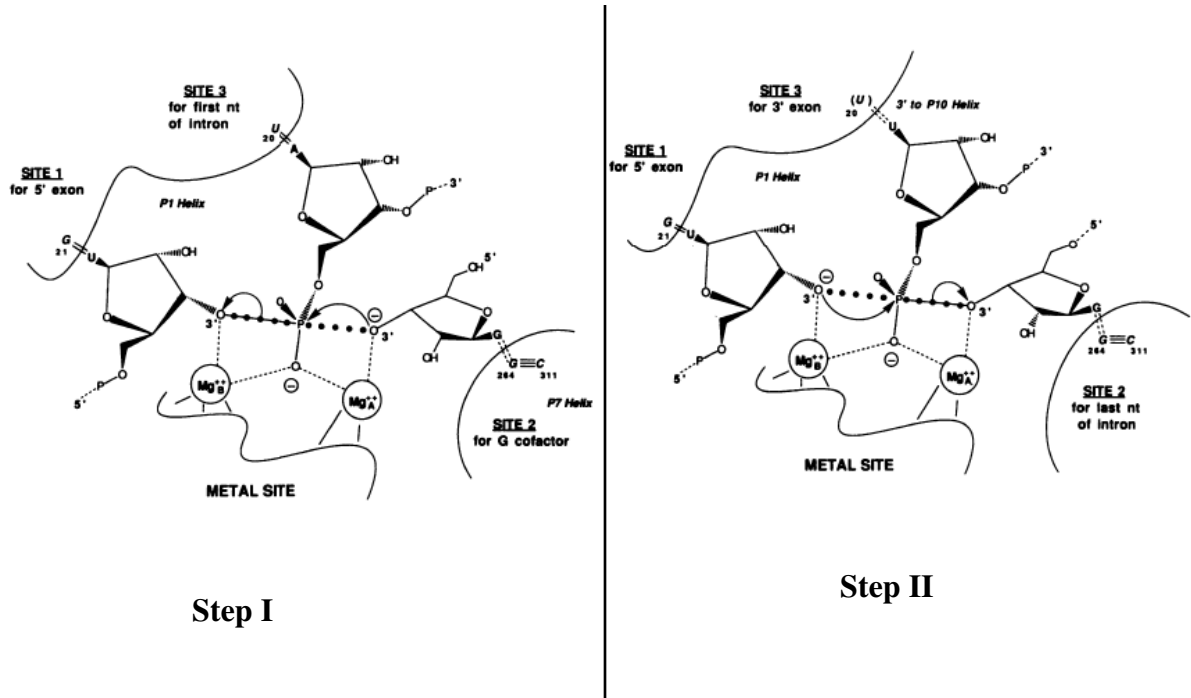


**Figure 1.6: Mechanism for the group I intron activity:** Step I is the removal of introns and step II is the ligation of the flanking exons. In step I of the splicing process the 3' OH group from the guanosine acts as the nucleophile and activates the  $Mg_A^{2+}$  ion. In the second step the  $Mg_B^{2+}$  ion activates the 3' OH group from the uridine, which acts as the nucleophile, and  $Mg_A^{2+}$  interacts with the leaving group. Adapted from (Steitz and Steitz, 1993).

$Mg_B^{2+}$  stabilizes the pentavalent transition state and coordinates with the 3' leaving group. At the second step of the reaction, there is a role reversal of the metal ions, the newly formed 3'OH group of the uridine is activated by the metal ion  $Mg_B^{2+}$  and the leaving group guanosine is bound to  $Mg_A^{2+}$  (Steitz and Steitz, 1993).

### **1.2.2 Role of metal sites: site A and site B in enzymes, e.g. BamHI.**

There are persistent questions regarding the number of metal ions required in the phosphodiester cleavage activity and the role of each metal ion in the catalytic process. BamHI, which is a well characterized enzyme from the PD...D/ExK, family recognizes the 5'-GGATCC-3' sequence and cleaves the DNA between GG residues. Crystal structure of BamHI shows that they bind two metals, but the role of each metal ion on the catalytic activity has to be characterized. In a study using molecular dynamics with free energy calculations, the role of each metal ion and the contribution of metal toward nucleophile generation were examined (Mones, et al., 2007). A reactive complex of BamHI was obtained from the crystal structures (Viadiu and Aggarwal, 1998). Metal ion at site A contributed more towards the nucleophile generation and stabilization of the pentavalent state than metal ion at site B. Metal ion at site A is a rigid entity whereas that at site B is more mobile and can cause conformational changes. It was proposed for BamHI that only one metal ion is required for the catalysis process and the metal at site B has a regulatory role.

### **1.3 Mixed metal studies: A biochemical approach for mechanistic details.**

Mixed metal kinetic studies were done on EcoRV, EndonucleaseV, etc., to dissect the role of metal ions during catalysis. These enzymes show evidence of mixed metal

complex formation (Vipond and Halford, 1995; Feng, et al., 2006). In these studies a catalytically active and catalytically inactive metal are paired.  $\text{Ca}^{2+}$  ions are used as the catalytically inactive metal since they are known to be involved in DNA binding but not DNA cleavage (Bowen, et al., 2004). EndonucleaseV, which is a DNA repair enzyme, is highly metal ion dependent during phosphodiester hydrolysis from a deaminated base. The analysis of catalytic activity of EndonucleaseV with  $\text{Mg}^{2+}/\text{Mn}^{2+}$  alone showed that a low concentration of  $\text{Mg}^{2+}$  is sufficient for enzymatic activity, whereas higher  $\text{Mn}^{2+}$  concentrations are required (Feng, et al., 2006). These studies imply that site 1 has higher affinity for  $\text{Mg}^{2+}$  than  $\text{Mn}^{2+}$ , and this site should be filled with  $\text{Mg}^{2+}/\text{Mn}^{2+}$  for catalytic activity. Filling of the second site does not have significant role in the activity. Mixed metal biochemical experiments where combinations of  $\text{Mg}^{2+}$ ,  $\text{Mn}^{2+}$ , and  $\text{Ca}^{2+}$  are used showed involvement of two metal ions in EndonucleaseV mediated catalysis (Feng, et al., 2006). They show an inhibitory or stimulatory effect when  $\text{Mn}^{2+}/\text{Ca}^{2+}$  metals are added with  $\text{Mg}^{2+}$ . From these experiments with the EndonucleaseV using different combinations of metal ions  $\text{Mg}^{2+}$ ,  $\text{Mn}^{2+}$ , and  $\text{Ca}^{2+}$  it was proposed that one metal binding site is catalytic and the other regulatory. Depending on which metal occupies the two sites, the activity of the enzyme varies. If  $\text{Ca}^{2+}$  ion occupies the catalytic site of the enzyme, they form an inactive complex (Feng, et al., 2006). It was gathered from these experiments that affinity of metal ions at site 1 is  $\text{Mg}^{2+} > \text{Mn}^{2+} > \text{Ca}^{2+}$ , and that at site 2 it is  $\text{Ca}^{2+} > \text{Mn}^{2+} > \text{Mg}^{2+}$ .  $\text{Mg}^{2+}$  at site 1 is required for catalysis, and  $\text{Ca}^{2+}$  at site 2 with  $\text{Mg}^{2+}$  at site 1 has stimulatory effects of the enzymatic activity (**Figure 1.7**) (Feng, et al., 2006). EcoRI and EcoRV endonucleases are studied for their structural differences at the active site, their metal ion binding properties, and the role of metal ions in catalytic activity.

Crystal structures have supported a one metal ion mechanism for the EcoRI enzyme, and a two or three metal ion mechanism for EcoRV (Vipond and Halford, 1995). Biochemical studies with mixed metals were performed to understand the involvement of metals in their catalytic activity. For EcoRI and EcoRV, the occupancy of metals at the active site has a varying effect on the enzymatic activity. In the mixed metal studies, the catalytic activity is measured in the presence of a mixture of a catalytically active ( $Mg^{2+}$  or  $Mn^{2+}$ ) and catalytically inactive ( $Ca^{2+}$ ) metal. With an increase in  $Ca^{2+}$  concentration, there was always an inhibition of activity seen for EcoRI with both  $Mg^{2+}$  and  $Mn^{2+}$  as seen in **Figure 1.8** (panel A and B) (Vipond and Halford, 1995). Many explanations were examined for this observation. The possibility that  $Ca^{2+}$  ions do not bind at the active site of the enzyme in presence of  $Mg^{2+}$  and  $Mn^{2+}$  ions was ruled out because that would mean no effect on the activity of the enzyme with the addition of  $Ca^{2+}$ . Another possibility is that on  $Ca^{2+}$  binding, a change in conformation of the protein occurs which forms an inactive complex. However, the crystal structure of the protein with  $Ca^{2+}$  and  $Mg^{2+}$  do not show big differences in conformation (Bauer, 1978). The data with mixed metals support a one metal ion mechanism for EcoRI, and the difference in affinity for the active site between metal ions shows the extent of inhibition. More inhibition of activity was seen in presence of  $Mg^{2+}$  and  $Ca^{2+}$  as compared to  $Mn^{2+}$  and  $Ca^{2+}$ , which shows a rank of affinity of EcoRI for the metals as  $Mn^{2+} > Ca^{2+} > Mg^{2+}$  (Vipond and Halford, 1995).

For EcoRV, there was an increase in the activity of the enzyme with the cognate and noncognate sequences in presence of  $Mn^{2+}$  and  $Ca^{2+}$ , whereas with  $Mg^{2+}$  and  $Ca^{2+}$  the increase in activity was seen only with the noncognate sequence. This difference in the

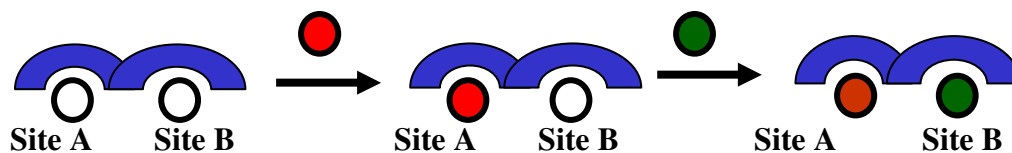


**Figure 1.7: Two metal ion model of Endonuclease V:** Two metal sites are shown in this model. Site A is a high affinity catalytic metal binding site, and site B is defined as a low affinity site which is also referred as the regulatory site. Metal binding at the catalytic site will lead to the DNA cleavage reaction. Depending on which metal binds at this site B, stimulation or inhibition of the activity is observed. Adapted from (Feng, et al. 2006).

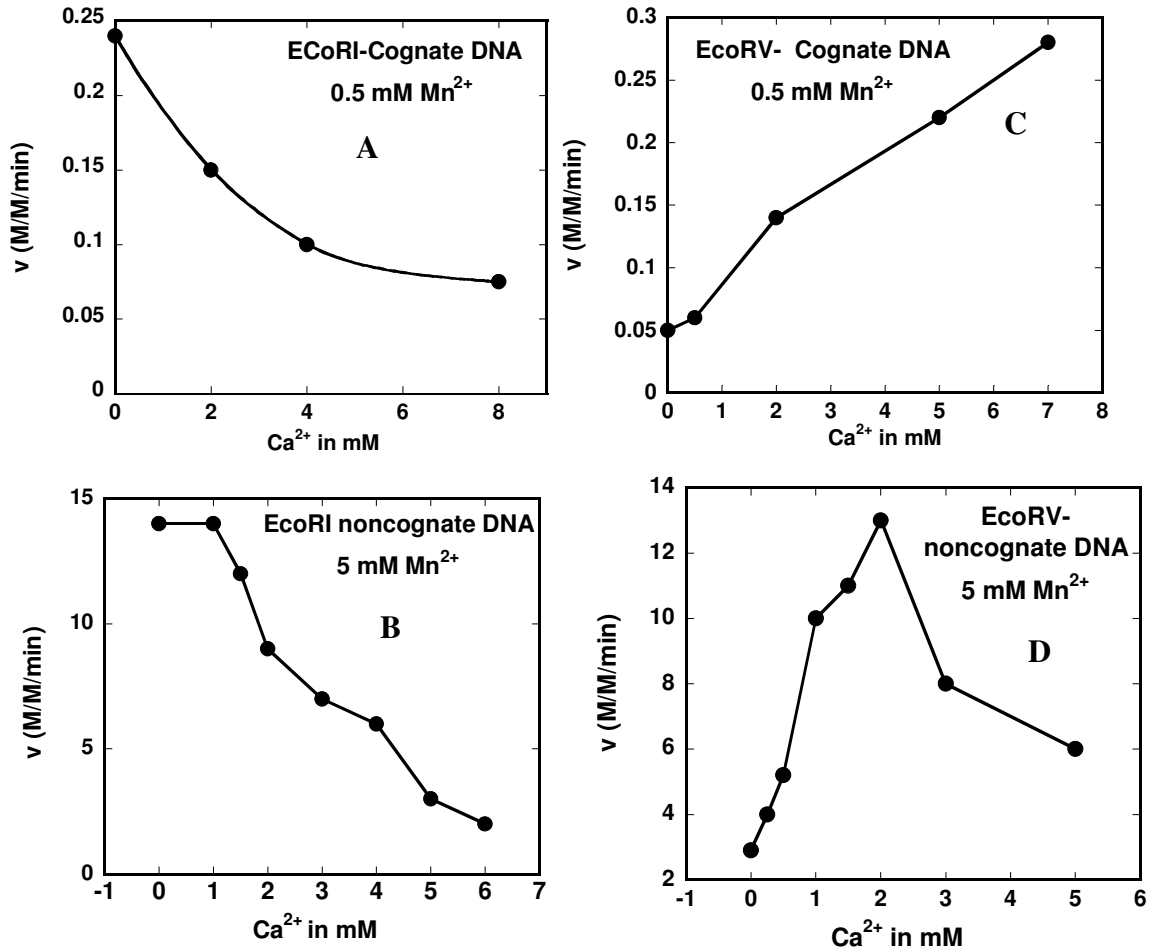


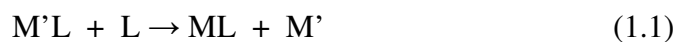
**Figure 1.8: Cleavage of cognate and non-cognate sequences by EcoRI and EcoRV enzymes under mixed metal conditions.** The line is not a fit and is shown here to guide the eye for the trend. Left hand panel (A and B) shows inhibition of activity of EcoRI enzyme with  $Mn^{2+}$  at increasing  $Ca^{2+}$  concentrations with cognate and noncognate sequences. Right hand panel (C and D) shows the effect of  $Ca^{2+}$  on the activity of EcoRV. With cognate sequence in presence of  $Mn^{2+}$  there is increase in activity with  $Ca^{2+}$ . With noncognate sequence EcoRV has an initial increase in activity and at  $Ca^{2+}$  concentrations above 2 mM the activity of the enzyme decreases. The trends seen with both enzymes under  $Mg^{2+}$  and  $Ca^{2+}$  conditions were similar to the  $Mn^{2+}/Ca^{2+}$  conditions. Adapted from (Vipond and Halford, 1995).

enzymatic activity of EcoRV was explained in this study with the presence of two metal binding sites and their differences in metal affinity. These studies implicated that the affinity for  $Mn^{2+}$  at the A site is more than  $Ca^{2+}$  and therefore with increasing  $Ca^{2+}$  concentrations, there is mixed metal complex formed ( $EMn^{2+}Ca^{2+}$ ) which is more active (**Figure 1.8**) (panel C and D).  $Ca^{2+}$  ions cannot displace  $Mn^{2+}$  ions from the site A; therefore the inactive  $E Ca^{2+} Ca^{2+}$  species is not formed. With the noncognate DNA, a lower affinity for the enzyme- $Mn^{2+}$  complex formation is mentioned. Therefore the increase in the activity of the enzyme at low  $Ca^{2+}$  concentrations is explained by the formation of a more active  $EMn^{2+}Ca^{2+}$  mixed complex. With increasing  $Ca^{2+}$  concentration, both metal sites are filled with  $Ca^{2+}$  to form the inactive  $E Ca^{2+} Ca^{2+}$  complex, and thus the activity of the enzyme decreases (Vipond and Halford, 1995).

A mixed metal study with the DNA repair enzyme ApeI endonuclease implicates a two metal ion mechanism for the enzyme where a stimulation of activity is seen with increasing  $Ca^{2+}$  ions (Beernink, et al., 2001). Strand transfer activity of Tn10 transposon with mixed metals  $Ca^{2+}$  and  $Mg^{2+}$  shows the inhibitory effect with increasing  $Ca^{2+}$  concentrations, thus indicating a one metal ion mechanism (Junop and Haniford, 1996).

### 1.3.1 Association and Dissociation rates of metal binding:

Characterization of metal binding at the active site of proteins or enzymes also involves studies by of association and dissociation rates. This is accomplished using metal exchange reactions. Metal exchange reactions explore the transfer of the ligand between two metal centers as shown in the **equation (1.1)**. Studies of metal exchange





provide details of the stability of a metal interaction (Berezin, et al., 2004). The mechanism of displacement in a kinetic process is determined using this method. These metal exchange reactions also help determine the stability constant and to prepare metal clusters and organometallic compounds (Suzuki, et al., 1994). A study with mesoporphyrins compares the stabilities of these porphyrins with  $\text{Zn}^{2+}$ ,  $\text{Mg}^{2+}$ , and  $\text{Cd}^{3+}$  (Berezin, et al., 2004). Most of these exchange studies with the small molecule chelators are done using solvent extraction techniques where the products are isolated and then characterized for the amount of species formed (Haraguchi and Frieser, 1983).

Exchange studies on transferrin, which is an iron transport protein, shows exchange of  $\text{Fe}^{3+}$  by other metal ions based on charge and coordination geometry of metals (Pakdaman, et al., 1999). The metal-transferrin interaction is studied using competition titration with many chelators, especially nitriloacetic acid (Harris, et al., 2003; Biver, et al., 2008). Exchange studies are done on  $\text{Fe}^{3+}$ -transferrin with different metals such as  $\text{Al}^{3+}$ ,  $\text{Fe}^{3+}$ ,  $\text{Ga}^{3+}$ , and  $\text{In}^{3+}$ . These metal ions are studied because they are medically important for diagnostic purposes (Hayes and Hubner, 1983). Calmodulin, parvalbumin, and calcineurin are other proteins where association and dissociation rates for metal binding are characterized using exchange kinetics (Corson, et al. 1983; Breen, et al., 1984; Tsai, et al., 1987). These studies are done using spectrophotometric techniques (Hayes and Hubner, 1983; Sun, et al., 1999).

Lanthanide metals are spectroscopically active and therefore used in the metal – protein interaction studies. Lanthanide ions have similarities with calcium ions with respect to their size, coordination sites, and the binding of the oxygen ligands (Moeller, 1963; Martin, 1984; Martell and Smith, 1989). Interaction of calcium with many calcium

binding proteins is explored with lanthanide spectroscopy. Using the luminescent property of the lanthanide ions, many metal ion coordination sites were studied (Horrocks, 1993).  $\text{Eu}^{3+}$  and  $\text{Tb}^{3+}$  are the most luminescent of the lanthanides; they have low molar absorptivity, which makes them absorb weakly with direct excitation (Martin and Richardson, 1979; Horrocks and Sudnick, 1981). Indirect excitation of lanthanides by exciting the aromatic residue close to the metal binding site (**Figure 1.9**), which then transfers the energy to the bound metal, overcomes this problem with direct excitation. This luminescence spectroscopy was explored in the exchange study of metals in the CD and EF metal binding sites of parvalbumin (Breen, et al., 1984). In one such study the dissociation rate of metal ions  $\text{Ca}^{2+}$ ,  $\text{Cd}^{2+}$ ,  $\text{Pr}^{3+}$ ,  $\text{Nd}^{3+}$ ,  $\text{Sm}^{3+}$ ,  $\text{Eu}^{3+}$ ,  $\text{Gd}^{3+}$ ,  $\text{Tb}^{3+}$ ,  $\text{Dy}^{3+}$ ,  $\text{Ho}^{3+}$ ,  $\text{Er}^{3+}$ ,  $\text{Yb}^{3+}$ , and  $\text{Lu}^{3+}$  from parvalbumin were measured. Kinetic traces which give the change in the luminescence signal with time was then fitted to the double exponential equation to obtain the dissociation rate constant of the metal ions from the two sites in parvalbumin (Breen, et al., 1984). There is no cooperativity between the metal sites in parvalbumin, and therefore the dissociation rate constants observed for the two sites are independent of each other (Breen, et al., 1984). In a study with murexide it was shown that the early and middle order lanthanides of the series have a bimolecular mechanism and therefore greater binding affinity for the protein (Geier, 1965). In the study with parvalbumin and lanthanide series, it was seen that the rate of exchange is fast when one site is filled with a metal ion. This indicates that with parvalbumin and early members of the lanthanide series there is a metal ion assisted exchange process that occurs (Breen, et al., 1984). In calmodulin the metal exchange reactions reflected stronger affinity of early

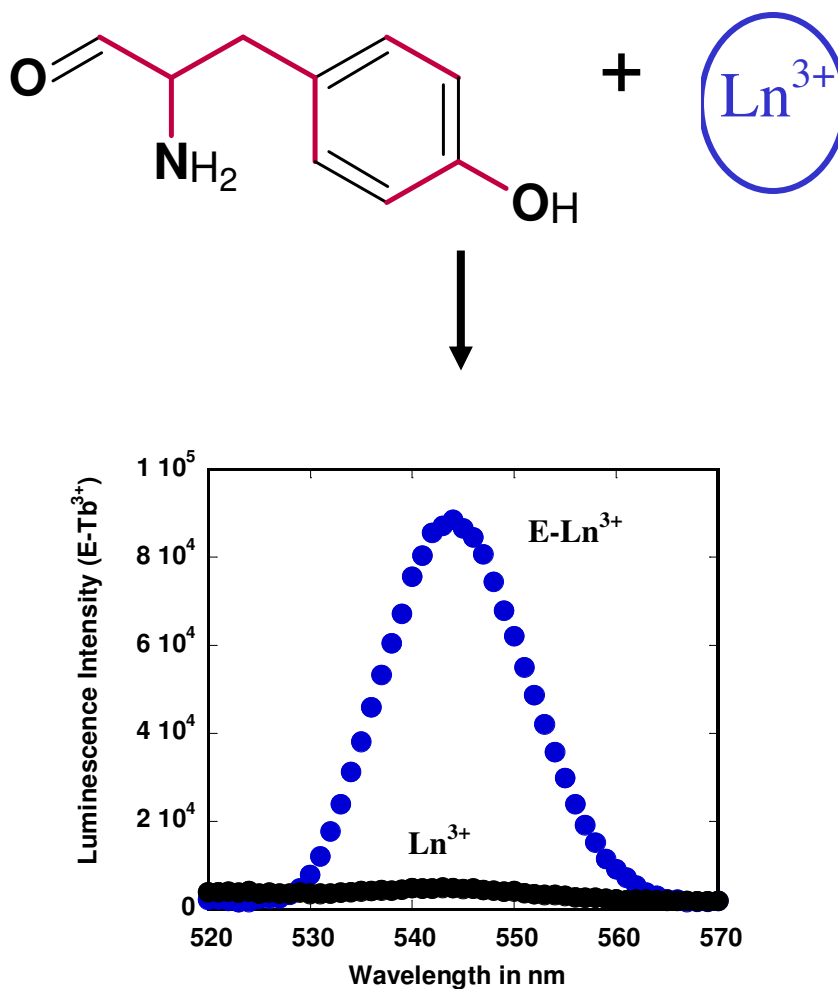


**Figure 1.9: Indirect excitation of the lanthanides using the aromatic residues closer to the metal binding site.** Tyrosine residue closer to the metal binding site of PvuII was excited, energy transfer to the lanthanide ions bound at the active site excites the lanthanide ions and the emission of these lanthanides is measured to observe the metal ion binding at the active site of the enzyme. The spectra here show the emission speak of the enzyme bound  $\text{Ln}^{3+}$  ions.

order lanthanides to EF site and the latter order lanthanides for the CD site (Corson, et al., 1983). Binding affinities and mechanism are being explored using the metal exchange reactions with lanthanides in many proteins, especially on calcium binding proteins.

#### **1.4 Model system: Restriction Endonucleases**

Restriction endonucleases are model systems for various protein-DNA interactions and catalysis. One percent of the genome in prokaryotic organisms consists of the genes from the restriction modification system (Pingoud and Jeltsch, 2001). The restriction modification system works as an immune system in bacteria and protects the host DNA from the invading foreign DNA. **Figure 1.10** shows the components in the restriction modification system of type II endonucleases and degradation of the foreign DNA by the enzymes. The host DNA is methylated in order to protect it from these nucleic acid cleaving enzymes (Tock and Dryden, 2005). Restriction endonucleases are characterized based on subunit arrangement and their cofactors. Type II enzymes are the most predominant type of restriction endonuclease. They are homodimeric or homotetrameric in nature, require  $Mg^{2+}$  as the cofactor and cleave DNA within or close to the recognition sequence (Pingoud and Jeltsch, 2001).

##### **1.4.1 Three dimensional structure of type II restriction endonucleases:**

These enzymes have a general structure with some variations. All of them have five strands, mixed  $\beta$ -sheet flanked by  $\alpha$ -helices. The catalytic residue motif PD...D/ExK is present at the second or third strand of  $\beta$ -sheet. There are structural differences between the different enzymes within the type II restriction endonucleases (Pingoud, et al., 2005). For example, the fifth  $\beta$ -strand can be parallel (EcoRI) or antiparallel (EcoRV) to the fourth strand. Also these subgroups of enzymes approach the DNA differently. EcoRI

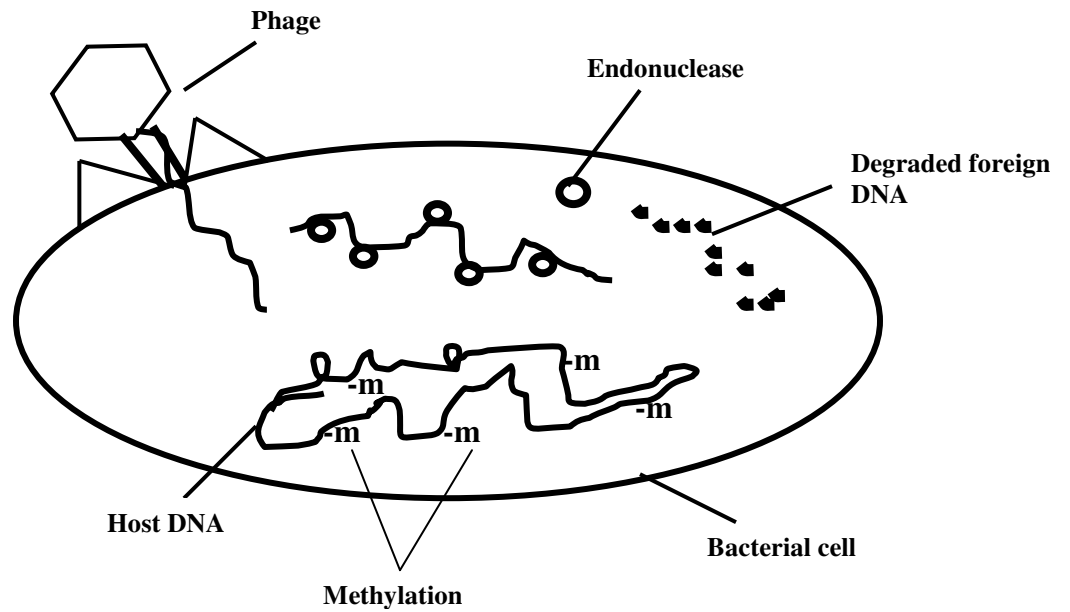


**Figure 1.10: Cartoon of the restriction modification system machinery:** The phage DNA or the foreign DNA is cleaved by the restriction endonuclease in presence of cofactors ( $Mg^{2+}$ ). Host DNA is protected from cleavage because of restriction modification (methylation). Adapted from (Tock and Dryden, 2005); and G. Papadakos thesis, 2008).

type enzymes approach the DNA from the major groove and produce 5' staggered product. The EcoRV type of enzyme approaches the DNA from the minor groove and produces blunt or 3' staggered end products (Pingoud, et al., 2005). Restriction endonucleases have functions similar to many other proteins which interact with the nucleic acids and are involved in recombination, DNA processing, and DNA repair (Etzkorn and Horton, 2004).

### **1.5 Introduction to PvuII Endonuclease:**

PvuII is a type II restriction endonuclease from the bacterium *Proteus Vulgaris* and it belongs to the PD..D(E)XK family of endonucleases. It requires  $Mg^{2+}$  as cofactor and recognizes a palindromic sequence of 5'-CAG|CTG-3'. PvuII works as a homodimer and hydrolyses a phosphodiester bond between G and C to produce blunt end products (Horton and Cheng, 2000). The active site of PvuII contains three residues two acidic (Asp58, Glu68) and one basic residue, (Lys70) which perform the binding of metal ions and binding and cleavage of the DNA (**Figure 1.11**). The metal ions bound at the active site of PvuII is characterized crystallographically as well as in solution (Jose, et al., 1999; Dupureur and Conlan, 2000; Horton and Cheng, 2000; Bowen, et al., 2004). Gel shift assays using site directed mutants demonstrated that the His83His84His85 triplet, Glu55 and the active site residue Lys70 do not contribute to the DNA binding specificity (Nastri, et al., 1997). Structure of PvuII with cognate DNA and  $Ca^{2+}$  ions shows the presence of two metal ions at the active site with octahedral coordination of the  $Ca^{2+}$  ions. These structures show that the active site residues mediate the binding to the metal ions and the substrate (**Figure 1.12**) (Horton and Cheng, 2000).

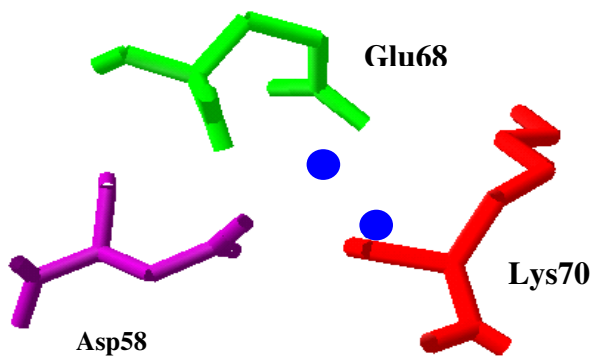


**Figure 1.11: Active site residues of PvuII endonuclease:** The Asp58, Glu68, and Lys70 residues are ligands to the metals in restriction enzyme PvuII (1F0O). The PD...D/ExK motif is conserved in the endonuclease family. The Ca<sup>2+</sup> ions are shown in blue. Adapted from (Horton and Cheng, 2000).

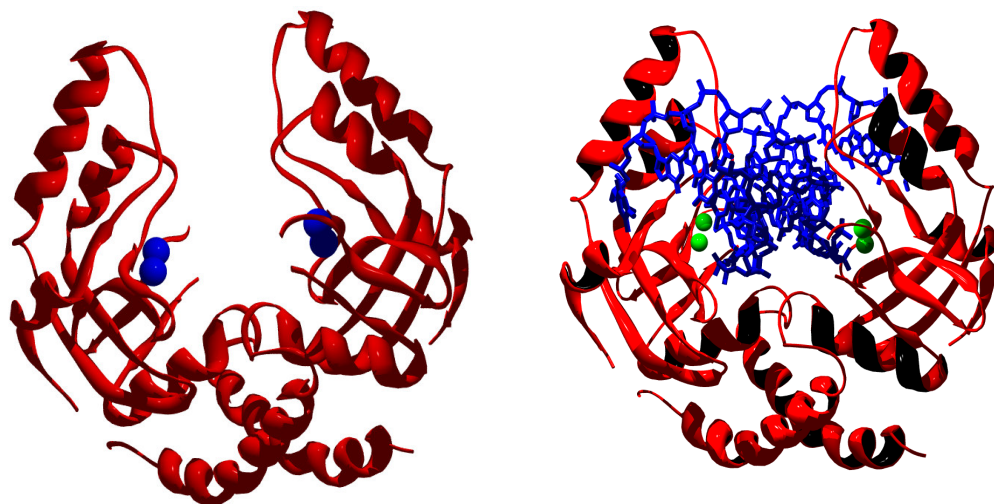


**Figure 1.12:** The crystal structure of PvuII endonuclease with the cognate DNA in presence of  $\text{Ca}^{2+}$  ions. The structures show the two subunits of the protein, the  $\text{Ca}^{2+}$  ions and the cognate DNA. The DNA molecule is positioned so that the cleavage site of DNA also coordinates with the metals. This structure is adapted from the 1F00 pdb structure (Horton and Cheng, 2000).



### 1.5.1 Metal binding to PvuII:

Metal binding in PvuII is characterized for the alkaline earth metals, the lanthanides and the transition metal  $Mn^{2+}$  using variety of techniques. Calorimetric titrations were done to monitor the binding of the  $Ca^{2+}$  and  $Mn^{2+}$  ion to the enzyme PvuII (Jose, et al., 1999). These direct titrations of metal binding indicated the presence of two metal sites. For  $Ca^{2+}$  ions the binding constants for the two sites were  $0.12 \pm 0.08$  mM and  $2.1 \pm 0.14$  mM (Jose, et al., 1999). For  $Mn^{2+}$  ions the direct titration data when fit to a model with independent sites fit for two sites with same binding constant of  $1.6 \pm 0.3$  mM (Jose, et al., 1999). Binding of metals  $Ca^{2+}$  and  $Mn^{2+}$  were also studied for the PvuII variants with mutations on the active site residues D58 and E68. The calorimetric titrations did not show any binding of the metal ions  $Mn^{2+}$  or  $Ca^{2+}$  to the E68A mutant, whereas for the D58A mutant the  $Mn^{2+}$  binding could be measured. The binding constant obtained for the  $Mn^{2+}$  binding to the D58A mutant using equivalent site model was  $2 \pm 0.3$  mM (Jose, et al., 1999).  $^{25}Mg$ - NMR spectroscopy was used to measure  $Mg^{2+}$  binding to the enzyme PvuII. It was observed that  $Mg^{2+}$  binding to PvuII fits to give a Hill coefficient of 1.4 which is consistent with two metal ions at the active site with apparent binding constant of  $1.9 \pm 0.4$  mM (Dupureur and Conlan, 2000).

PvuII variants D58A and E68A were also studied for the  $Mg^{2+}$  binding. For D58A a Hill coefficient of 0.7 was observed with an apparent binding constant of  $3.6 \pm 0.5$  mM (Dupureur and Conlan, 2000). This indicates the loss of one metal site from the mutation and therefore weaker binding than the WT enzyme. For the E68A mutant it was difficult to get the signal, and an approximate  $K_d$  of 40 mM was obtained (Dupureur and Conlan, 2000). The size and the coordination sites for these metal ions are different and

therefore the geometry of the active site will decide the metal ion binding. The active site geometry with the D58A mutation is suitable for the binding of  $Mg^{2+}$  and  $Mn^{2+}$  ions but not the  $Ca^{2+}$  ions.

### **Lanthanide binding to PvuII:**

Binding of lanthanides ions  $Tb^{3+}$  and  $Eu^{3+}$  to PvuII was studied using lanthanide spectroscopy. Tyrosine sensitized luminescence spectroscopy was measured for PvuII enzyme with the addition of these metal ions. The data was fit to the sequential two-site equilibria model and binding constants with strong and weak binding affinity were obtained. The two constants obtained for  $Tb^{3+}$  were  $2.3 \pm 1.7$   $\mu$ M (strong site) and  $117 \pm 46$   $\mu$ M (weak site) and for  $Eu^{3+}$  were  $3.3 \pm 2.3$   $\mu$ M (strong site) and  $223 \pm 161$   $\mu$ M (weak site) respectively (Bowen, et al., 2004). This was further confirmed by the direct excitation spectra of the  $Eu^{3+}$  with PvuII where the line shape analysis showed two metal ions binding. In the PvuII mutant E68A it was seen that at high metal concentrations the weak site was occupied. Glutamic acid 68 is thus a ligand for the lanthanide ion at the strong site, and it is not a bridging ligand for the lanthanide metals (Bowen, et al., 2004).

### **1.5.2 DNA binding of PvuII:**

DNA binding domain of the enzyme reaches the major groove and interacts with the histidine triplet (His83, His84, His85), an asparagine doublet (Asn140, Asn141) and Ser81. Gel shift assays with the radiolabeled DNA containing the PvuII recognition site characterize the DNA binding residues as Glu33, Asp34 and Asn 35 (Nastri, et al., 1997). The histidine triplet His83His84His85, which was shown to participate in DNA binding by crystal structures, was analyzed with alanine mutants. Using the different mutants it was shown that the specificity of the DNA binding does not depend on the histidine triplet, the lysine 70, or glutamine 55 residues. The D34G variant of PvuII showed a

nonspecific DNA binding, which shows the importance of the D34 residue for specific binding (Nastri, et al., 1997). Metal dependence on the DNA binding was studied since no DNA binding was seen in the absence of metal ions (Nastri, et al., 1997). Nitrocellulose filter binding and fluorescence anisotropy studies with PvuII showed metal ion dependence on DNA binding. Under metal free conditions the binding of DNA was observed to be 300 nM, and there was higher affinity to the DNA in presence of metals. With  $\text{Ca}^{2+}$ , which supports the DNA binding but not cleavage, a picomolar affinity (53-125 pM) was observed for different oligonucleotides used (Conlan, et al., 2002). An apparent  $\text{Ca}^{2+}$  dissociation constant of  $2.9 \pm 1.9$  mM was obtained with a Hill coefficient of  $3.5 \pm 0.2$  from the DNA binding analysis which indicates two metal ions per subunit of the enzyme (Conlan, et al., 2002). Increased DNA binding of PvuII was seen with other metal ions like  $\text{Eu}^{3+}$ ,  $\text{Tb}^{3+}$ ,  $\text{Ba}^{2+}$ ,  $\text{Sr}^{2+}$ , and  $\text{Cd}^{3+}$  as compared to the metal free conditions (Bowen and Dupureur, 2003).  $\text{Zn}^{2+}$  metal, which has a similar ionic radius to that of  $\text{Mg}^{2+}$  and  $\text{Mn}^{2+}$  (0.9-1.0 Å) ions, does not support the DNA binding any more than the metal free condition (Bowen and Dupureur, 2003). From these studies it is evident that the PvuII-DNA complex formation depends on the ligand preference and electrostatics of the metal ions and not on the ionic sizes. DNA binding studies with the E68A mutant in presence of  $\text{Ca}^{2+}$  ions showed a 400 fold decrease in affinity, which indicates the involvement of the glutamic acid 68 in metal complex formation.

The involvement of  $\text{Mg}^{2+}$  in the DNA binding was difficult to study directly because of the hydrolysis of the DNA. A noncleavable substrate analog with phosphoramidate DNA was used to study the DNA binding in presence of  $\text{Mg}^{2+}$  (King, et al. 2004). The dissociation constant value obtained with  $\text{Mg}^{2+}$  was weaker (10 nM) as

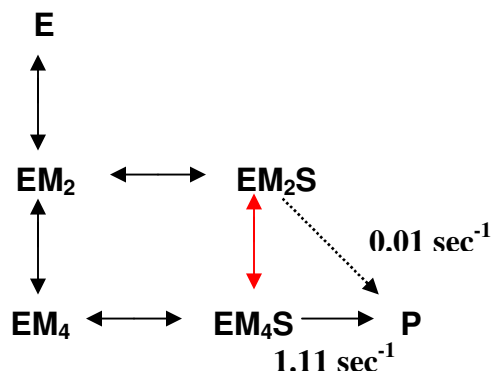
compared to  $\text{Ca}^{2+}$  ( $\approx 200$  pM) (King, et al., 2004). The dissociation rate constant for the metal ions  $\text{Ca}^{2+}$  and  $\text{Mg}^{2+}$  did not vary very much and was assigned to  $10^{-3} \text{ sec}^{-1}$  (Conlan and Dupureur, 2002; Xie and Dupureur, 2009). Based on the dissociation constant ( $K_d$ ), and the dissociation rate constant ( $k_{\text{off}}$ ) values, the association rate constant ( $k_{\text{on}}$ ) values were calculated for the DNA binding of the substrate analog in presence of  $\text{Mg}^{2+}$ . The association rate obtained was 100 fold slower than in the presence of  $\text{Ca}^{2+}$  ions (Xie, et al., 2008). Since this association rate constant obtained is for a substrate analog, another analysis for the association rate constant was done with data for the cleavage kinetics under the steady state conditions using the  $k_{\text{cat}}$  and the  $K_m$  values.  $K_m$  is a function of the substrate association rate constant ( $k_1$ ), the dissociation rate constant ( $k_{-1}$ ), and the catalytic constant ( $k_{\text{cat}}$ ). Since  $k_{\text{cat}}$  and  $k_{-1}$  are known experimentally, the association rate constant ( $k_1$ ) was calculated. The DNA association rate constant derived from this analysis with  $\text{Mg}^{2+}$  ions is  $2 \times 10^5 \text{ M}^{-1} \text{ sec}^{-1}$ . The association rate constant for DNA in presence of  $\text{Mg}^{2+}$  ion from this analysis is also 100 times slower than in the presence of  $\text{Ca}^{2+}$  ( $2 \times 10^7 \text{ M}^{-1} \text{ sec}^{-1}$ ) which compares well to the data obtained for phosphoramidate DNA (Conlan and Dupureur, 2002; Xie, et al., 2008; King, et al., 2004).

### 1.5.3 Hydrolysis activity of PvuII:

DNA binding of the enzyme requires two metal ions. A sigmoidal dependence of cleavage rate as a function of  $\text{Mg}^{2+}$  dependence and the derived Hill coefficients indicates the presence of multiple ions at the cleavage process for EcoRV and PvuII (Groll, et al., 1997; Spyridaki, et al., 2003; Xie, et al., 2008). This sigmoidal dependence does not prove the number of metal ions that participate in the catalytic step; it only indicates the

involvement of multiple classes of metals (Groll, et al., 1997). Hill coefficient also depends on the cooperativity of sites, which is not very well understood for the metal binding of PvuII. From a study with the global analysis, it was suggested that the two metal sites are independent of each other and no cooperativity is seen (Xie and Dupureur, 2009). A two metal ion mechanism is proposed for DNA catalysis of PvuII. There are ambiguities regarding the role of each metal site.

Mutation studies were done on the enzyme PvuII in order to understand the metal ions in the catalytic step. D58A and E68A mutants showed that there was 1000 and 50 fold lower activity, respectively, as compared to the WT PvuII (Dupureur and Conlan, 2000). From the crystal structure it is seen that both these residues ligate  $\text{Ca}^{2+}$  ions, and from the analysis of  $^{25}\text{Mg}$  NMR titration the mutant E68A hinders the  $\text{Mg}^{2+}$  binding (Dupureur and Conlan, 2000; Horton and Cheng, 2000). It is proposed from these analyses that the Glu68 might be the bridging ligand for the metals. Metal ions bound to these active site residues as well as their orientation support efficient catalysis. By global fitting analysis of single turnover cleavage data, it was shown that one metal ion at the PvuII active site can cleave the DNA, as shown in the model **Scheme 1.1**. Two possible models were analyzed; one where catalysis occurs only with the two metal ions at the active site (with interconversion) and another where one/two metals at the active site (without interconversion) can support cleavage (Xie, et al., 2008). The enzymatic model for catalysis of DNA shows that enzyme binds to the metal first and then DNA (Xie, et al., 2008). The global analysis on the single turnover kinetic data shows that the rate of cleavage by one metal species is slower than that of the two metal species (Xie, et al., 2008).



**Scheme 1.1: Kinetic models with and without interconversion step:** Models with single metal species studied earlier in the lab to assess the amount of product formed from a one metal and two metal enzyme species. The red arrow represents the interconversion step where a less active EM<sub>2</sub>S species can bind metals and get converted to a more active EM<sub>4</sub>S species. Dotted line represents the less active EM<sub>2</sub>S species, which do not convert to product if interconverted to EM<sub>4</sub>S. Adapted from (Xie, et al., 2008).

## 1.6 Global Data Analysis:

Global analysis of the data provides more confidence on the analysis. There are many software packages which are available for the global analysis of the kinetic data (Barshop, et al., 1983). Dynafit is a software package for the enzyme kinetic studies which can use the initial concentrations of substrate/inhibitor for the fits. It can also accept an initial guess value for a parameter and adjust the value based on the datafit (Kuzmic, 1996). This adjusted parameter output is represented with the error on that parameter, the model fit and standard deviation of the fit. Kinetic studies provide a time dependent signal and therefore a rate constant can be obtained. Dynafit can fit the large set of data to a set of equations which describe a reaction scheme (Zhang, et al., 2008). The key to this analysis is the availability of multiple sets of data and reasonable knowledge about most steps in the reaction scheme that is analyzed. The major advantage of using software such as Dynafit for the analysis of kinetic data is that this software can use the progress curves to analyze the mechanism instead of using the output from the Michaelis-Menten fit (Zhang, et al., 2008). Kinetic data can be fit to reactions with a simple scheme using linear or exponential derived terms. Analysis of the reactions with multiple steps is complicated (Fierke and Hammes, 1995). The global analysis of the kinetic data minimizes the uncertainty in the analysis of reactions with multiple steps where there are multiple ligands or cofactors or conformational structures.

Analysis using the software has been performed on many enzymes. Serine hydrolase and HIV-proteinase were studied for their inhibition activity and with the progress curves obtained at different inhibitor concentrations, the constants for inhibition were obtained similar to that with other analysis (Kuzmic, et al., 1996; Fersht, 1999). In

the study with HIV-proteinase using the data for poor inhibitors, which did not saturate the active site, could also be analyzed using the program Dynafit (Kuzmic, 1996). We used program Dynafit to analyze the cleavage kinetic data of the enzyme PvuII in presence of mixed metals and in the light all the earlier studies.

### **1.7 Overview of dissertation:**

In the earlier studies mentioned here, number and type of metal ions involved and its characteristics in metal binding to the protein and enzymatic process were explored. In our study we want to understand the contribution of each metal at the active site towards the activity of the enzyme. Mixed metals with varying effects on the activity were used to understand the metal binding to the active site and its contribution to the enzymatic activity. In this study the affinity of different metals at the metal binding sites of the protein was used to form mixed metal complexes. Kinetics of these complexes were observed to understand the catalytic or regulatory role of these metal sites as well as the association and dissociation rate of the metals from these sites.

Chapter II describes the methods used in this study. Details about sample preparation, collection of data, and its analysis are provided in this section.

Chapter III involves enzymatic models from the global analysis of kinetic data. Cleavage kinetics data obtained for PvuII with mixed metals  $\text{Ca}^{2+}$  and  $\text{Mg}^{2+}$  were used for this analysis. Many of the kinetic and thermodynamic constants for the enzymatic reaction steps were characterized earlier. Enzymatic model described in this chapter with the values for the dissociation constants explain the data collected under mixed metal conditions. The model trials show that for PvuII with the proposed two metal ion mechanism in the presence of  $\text{Ca}^{2+}$  and  $\text{Mg}^{2+}$ , there was always an inhibition of activity



seen with increasing  $\text{Ca}^{2+}$  concentration unlike EcoRV and EndonucleaseV. The model analysis also shows the mixed metal complexes formed in these conditions do contribute to product formation.

Chapter IV shows a study of metal exchange reactions on PvuII. Lanthanide spectroscopy was used to compare and characterize the association and dissociation rate of metals to the active site of PvuII. One metal site was specifically filled with a lanthanide and competition of the lanthanide with other metal ions was observed. The datasets for this competition was analyzed to understand relative association and dissociation rate for different metals.

## CHAPTER II

### MATERIALS AND METHODS.

#### 2.1 Enzyme Preparation:

PvuII is cloned into the pBBE vector with a pTac promoter and ampicillin resistance (Balendiran, et al., 1994). The gene is transformed into *E.coli* strain PR1206, which has a methyltransferase gene that provides protection of DNA from PvuII expression. The strain has kanamycin and chloramphenicol resistance (Jack, et al., 1991; Balendiran, et al., 1994).

Competent cells of pR1206 *E. coli* strain were prepared using the calcium chloride chemical treatment method. 2 mL seed culture was used to inoculate 50 mL LB (Lurea Broth, Sigma) media without any drug. Cells were grown until the culture gave an absorbance of 0.4 at 595 nm. The pellet was treated with 0.1 M CaCl<sub>2</sub> to make the cells competent. 200 µL of the competent cells was used to transform the plasmid pBBE-PvuII. Approximately 1 µL of the plasmid DNA was added to the 200 µL aliquot of competent cells and allowed to sit on ice for 30 minutes. This mixture is then treated with heat shock at 42 °C for 45 seconds in order to perform the transformation. LB media was added and cells were grown for 2 hours. The cell suspension was then plated on LB-agar plates with ampicillin (Sigma) concentration 150 µg/ µL to select the cells with PvuII gene.

Minimal 9 media was used to express the protein. 10 litre cultures were grown with M9 media (22 mM potassium phosphate monobasic, 46 mM sodium phosphate dibasic, 8.6 mM sodium chloride and 18.6 mM ammonium chloride). Also media supplements, 40 mg/mL CAS amino acids (Difco), 10 mg/mL biotin, 10 mg/mL uracil, 50 mg/mL thiamine, 40 mg/mL methionine and 40 mg/mL tyrosine, 1 mM CaCl<sub>2</sub>, 2 mM

MgSO<sub>4</sub>, and 0.5 % glucose were added to enrich the media. All the cells were grown with continuous shaking at 37 °C with 30 mg/mL ampicillin. When the OD<sub>595</sub> reached 0.6-0.8, expression was induced with 100 μM isopropyl thio-β-d-galactoside (Anatrace). Cells were grown for 4 hours after induction, and harvested cells were stored at -20 °C until further use.

Pelleted cells were then resuspended in resuspension buffer (50 mM potassium phosphate monobasic, β-mercaptoethanol, 1 mM EDTA, pH 7.4) and lysed with a French press treatment to break open the cells. The solution was subjected to centrifugation in order to separate the cell debris and insoluble protein from the soluble nucleic acid-protein mixture. The supernatant from the French press was treated with streptomycin sulfate (0.05 % w/v) (Sigma) to precipitate nucleic acids. The supernatant after streptomycin treatment was then treated with 45 % w/v ammonium sulfate (Sigma) to precipitate proteins. Precipitated protein was dissolved in a desired volume and dialyzed versus buffer (30 mM potassium phosphate dibasic, 50 mM potassium chloride and 1mM EDTA, pH 7.4). Cellulose phosphate was first precycled as mentioned by the manufacturer, and the column was equilibrated using the same buffer as the protein dialysis buffer. A cation exchange column of Cellulose phosphate (Sigma) was poured into an Econo column (Bio-Rad). Protein solution was loaded on the column and eluted with a gradient (0.5 mM to 0.8 mM potassium chloride) using Akta purifier (Amersham Pharmacia Biotech). Fractions were analyzed for purity using SDS- PAGE analysis. Fractions with PvuII that were relatively pure were pooled together and dialyzed in dialysis buffer and subjected to another ion exchange purification using a heparin column. Heparin sepharose (Amersham Biosciences) was poured on an Econo column

and equilibrated with dialysis buffer. Protein was eluted off the column with the same salt gradient. SDS-PAGE analysis identified the purified fractions which were lyophilized and stored until further use. An image of elution profile obtained using an ion exchange column (heparin resin) and an SDS page gel for the eluted fractions are shown in **Figure 2.1**.

Purified enzyme was quantitated by a UV-Vis spectrophotometer (Hewlett Packard 8453) using the extinction coefficient  $\epsilon_{280} = 36900 \text{ cm}^{-1} \text{ M}^{-1}$  (Pace, et al., 1995) for a single subunit. Enzyme samples for the assays were prepared by dialysis of the enzyme in the required buffer using Slide-A-lyzers (Pierce). The buffer used for assay was made metal free by passing the buffer through a Chelex column (Sigma).

## **2.2 Preparation of substrates:**

14mer oligonucleotides with the recognition site for PvuII used for the assay are Sq3121-1 (5'-CAGGCAGCTGCGGA-3') and Sq3121-2 (5'-TCCGCAGCTGCCTG-3'), with the PvuII recognition site in the middle (bolded). Synthesized oligos were purchased from IDT technologies and purified with PAGE and extracted using Elutrap (Schleicher and Schuell). Double stranded DNA was prepared by annealing the two strands together. Both the strands were mixed in a 1:1 ratio, heated to 100 °C, and slowly cooled to room temperature in order to form the duplex. The duplex formed is quantitated by UV- absorbance at 260 nm applying Beer's law with the extinction coefficient calculated as  $6600 \text{ M}^{-1} \text{ cm}^{-1} \text{ nucleotide}^{-1}$ . Radiolabelled substrates were prepared with the duplexed oligonucleotides by end labeling it using T4 polynucleotide kinase (New England Biolabs) and  $^{32}\text{P}$ - $\gamma$ ATP (Perkin Elmer). The radiolabelled duplex was purified using G-50 sephadex resin (Sigma) and eluted in water.

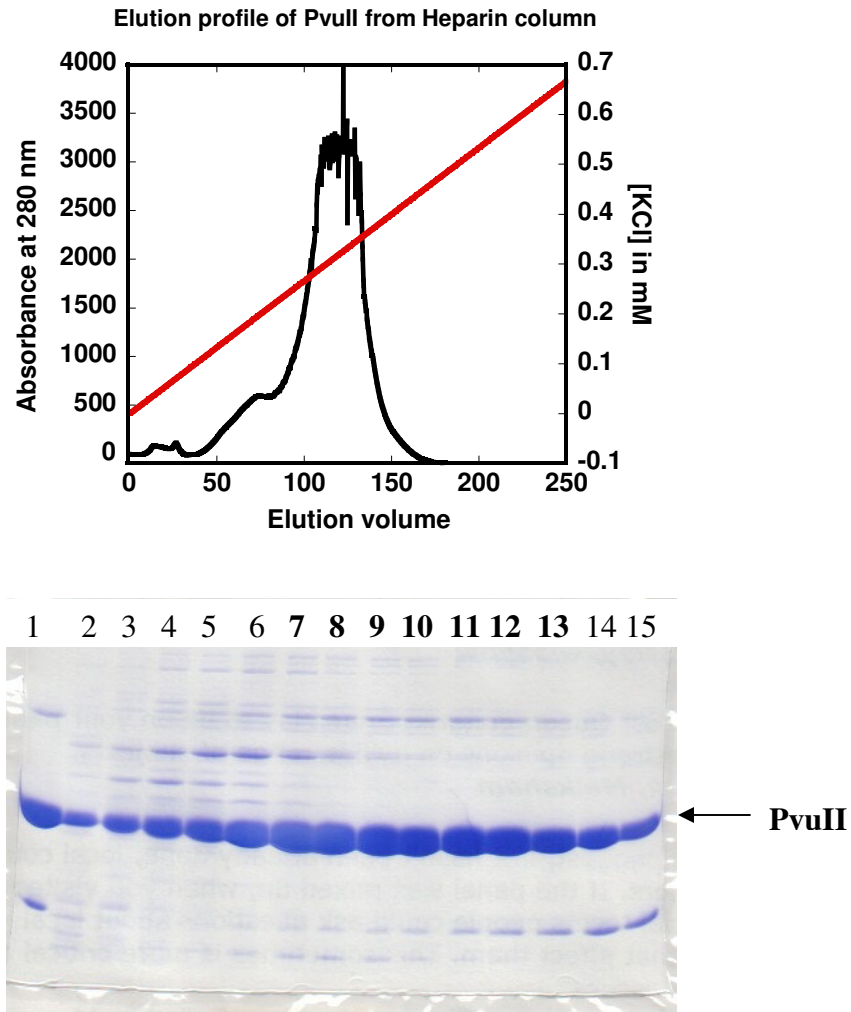


**Figure 2.1:** An elution profile and SDS-PAGE gel from PvuII purification using heparin column. Linear salt gradient was used to elute the bound protein from column as shown in curve with the percentage of high salt solution. Absorbance at 280 nm shows the presence of protein at different fractions. SDS gel image shows the amount of protein present in each fraction and its purity. Lane 1 is the marker for PvuII where a dominant band of PvuII is seen as shown by arrow. Lane 7-13 are the fractions that were pooled together as the purest fraction of PvuII.

**Metal salt stocks:**

Puratronic  $\text{MgCl}_2$ ,  $\text{CaCl}_2$  and  $\text{MnCl}_2$  used to prepare metal stock solutions were purchased from (Alfa Aesar) and quantitated with flame absorption spectroscopy with a double beam atomic absorption spectrometer model GBC904BT (GBC Scientific). Standard solutions were purchased from Fisher (Pittsburgh, PA) and diluted in 5% nitric acid. For DNA cleavage kinetic experiments, metal solutions were adjusted to pH 7.5 in a buffer with Tris and NaCl.

Lanthanides were quantitated using colorimetric titrations. Arsenazo III dye was used to detect the EDTA titration. Stocks of lanthanide ions  $\text{Tb}^{3+}$  and  $\text{Eu}^{3+}$  were prepared in MQ water. Unknown lanthanide solutions were diluted to approximately 10 mM concentration; 250  $\mu\text{L}$  of this diluted solution was added to 2.5 mL of 100 mM ammonium acetate ( $\text{CH}_3\text{COONH}_4$ ) buffer pH 7.2 and 5  $\mu\text{L}$  of 4mg/mL Arsenazo dye. Lanthanide solutions were titrated using 10 mM standard EDTA solution (Mallinckrodt). Arsenazo dye gives a pink color in the absence of lanthanides, whereas in the presence of lanthanides the solution is blue. With the addition of increasing concentrations of EDTA, a color change of Arsenazo dye is seen from blue to pink. The concentration of the unknown lanthanide solution was then determined using equation,

$$[\text{Ln}^{3+}] = [\text{EDTA}][\text{volume of EDTA}] / [\text{volume of Ln}^{3+}]$$

where volume of  $\text{Ln}^{3+}$  used is 250  $\mu\text{L}$ , the concentration of EDTA used is 10 mM and the volume of EDTA is measured from the titration. Samples were titrated with 10 mM EDTA solution and a color change of blue to pink was observed at the end point.

**Cleavage kinetics:**

Single turnover experiments were performed with 2  $\mu\text{M}$  enzyme and 300 nM DNA duplex. Reactions were done with a mixture of  $\text{Mg}^{2+}$  and  $\text{Ca}^{2+}$ . The reaction buffer has 50 mM Tris, NaCl adjusted to a constant ionic strength and the desired amount of  $\text{Ca}^{2+}$  and  $\text{Mg}^{2+}$ . Buffer pH was adjusted at 7.5 at 37 °C. Ionic strength was fixed to a constant at 100 mM NaCl at 10 mM  $\text{MgCl}_2$ . The DNA used was radiolabelled with  $^{32}\text{P}$  gamma ATP and for the reaction conditions; a small amount of radiolabelled DNA was added to the cold DNA in order to observe the reaction. Reactions were quenched with stop dye (100mM EDTA and 10% glycerol). Samples were loaded on a 20% PAGE gel with 8 M urea and run for 4 hours at 1500 V in TBE buffer (Tris-Boric acid- EDTA). The gel was scanned using the Storm Phosphoimager and image quantitated using ImageQuant software. Single turnover rates at each condition were obtained by fitting the cleavage product obtained to a first order single exponential equation ( $y = 1 - e^{-kt}$ ) using Kaleidagraph (Synergy). A gel image and the corresponding progress curve for the rate are shown in **Figure 2.2**.

**Quench Flow:**

The technique is used to monitor fast reaction kinetics of millisecond timescale. Biologic SFM4/Q quench flow model has four syringe ports and can process two mixing events. For the quench flow reactions at higher  $\text{MgCl}_2$  (5-15 mM) conditions, port 1 was filled with DNA (600 nM), metal, and buffer and port 2 with enzyme (4  $\mu\text{M}$ ), metal, and buffer. At the delay lines solutions were mixed 1:1 so that the enzyme concentration is 2  $\mu\text{M}$  and DNA 300 nM, respectively. Reaction was quenched with 100 mM EDTA filled at port 4. A scheme for the quench flow module is shown in **Figure 2.3**, from the

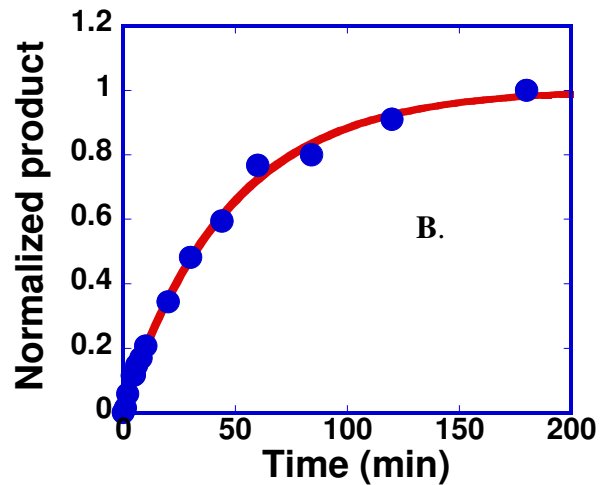
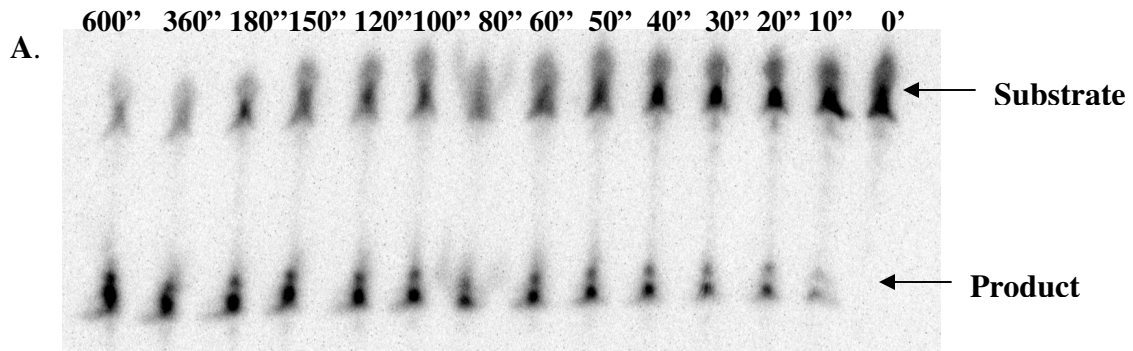
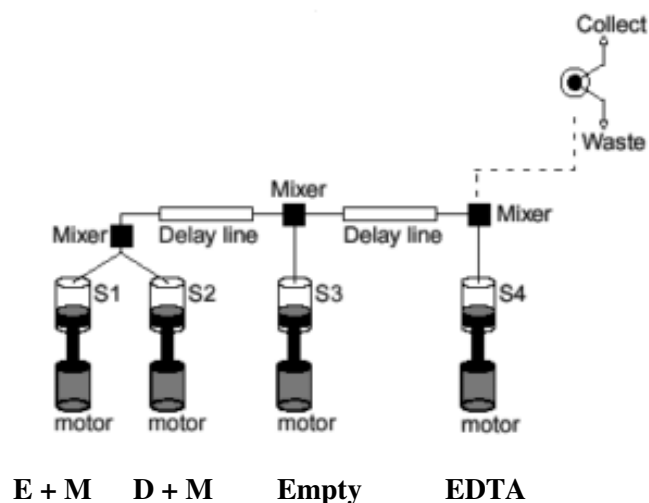


**Figure 2.2: Cleavage kinetics polyacrylamide- urea gel and the corresponding progress curve.** Cleavage kinetics reactions performed at different metal concentrations were quenched with EDTA and run on polyacrylamide-urea gel. A) Substrate DNA labeled with  $^{32}\text{P}$ - $\gamma$ ATP runs slowly and is seen on the top of the gel, whereas the cleavage product formed runs faster and is seen at the bottom. B) Amount of product formed quantitated to obtain the progress of the reaction and this curve is fitted to the first order rate equation,  $y= 1-e^{-kt}$  to obtain the rate of the reaction.





[www.biologic.info/rapid\\_kinetics](http://www.biologic.info/rapid_kinetics).

**Figure 2.3: Quench flow Module for SFM 400:** This figure shows the design for the quench flow module; it is adapted from the manual of Bio logic Science Instruments. Here it is seen that there are four ports (S1, S2, S3 and S4), two delay lines, and three mixers. There is an outlet which is connected to the waste or the collector. We fill S1 with enzyme and metal (E + M), S2 with DNA and metal (D + M), and S4 with EDTA. Reaction is quenched at the third mixer and initiated at the first one. 1:1 ratio of Enzyme:DNA is mixed together at mixer 1. The machine can be programmed so that the desired volume would be pushed in the mixer from the syringes. Delay line 1 used here is 90  $\mu\text{L}$  and delay line 2 is 40  $\mu\text{L}$ . The calculated aging time from the delay lines used is 260 ms.

Biologic website for SFM 400. Two runs were done at each required time points so that we flush the delay lines first and then collect the samples. The equipment has different delay line modules, which can be used to obtain the volume of interest. MPS program software was used to monitor the injection volume and flowing rates. The delay lines used for the experiments are a combination of 90  $\mu\text{L}$  and 40  $\mu\text{L}$  and the flow rate for the solutions is 0.5 mL/s. Reaction time is calculated from the amount of time specified for the interrupt phase plus the aging time. Aging time calculated in this set of delay lines is 260 ms.

### **Fluorescence spectroscopy:**

A Fluorolog 3 spectrofluorimeter (Horiba Jobin Yvon) was used to perform the experiments. A nitric acid cleaned quartz cuvette (NSG scientific) was used and 25  $^{\circ}\text{C}$  temperature was maintained during the experiments using an external water bath.

### **Luminescence of lanthanide ions:**

Enzyme bound lanthanide ion was excited by indirect excitation using the tyrosine residues that are close to the active site of the enzyme. Energy transfer from the direct excitation of the tyrosine residues allows monitoring of the binding of the lanthanide ions. Binding of lanthanide ions to the enzyme was performed at 5 mM HEPES pH 7.0 at 25  $^{\circ}\text{C}$  and 400 mM NaCl. Experimental conditions used were to avoid the interference of buffer. Conditions used also have the optimum solubility of the enzyme in presence of lanthanide metals (Bowen, et al., 2004).

Tyrosine residues of the enzyme were excited at 274 nm, and emission spectra were recorded from 450 to 650 nm for  $\text{Tb}^{3+}$ . An intensity maximum at 543 nm was obtained in case of  $\text{Tb}^{3+}$  which represents the enzyme bound metal (Bowen, et al., 2004).

All experiments were performed with constant stirring, and spectra were collected at 1 nm increment with an integration time of 1 second. An emission cutoff filter (Andover Corp.) at 450 nm was used to prevent Rayleigh scattering, which is the scatter of light from the excitation source. This scatter occurs at twice the excitation wavelength and this is a second order component of the excitation source light (Lakowicz, 1983). This scattered light interferes with the emission signal (Bowen, et al., 2004). Time dependent and competition experiments were performed using different metal ions  $\text{Ca}^{2+}$ ,  $\text{Mg}^{2+}$ , and  $\text{Mn}^{2+}$  independently, and changes in the intensity due to the bound lanthanide ion was monitored. A control experiment was run with the lanthanide ions in buffer to correct for the background signal from the unbound lanthanide ions. The observed change in intensity with time was analyzed further to obtain details about the metal exchange process.

## **CHAPTER III**

### **GLOBAL KINETIC ANALYSIS FOR MIXED METAL COMPLEXES OF PvuII.**

#### **Introduction:**

Most of the deoxyribonucleic acid cleaving enzymes require divalent metal ions for their activity (Etzkorn and Horton, 2004). Restriction enzymes are well studied enzymes for the mechanism of catalysis. It is proposed that restriction enzymes with similar active site motifs will have similar mechanisms for catalysis, but this is subject to debate (Pingoud and Jeltsch, 2001; Dupureur, 2008). Crystallographic studies of RNaseH, integrases, 3'-5' exonuclease of Klenow fragment, restriction enzymes, etc., have shown two metal ions at the active site (Steitz and Steitz, 1993; Horton and Perona 2004; Nowotny, et al., 2005; Diamond and Bushman, 2006), which implicates a two metal ion mechanism for the enzymes. In light of the important structural data on these enzymes, the question about the number of metal ions needed for phosphodiester hydrolysis is yet to be answered. Also there are questions about the role of each metal ion in the process of catalysis: Do both metal ions have an equal role in the catalysis reaction, or does one metal ion have an electrostatic role? In a study based on analysis using molecular dynamics of transition state stabilization, it was proposed that the BamHI enzyme requires a single ion at the catalysis step even though it has two metals at its active site. The second metal ion is proposed to have a regulatory function (Mones, et al., 2007). This regulatory function of the second metal ion at site B is also proposed for Endonuclease V (Feng, et al., 2006).

There are a number of solution approaches for testing two metal ion mechanisms that involve metal ion substitution. Metal rescue studies done on *Tetrahymena* group I ribozyme, HIV-1 integrase, *Escherichia coli* DNA polymerase I, and isocitrate dehydrogenase map their metal binding sites (Shan, et al., 2001; Diamond and Bushman, 2006; Soundar, et al., 2006). In these studies, the probable metal binding residues are substituted by cysteines that bind  $Mn^{2+}$  ions. The effect of  $Mn^{2+}$  binding on the activity of the enzyme indicates the location of metal ion binding sites (Diamond and Bushman, 2006). When metal ion binding sites are very similar and also very close to each other, it becomes difficult to interpret these results.

Another approach used to test two metal ions mechanisms is to work with mixed metals. Enzymes are assayed in presence of two metal ions which have differing abilities to support enzymatic activity. Studies of mixed metal experiments on EcoRV, Endonuclease V, and apurinic/aprimidinic endonucleases (Vipond, et al., 1995; Beernink, et al., 2001; Feng, et al., 2006) provide information about number of metal ions involved in the reaction. In these studies, an increase in the  $Mg^{2+}$  dependent activity of the enzyme with the addition of a catalytically inactive metal like  $Ca^{2+}$  shows evidence for a mechanism involving more than one metal ion. EcoRV and EcoRI enzymes were studied with cognate and noncognate sequences. In this study it was seen that for noncognate complexes under mixed metal conditions using  $Mn^{2+}/Mg^{2+}$  and  $Ca^{2+}$ , there was stimulation of EcoRV activity at low  $Ca^{2+}$  concentration and inhibition at high  $Ca^{2+}$  concentration. This biphasic behavior was seen only for EcoRV and not for the EcoRI enzyme (Vipond, et al., 1995). Results are consistent with a one metal ion mechanism for the cleavage process of EcoRI and a two metal ion mechanism for EcoRV (Vipond, et

al., 1995). Another study with EndonucleaseV also showed the biphasic behavior of cleavage activity with increasing concentrations of  $Mn^{2+}$  in the presence of  $Mg^{2+}$  (Feng, et al., 2006). This process was described as a two metal ion mechanism for the EndonucleaseV cleavage activity where one site is catalytic and the other regulatory (**Figure 3.1**) (Feng, et al., 2006). The catalytic metal binding site must be occupied with a catalytically active metal in order for the hydrolysis to occur.

### **Regulatory role of metal ions:**

In prokaryotes, metal ion homeostasis is regulated by proteins that maintain the cellular needs and restrict the excess of metals in all cells (Pennella and Giedroc, 2005). Regulatory proteins that are specific metal sensor proteins maintain metal ion homeostasis, and they discriminate between identical ligands very well (Pennella and Giedroc, 2005). This phenomenon leads to speculation that mixed metal species may exist in the cell as a means of regulating metallo nuclease activity.  $Ca^{2+}$  ions studied in the DNA cleaving enzymes are known to assist DNA binding but inhibit catalysis, except in staphylococcal nuclease where  $Ca^{2+}$  ions are required for catalysis (Cuatrecasas, et al., 1967). Since both  $Ca^{2+}$  and  $Mg^{2+}$  ions have the same octahedral geometry but one inhibits and the other favors catalysis in some metallo nucleases, it would appear that there are other factors which govern the metal ion selectivity in restriction enzymes (Kostrewa and Winkler, 1995; Viadiu and Aggarwal, 1998; Horton and Perona, 2004).

In this study we are examining the behavior of mixed metal complexes using PvuII endonuclease as the model system. Our goal is to test the possibility that metal B has a regulatory role. It is proposed that PvuII has a two metal ion mechanism as

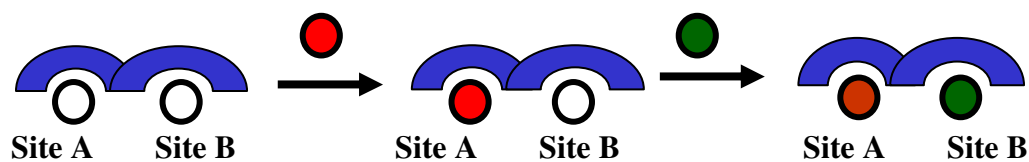


**Figure 3.1: Two metal ion model of Endonuclease V:** Two metal sites are shown in this model. Metal binding at the catalytic site A will lead to the DNA cleavage reaction. Depending on which metal binds at this site B, stimulation or inhibition of the activity is observed. In this model, a catalytically active metal has to bind at site A, the catalytic site, in order for the DNA cleavage to occur. Adapted from (Feng, et al., 2006).

discussed in Chapter 1. The active site residues Asp58 and Glu68 ligate two metal ions (Pingoud, et al., 2005), so in order to form the mixed metal complexes we have to choose the metal ions carefully because metals have to occupy sites A and B.

It was previously seen that smaller ions like  $Mn^{2+}$ ,  $Mg^{2+}$  and  $Co^{2+}$  support cleavage of the DNA, whereas larger ions like  $Ca^{2+}$ ,  $Tb^{3+}$ , and  $Eu^{3+}$  do not (Bowen and Dupureur, 2003). These studies help determine the combinations of metal ions that can be used for the mixed metal complex formation. In this study we chose to do reaction kinetics in presence of  $Ca^{2+}$  and  $Mg^{2+}$  and analyze the data to model the mixed metal complex formation. Single turnover kinetic data was fit to different models by global analysis, which can provide information about the role of each species in the reaction mixture (Xie, et al., 2008). Comparing the data fits to different model schemes, we discuss the behavior of mixed metal species formed in presence of  $Ca^{2+}$  and  $Mg^{2+}$ .

### **Methods:**

The enzyme was prepared and kinetics performed as described in Chapter 2. 20 different  $Mg^{2+}/Ca^{2+}$  concentrations with 28 progress curves and 379 points were used in the global analysis.

### **Dynafit Program:**

The experimental rates obtained were analyzed for the best fit to a mechanism. Models for the mechanism were written and run using Dynafit, a program that performs nonlinear least square regression. Mechanisms are written symbolically either for initial velocities, progress of an enzyme reaction, analysis of binding curves or analysis of inhibition data. Numerical and graphical tests are applied to test the data in the program (Kuzmic, 1996). We express the processes of the mechanism in the form of chemical



equations. Data used is the amount of product formed with time at all experimental conditions. The program uses differential equations to calculate the amount of product formed over time using the set of equations and the parameters provided. Different runs for the global fits of the data provide the standard deviation and percentage error, which defines the best fit (Zhang, et al., 2008). Data and parameters are expressed in units so that the number is close to unity. In our case for all the fits and simulations used here, values are expressed in micromolar units.

A representation of the script is shown in **Figure 3.2**, where data is provided as a text file. There are three windows during the run of the program: a graphic window, text window and status window. A snapshot of a Dynafit run is shown in **Figure 3.3**. The results were saved in a folder that contains information on the fitted curves, the errors on the parameters floated, and the standard deviation values.

### **Results:**

In order to determine the role of each metal site (catalytic and regulatory), we studied mixed metal single turnover kinetics on enzyme PvuII. Cleavage kinetics of the enzyme at different  $\text{Mg}^{2+}$  and  $\text{Ca}^{2+}$  concentrations were measured using a gel cleavage assay as described in Chapter 2. Kinetic rate profiles from the experiments are shown in **Figure 3.4**. Two types of datasets are shown: rate of product formed at a fixed  $\text{Mg}^{2+}$  and varying  $\text{Ca}^{2+}$  concentrations and the rate of product formed at fixed  $\text{Ca}^{2+}$  and varying  $\text{Mg}^{2+}$  concentration. As shown in **Figure 3.4**, cleavage rate constants decrease as  $\text{Ca}^{2+}$  concentration is increased. The simplest explanation for this decrease is that, in presence of both active metal  $\text{Mg}^{2+}$  and the inactive metal  $\text{Ca}^{2+}$ , the enzyme is distributed to form the active  $\text{EM}_2$  and  $\text{EM}_4$  species and the inactive  $\text{EC}_2$  and  $\text{EC}_4$  species.  $\text{EM}_2$  and  $\text{EC}_2$

**[task]**

task = fit

data = progress

**[mechanism]**

$E + M + M \xrightleftharpoons{k_1} EM_2$  : k1 k-1

$EM_2 + M + M \xrightleftharpoons{k_2} EM_4$  : k2 k-2

$EM_2 + S \xrightleftharpoons{k_3} EM_2S$  : k3 k-3

$EM_4 + S \xrightleftharpoons{k_4} EM_4S$  : k4 k-4

$EM_2S \xrightarrow{k_5} EM_2 + P$  :k5

$EM_4S \xrightarrow{k_6} EM_4 + P$  :k6

**[constants]**

k1 = 1e-4 ?

k-1 = 1000

k2 = 2.01e-4

k-2 = 1000

k3 = 0.1

k-3 = 0.001

k4 = 0.19

k-4 = 0.001

k5 = 0.02 ?

k6 = 1.12

**[responses]**

P = 1

**[Progress]**

directory ./examples/charu/cp80618/data

extension txt

delay 2

**[Data]**

file fx70103(5) | concentration E = 2, M = 5000, S = 0.3, C = 0

file fx70103(10) | concentration E = 2, M = 10000, S = 0.3, C = 0

**[output]**

directory ./examples/charu/CP81103/Cp81103f

**Figure 3.2: Script for a cleavage model written for Dynafit run.**

**Note:** Parameters k1 and k5 were floated in this model; it is represented as the question mark in front of the parameter that is detected by the program. Numbers from the fit for these parameters, the model fit to the experimental data, error on each parameter, and the standard deviation for the fit are all obtained from the output file.

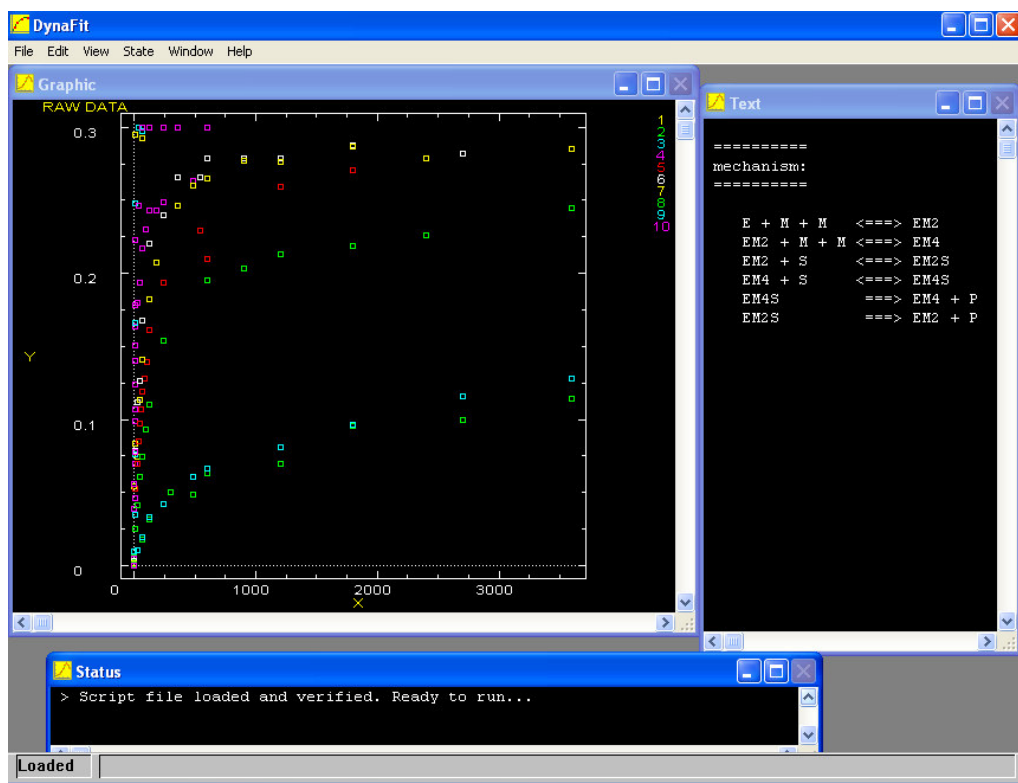


**Figure 3.3:** A snapshot during the program run of Dynafit. There are three windows where we can observe the status of the fit. The graphic window here shows the data set provided for the fit, and the text window shows the model used. The status window defines the run status of the program. In this snapshot, the models and the datasets are uploaded and the program is ready to run the fit trial.

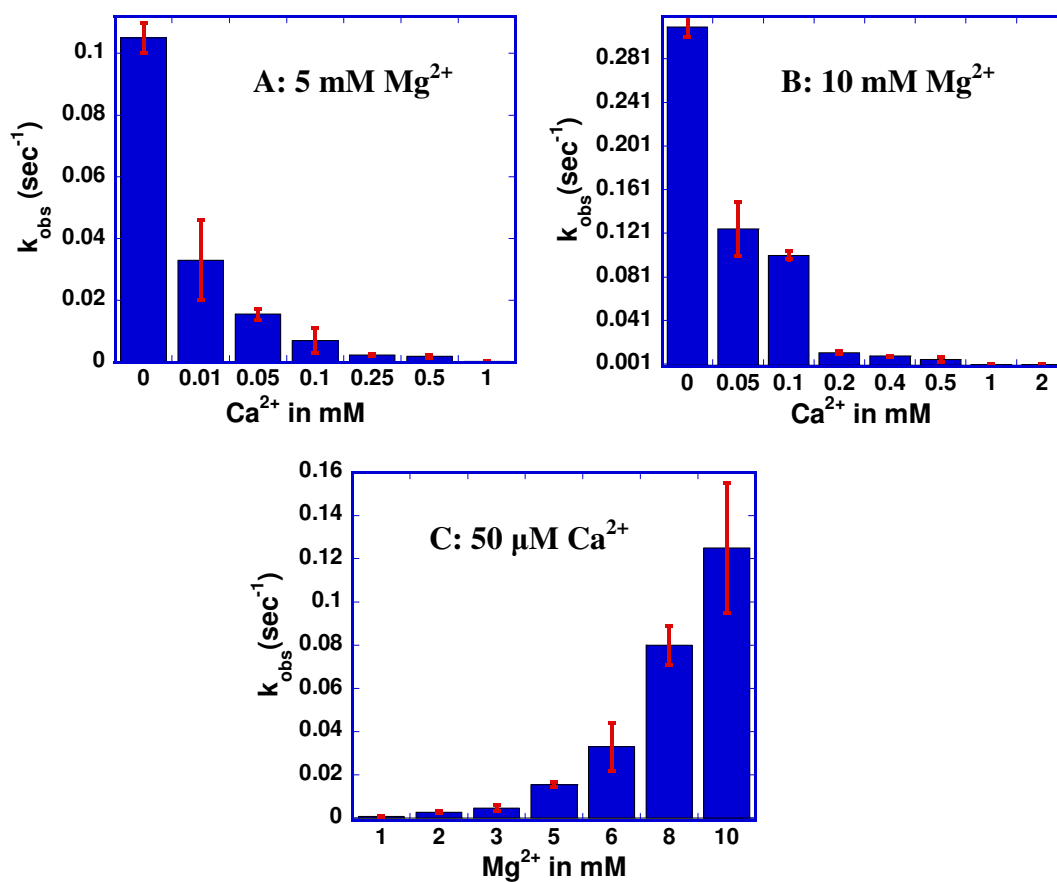
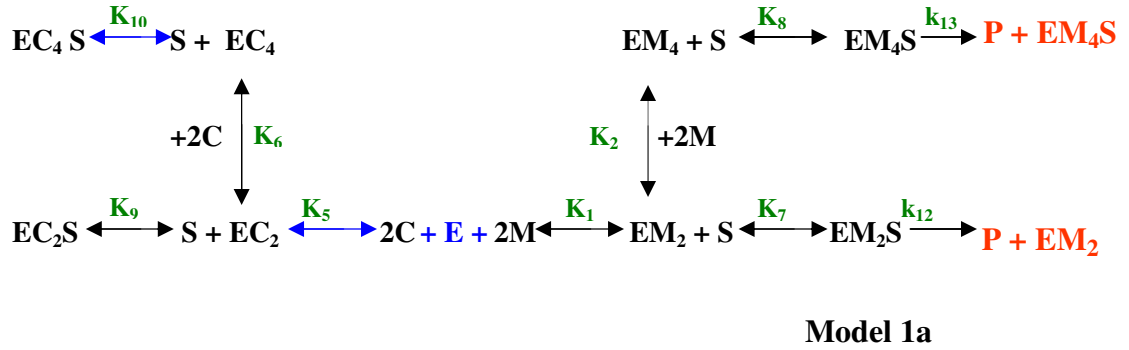


**Figure 3.4: Plot of experimental  $k_{\text{obs}}(\text{sec}^{-1})$  at varying  $\text{Mg}^{2+}$  and  $\text{Ca}^{2+}$  concentrations:** Reaction at A: 5 mM  $\text{Mg}^{2+}$  and B: 10 mM  $\text{Mg}^{2+}$  with 2  $\mu\text{M}$  PvuII dimers, 300 nM 14 mer cognate DNA duplex and varying  $\text{Ca}^{2+}$  concentrations. C: Reaction at 50  $\mu\text{M}$   $\text{Ca}^{2+}$  with 2  $\mu\text{M}$  PvuII dimers, 300 nM 14 mer cognate DNA duplex and varying  $\text{Mg}^{2+}$  concentrations. All the reactions were done at 37  $^{\circ}\text{C}$  in 50 mM Tris pH 7.5 and at a constant ionic strength of 130 mM using NaCl. We see a decrease in the rate of product formation in the presence of  $\text{Ca}^{2+}$ .

represent species with one metal at each monomer unit of the enzyme; EM<sub>4</sub> and EC<sub>4</sub> shows two metals at each monomer unit. These metal species can bind the substrate DNA which is represented here as 'S' and form species EM<sub>2</sub>S, EM<sub>4</sub>S, EC<sub>2</sub>S, and EC<sub>4</sub>S. In our analysis, experimental cleavage kinetics data with mixed metals were fitted to enzymatic models where enzyme PvuII is partitioned between Mg<sup>2+</sup> and Ca<sup>2+</sup> ions to form the active (EM<sub>2</sub>S and EM<sub>4</sub>S), inactive (EC<sub>2</sub>S and EC<sub>4</sub>S) species, and the mixed species (EM<sub>2</sub>C<sub>2</sub>S and EC<sub>2</sub>M<sub>2</sub>S). The single metal species and the parameters which are characterized from the earlier work are shown in **Scheme 3.1** and **Table 3.1**. The parameters for the mixed metal species are also listed in **Table 3.1**, which will be explained in the later sections of this chapter.

The DNA binding parameters are in the nanomolar to picomolar range, whereas the metal binding parameters have millimolar to micromolar constants. Association rates were calculated from the experimental equilibrium constants using dissociation rate constant values. Dissociation rate constant values for metal binding step used was 1000 sec<sup>-1</sup> from earlier studies done on enzymes such as enolase, phospholipase A2 and troponin C (Andersson, et al., 1981; Forsen, et al., 1983; Drakenberg, et al., 1984; Lee and Nowak, 1992; Xie, et al., 2008). The DNA binding association and dissociation rates were measured by fluorescence anisotropy and DNA trap experiments, respectively (Conlan and Dupureur, 2002). The association rate of DNA binding with Mg<sup>2+</sup> ions was obtained using steady state cleavage data (Xie and Dupureur, 2009). For the mixed metal species, we made some educated estimates for initial parameter values based on the values for the single metal species. These numbers were floated in the model fits in order to get the parameter values from the fit. Various trials were attempted to get a best fit



**Scheme 3.1: Model 1a, mixed species not formed:** E: homodimeric enzyme, S: Cognate 14mer DNA duplex, M= Mg<sup>2+</sup> ion, C= Ca<sup>2+</sup> ion. The equilibrium step is represented by double arrow, and the cleavage step is represented by single arrow. The equilibrium constants and the kinetic parameters are numbered and represented here in green. The cleavage products are shown in red. The arrows in blue indicate parameters which were varied in the trials.

**Table 3.1: List of parameters used in the models and their sources.**

Parameters	Values used	Source for the parameter values
k <sub>1</sub>	4.72 x 10 <sup>-5</sup> μM <sup>-2</sup> sec <sup>-1</sup>	K <sub>d</sub> = 4.6 mM (Xie, et al., 2008)
k <sub>2</sub>	1 x 10 <sup>-4</sup> μM <sup>-2</sup> sec <sup>-1</sup>	K <sub>d</sub> = 3.16 mM (Xie, et al., 2008)
k <sub>3</sub>	0.0137 μM <sup>-2</sup> sec <sup>-1</sup>	From the earlier fits for EM <sub>2</sub> C <sub>2</sub> K <sub>d</sub> = 270 μM
k <sub>4</sub>	1 x 10 <sup>-4</sup> μM <sup>-2</sup> sec <sup>-1</sup>	Assumed to be the same as k <sub>2</sub> for EC <sub>2</sub> M <sub>2</sub> K <sub>d</sub> = 3.16 mM
k <sub>5</sub>	0.069 μM <sup>-2</sup> sec <sup>-1</sup>	Calcium binding constant K <sub>d</sub> = 120 μM (Jose, et al., 1999), the value is floated
k <sub>6</sub>	2.5 x 10 <sup>-4</sup> μM <sup>-2</sup> sec <sup>-1</sup>	Calcium binding constant K <sub>d</sub> = 2 mM (Jose, et al., 1999)
k <sub>7</sub>	0.037 μM <sup>-1</sup> sec <sup>-1</sup>	K <sub>d</sub> = 27 nM (Xie, et al., 2008)
k <sub>8</sub>	0.19 μM <sup>-1</sup> sec <sup>-1</sup>	K <sub>d</sub> = 5 nM (Xie, et al., 2008)
k <sub>9</sub>	0.1 μM <sup>-1</sup> sec <sup>-1</sup>	10 nM, averaged from (Bowen and Dupureur, 2003)
k <sub>10</sub>	20 μM <sup>-1</sup> sec <sup>-1</sup>	56 pM averaged from (Bowen and Dupureur, 2003) This value is floated
k <sub>11</sub>	3 μM <sup>-1</sup> sec <sup>-1</sup>	0.33 nM as the initial guess equilibrium constant value The values obtained from the fit was 94 pM
k <sub>15</sub>	1 μM <sup>-1</sup> sec <sup>-1</sup>	1 nM as the initial guess equilibrium constant value The value obtained from the fit was 3 nM
k <sub>12</sub>	0.01 sec <sup>-1</sup>	(Xie, et al., 2008)
k <sub>13</sub>	1.11 sec <sup>-1</sup>	(Xie, et al., 2008)
k <sub>14</sub>	0.01 sec <sup>-1</sup>	0.08 sec <sup>-1</sup> value obtained from the fit.
k <sub>16</sub>	0.001sec <sup>-1</sup>	0.008 sec <sup>-1</sup> value obtained from the fit.

The dissociation constant rate used for metal binding step was 1000 sec<sup>-1</sup> (Xie, et al., 2008) and the dissociation constant rate used for the DNA binding step was 0.001 sec<sup>-1</sup> (Conlan and Dupureur, 2002). The dissociation constants for metal binding is expressed in mM units and the second order reaction was accounted for in the association rate constant.

parameter value. Some of these parameters had no effect on the model fits, and others could be varied only to a certain range. These trials are explained in detail in the Appendix section.

**Model 1a: No mixed species formed:**

**Scheme 3.1** features the kinetic model 1a without the mixed metal species for the enzymatic reaction of PvuII in presence of  $\text{Ca}^{2+}$  and  $\text{Mg}^{2+}$ . Model 1a is based on the assumption that under the experimental conditions, there is a distribution of the enzyme and substrate to form both active ( $\text{EM}_2\text{S}$  and  $\text{EM}_4\text{S}$ ) and inactive species ( $\text{EC}_2\text{S}$  and  $\text{EC}_4\text{S}$ ). The decrease in the rate of the product formed is associated with the amount of inactive species formed in this model. This model was run using the data sets obtained from the mixed metal cleavage kinetics at different  $\text{Mg}^{2+}$  and  $\text{Ca}^{2+}$  concentrations as documented in **Figure 3.4**. The association rate constant for the formation of  $\text{EC}_2$  complex ( $k_5$ ) and the association rate constant for the formation of  $\text{EC}_4\text{S}$  ( $k_{10}$ ) were varied in the trials in order to facilitate the model runs (represented using blue arrows in **Scheme 3.1**). An overlay plot of the raw data with the simulated curves for model 1a is shown in **Figure 3.5A**. The datasets for 10 mM  $\text{Mg}^{2+}$ , the 5 mM  $\text{Mg}^{2+}/250 \mu\text{M Ca}^{2+}$  and 5 mM  $\text{Mg}^{2+}/1 \text{ mM Ca}^{2+}$  were chosen here to illustrate the difference in the fit. The fitted product curves underestimated the amount of product formed when  $\text{Ca}^{2+}$  is present. These fitted curves were used to obtain the  $k_{\text{obs}}$  ( $\text{sec}^{-1}$ ) at each reaction condition. **Figure 3.5BC** is an overlay plot of experimental and fitted  $k_{\text{obs}}$  ( $\text{sec}^{-1}$ ) obtained at 10 mM  $\text{Mg}^{2+}$  and 5 mM  $\text{Mg}^{2+}$  at varying amounts of  $\text{Ca}^{2+}$ . The fitted values for  $k_{\text{obs}}$  ( $\text{sec}^{-1}$ ) obtained from the model fit do not represent the experimental data at different  $\text{Ca}^{2+}$  concentrations. In all these trials, fitted curves for the sets with  $\text{Ca}^{2+}$  underestimated the amount of



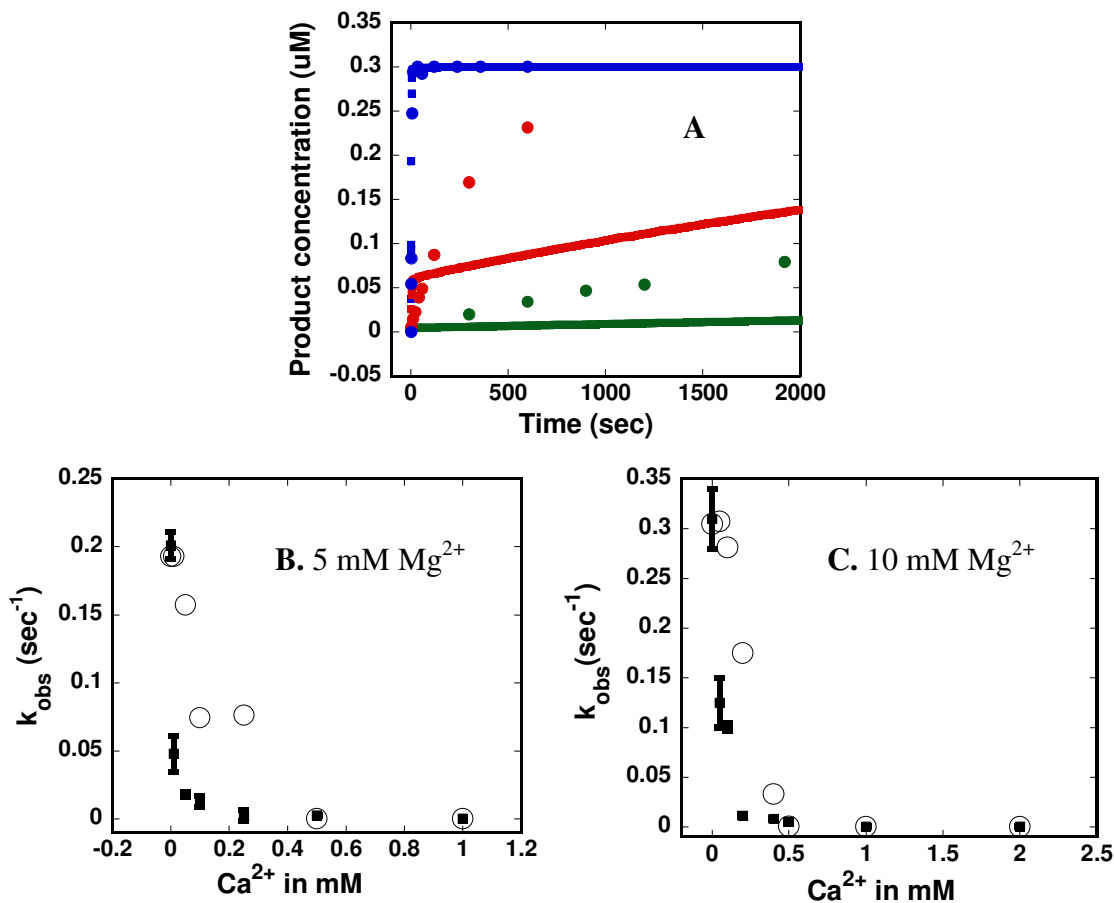


**Figure 3.5: Overlay plot of the experimental and fitted values for model 1a (no mixed species formed).** A). Representative experimental data and fitted curves for 10 mM Mg<sup>2+</sup> set is shown in blue, 5 mM Mg<sup>2+</sup>/ 250 μM Ca<sup>2+</sup> set is shown in red and 5 mM Mg<sup>2+</sup>/ 1 mM Ca<sup>2+</sup> is shown in green for model 1a. In the datasets with Ca<sup>2+</sup> (red and green), fitted curves underestimates the data. B and C). The overlay plots of experimental (filled squares) and fitted (open circles)  $k_{\text{obs}}$  (sec<sup>-1</sup>) values at fixed Mg<sup>2+</sup> and varying Ca<sup>2+</sup> concentrations.

product formed. As shown in **Table 3.2**, the parameter value for EC<sub>4</sub>S formation fits to an unreasonable number. These numbers are compared to what is already known about these parameters from the earlier work (**Table 3.1**). The DNA binding constant cannot have micromolar values since for PvuII even in the absence of metals the enzyme can bind DNA in nanomolar range (Conlan and Dupureur, 2002). The standard deviation obtained for this model run (6.62e-8) was the largest among all the models shown here, which indicates a poor fit of the data to the model.

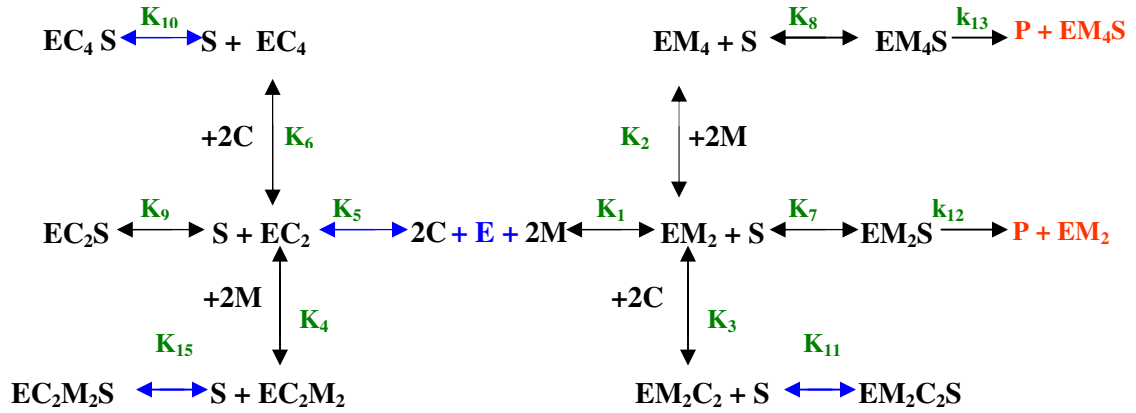
**Model 1b: Mixed metal species formed and not active:**

Since PvuII binds two metal ions per monomer unit, it is possible that there are some mixed species formed. There can be four types of species depending on which metal is in which site. Models with mixed metals species that do not differentiate between the two sites are shown here and models with site specificity is shown in Appendix section. **Scheme 3.2** features model 1b, where the mixed species are formed and are assumed to be not contributing towards the product formation. Since there are no known binding or cleavage parameters for these species we made some estimates for these parameters based on the values that are known for the single metal species. The value for EC<sub>2</sub>M<sub>2</sub> formation (K<sub>4</sub>) from EC<sub>2</sub> was fixed to 3.16 mM, as the value for the EM<sub>4</sub> (K<sub>2</sub>) formation from EM<sub>2</sub>. Simulations done on the parameters for these species shows a range of values that do not effect the model fit (described in Appendix section). Parameters k<sub>5</sub> (association rate constant for formation of EC<sub>2</sub>), k<sub>10</sub> (association rate constant for the formation of EC<sub>4</sub>S), k<sub>11</sub> (association rate constant for the formation of EM<sub>2</sub>C<sub>2</sub>S) and k<sub>15</sub> (association rate constant for the formation of EC<sub>2</sub>M<sub>2</sub>S) were always

**Table 3.2: Table shows the initial guess and the fitted values for the parameters obtained for model 1a and model 1b**

		<b>Model 1a</b> (No mixed species formed)	<b>Model 1b</b> (Mixed species formed and not active)
Parameters	Initial guess	Fitted value (Errors for association rates)	Fitted value (Errors for association rates)
$K_5$ (E + 2C)	120 $\mu$ M	49.6 $\mu$ M (11.6 %)	77 $\mu$ M (21%)
$K_{10}$ (EC <sub>2</sub> +S)	50 pM	2.12 $\mu$ M (12510%)	50.0 $\mu$ M (11700%)
$K_{11}$ (EC <sub>2</sub> M <sub>2</sub> +S)	0.33 nM	N/A	0.33 mM (9049%)
$K_{15}$ (EM <sub>2</sub> C <sub>2</sub> +S)	1 nM	N/A	50.0 nM (44%)
Standard deviation		6.56e-8	5.89e-8

The errors shown here are for the floated association rate constant values. Parameters obtained have high errors as described in the results section. Specifically parameter  $K_{10}$  cannot have micromolar affinity; this is too weak a constant for the DNA binding by a nuclease.



**Scheme 3.2: Model 1b, mixed species formed and not active:** E: homodimeric enzyme, S: Cognate 14mer DNA duplex, M=  $\text{Mg}^{2+}$  ion, C=  $\text{Ca}^{2+}$  ion. The equilibrium step is represented by double arrow and cleavage step is represented by single arrow. The equilibrium constants and the kinetic parameters are numbered and represented here in green. The cleavage products are shown in red. The arrows in blue indicate parameters, which were varied in the trials.

floated in the model runs; they are represented with blue arrows in **Scheme 3.2**. **Figure 3.6A** shows an overlay plot of the fitted curves and experimental data for model 1b. All the progress curves obtained from the models were fitted to a first order rate equation to derive  $k_{\text{obs}}$  ( $\text{sec}^{-1}$ ). The calculated  $k_{\text{obs}}$  from the fits and the experimental  $k_{\text{obs}}$  were plotted to compare the model fit to the data. **Figure 3.6BC** summarizes the result for this model run with an overlay of fitted  $k_{\text{obs}}$  ( $\text{sec}^{-1}$ ) and experimental data for 10 mM  $\text{Mg}^{2+}$  and 5 mM  $\text{Mg}^{2+}$  at varying amounts of  $\text{Ca}^{2+}$  for model 1b. Datasets with fixed  $\text{Ca}^{2+}$  and varying  $\text{Mg}^{2+}$  concentrations also showed similar trend (data not shown).

When compared to model 1a, we expected that model 1b would have even lower product since in this model there are more inactive species, but we see a similar fit as model 1a (**Figure 3.5A and Figure 3.6A**). Underestimation of the product formed using model 1a could be due to underestimation of the active species ( $\text{EM}_2\text{S}$  and  $\text{EM}_4\text{S}$ ) formed or overestimation of the inactive species ( $\text{EC}_2\text{S}$  and  $\text{EC}_4\text{S}$ ) formed. From the parameter values for the fits as shown in **Table 3.2**, the DNA binding by the  $\text{EC}_4$  ( $K_{10}$ ) complex and the  $\text{EM}_2\text{C}_2$  ( $K_{11}$ ) complex were fit to millimolar to micromolar values, which are excessively weak for the DNA binding step of a nuclease. This number should be in the picomolar-nanomolar range (Conlan and Dupureur, 2002). The unreasonable values for these constants decreases the amount of inactive species formed for model 1b, making the fit more similar to model 1b than anticipated.

#### **Model 1c, 1d, and 1e: Mixed metal species are active:**

In the next approach the amount of active species was increased. We looked at

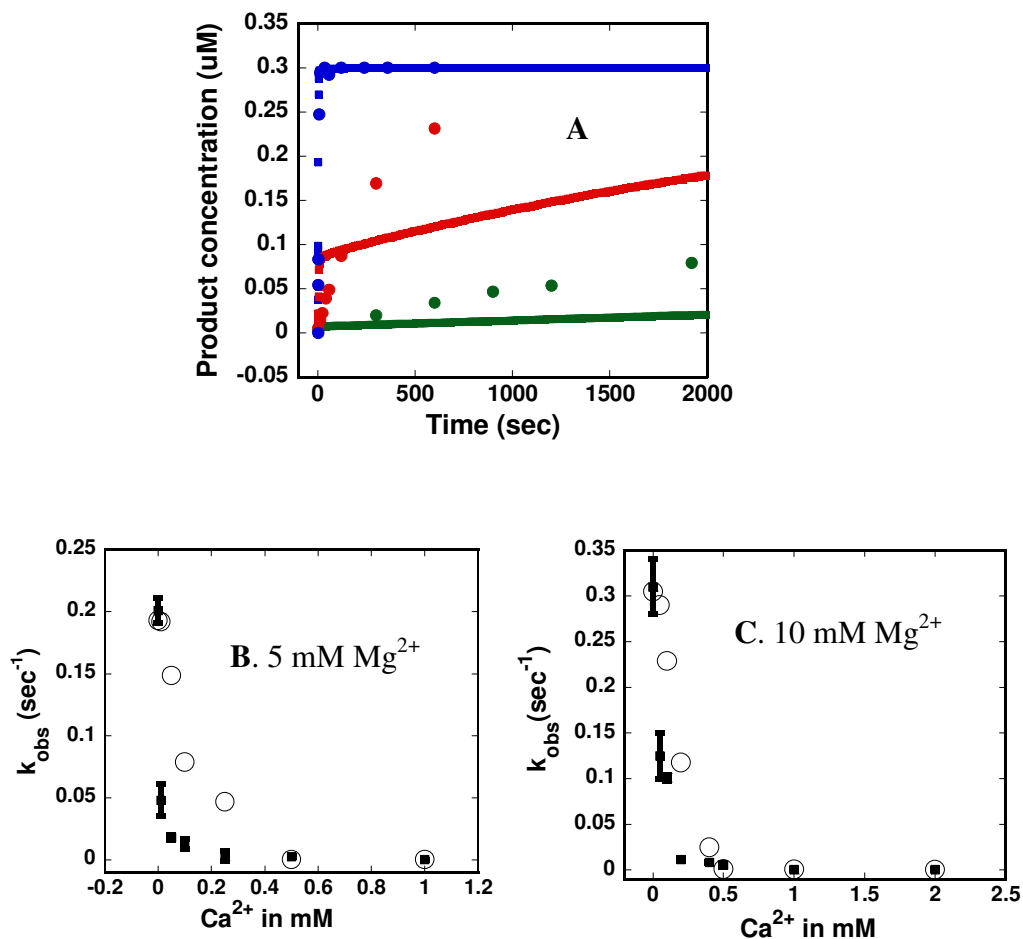
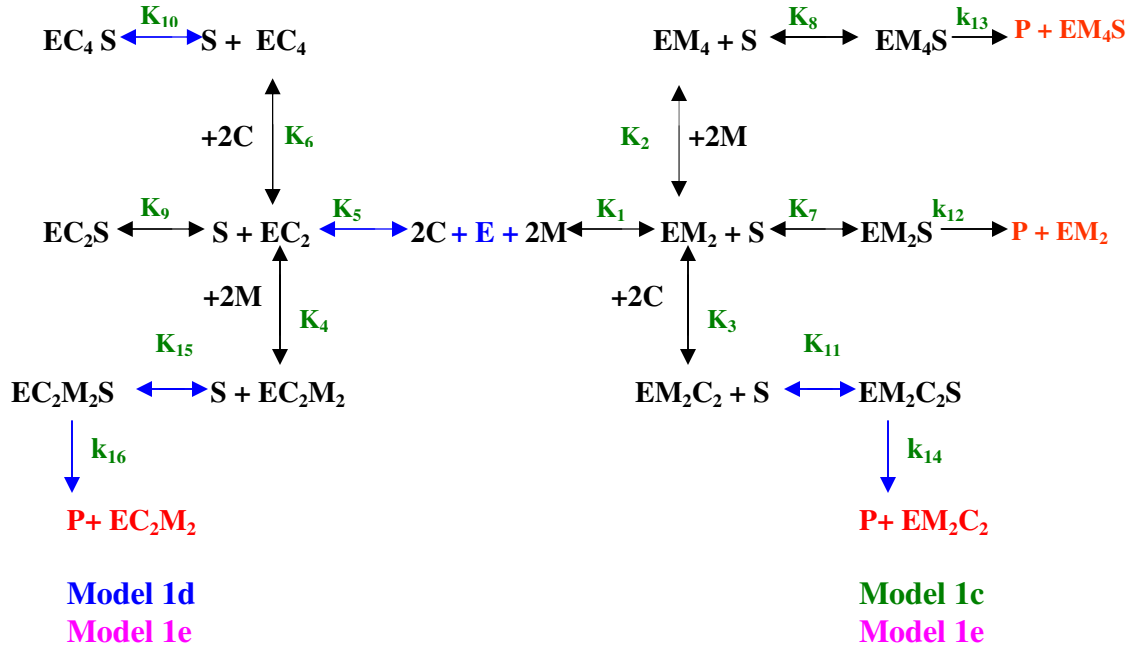


**Figure 3.6: Overlay plot of the experimental and fitted values for model 1b.** A). Experimental data and fitted curves for 10 mM Mg<sup>2+</sup> set is shown in blue, 5 mM Mg<sup>2+</sup>/ 250  $\mu$ M Ca<sup>2+</sup> set is shown in red and 5 mM Mg<sup>2+</sup>/ 1 mM Ca<sup>2+</sup> is shown in green for model 1b. In the datasets with Ca<sup>2+</sup> (red and green), fitted curves underestimates the data. B and C). The overlay plots of experimental (filled squares) and fitted (open circles) k<sub>obs</sub> (sec<sup>-1</sup>) values at fixed Mg<sup>2+</sup> and varying Ca<sup>2+</sup> concentrations.

models where either one or both of the mixed species formed are active. There are three different possibilities: either one of the mixed species is active or both species ( $EM_2C_2S$  and  $EC_2M_2S$ ) are active. From the work done on EcoRI and EcoRV as discussed in the introduction, it was observed that occupation of native or non-native metal at a particular site has varying effects on the activity of the enzyme (Vipond and Halford, 1995). Depending on which metal occupies the regulatory site B, there will be stimulation or an inhibition of activity (Feng, et al., 2006). In order to specify the effect of metal ion occupation at each metal site, models with one mixed species being active were tested. **Scheme 3.3** features models with mixed species active: model 1c where  $EM_2C_2S$  species is active; model 1d where  $EC_2M_2S$  species is active; and model 1e where both of the mixed species are active. In model 1e, the rate constant for  $EM_2C_2S$  species forming product ( $k_{14}$ ) and that for  $EC_2M_2S$  species forming product ( $k_{16}$ ) were given initial values of  $0.01 \text{ sec}^{-1}$  and  $0.001 \text{ sec}^{-1}$  respectively.

**Figure 3.7** summarizes the results, where models 1c, 1d, and 1e fit well to the experimental data. Errors obtained on the floated parameters were also better for these models (**Table 3.3**). Standard deviations for model 1c, 1d and 1e are comparable to each other and lower than for models 1a and 1b (**Table 3.3 and Table 3.2**). The overlay plot of the experimental and fitted  $k_{\text{obs}}$  ( $\text{sec}^{-1}$ ) for models 1c, 1d, and 1e indicates good agreement with one another (**Figure 3.8**). Models with mixed species formed and active showed better fit to the experimental data and better errors than models with mixed species formed and not active (model 1b). However from the fit of the models, or the error on the fitted parameters, or from the standard deviation, we cannot distinguish whether one or both mixed species are active. Studies on enzymes, BamHI and



**Scheme 3.3: Models with mixed species active:** E: homodimeric enzyme, S: Cognate 14 mer DNA duplex, M= Mg<sup>2+</sup> ion, C= Ca<sup>2+</sup> ion. The equilibrium step is represented by double arrow and cleavage step is represented by single arrow. The equilibrium constants and the kinetic parameters are numbered and represented here in green. The cleavage products are shown in red. The arrows in blue indicate parameters which were varied in the trials. Model 1c where EM<sub>2</sub>C<sub>2</sub>S species is active, model 1d where EC<sub>2</sub>M<sub>2</sub>S species is active and model 1e where both of the mixed species are active are labeled.



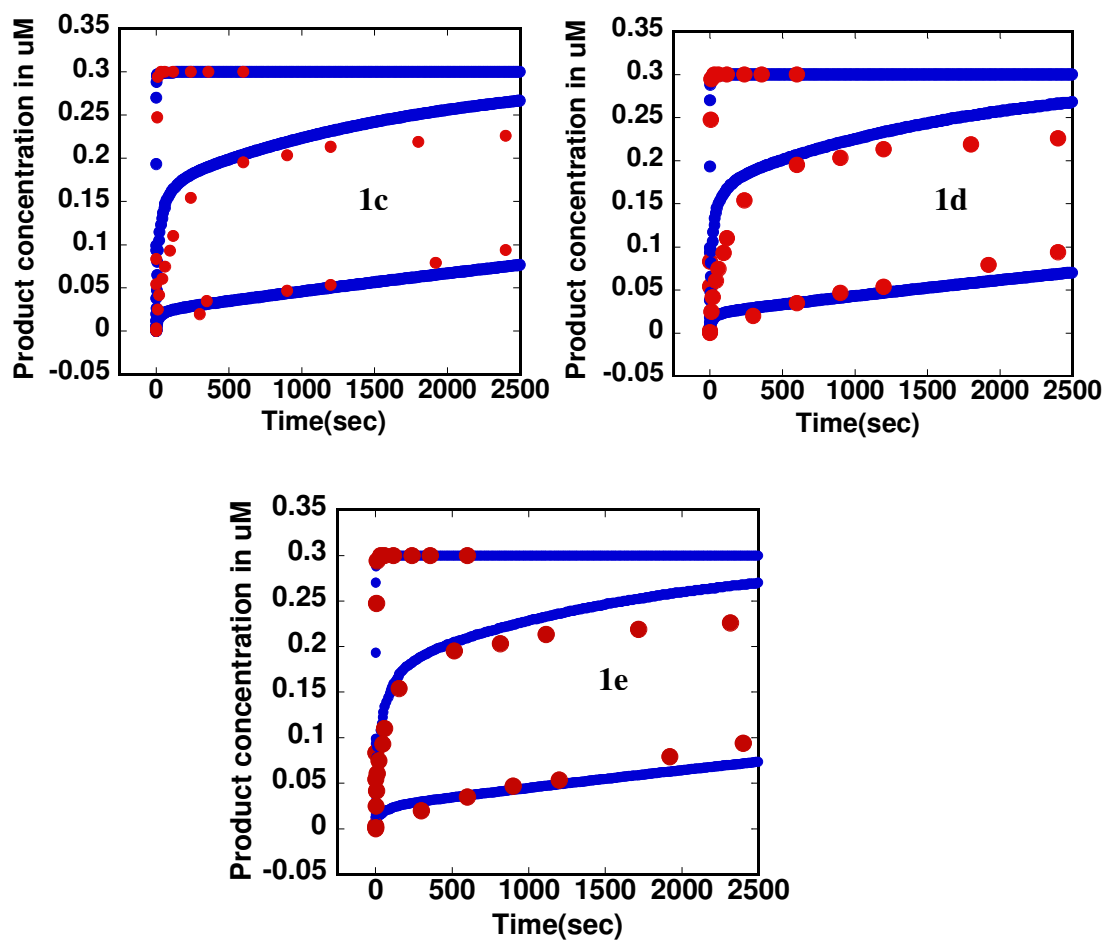


**Figure 3.7: Overlay plot of the experimental and fitted curves.** Experimental data is shown in red and fitted curves are shown in blue. Three different curves seen here are for the datasets with 10 mM  $Mg^{2+}$  alone, 10 mM  $Mg^{2+}$ ; 500  $\mu M$   $Ca^{2+}$  set and 5 mM  $Mg^{2+}$ ; 1 mM  $Ca^{2+}$  data sets for model 1c, model 1d and model 1e as labeled. Experimental data does fit well to the model with mixed species being formed and active.

**Table 3.3: The initial guess and the fitted values for comparison of the parameters in models with both mixed species formed and either one or both species active.**

Parameters	Initial guess	Model 1c (EM <sub>2</sub> C <sub>2</sub> S active) (% error)	Model 1d (EC <sub>2</sub> M <sub>2</sub> S active) (% error)	Model 1e (both species active) (% error)
K <sub>5</sub> (E+2C)	120 μM	60.6 μM (37.4%)	36.3 μM (17.4%)	34 μM (23.5%)
K <sub>10</sub> (EC <sub>2</sub> +S)	50 pM	16.6 pM (35.2%)	33.5 pM (19.2%)	29.5 pM (20.3%)
K <sub>11</sub> (EM <sub>2</sub> C <sub>2</sub> + S)	0.33 nM	38.6 pM (13.1%)	<b>0.645 μM</b> <b>(1354 %)</b>	93.8 pM (56.5%)
K <sub>15</sub> (EC <sub>2</sub> M <sub>2</sub> +S)	1 nM	12 nM (67.8%)	4 nM (36.90%)	4 nM (22.6%)
k <sub>14</sub> (EM <sub>2</sub> C <sub>2</sub> S)	0.01 sec <sup>-1</sup>	0.0127 sec <sup>-1</sup> (12.8%)	n/a	0.083 sec <sup>-1</sup> (97.7%)
k <sub>16</sub> (EC <sub>2</sub> M <sub>2</sub> S)	0.001 sec <sup>-1</sup>	n/a	0.013 sec <sup>-1</sup> (10.5%)	0.008 sec <sup>-1</sup> (28.3%)
Standard deviation		3.40e-8	3.33e-8	3.26e-8

Model 1c is with EM<sub>2</sub>C<sub>2</sub>S species active, model 1d with EC<sub>2</sub>M<sub>2</sub>S species active and model 1e with both EC<sub>2</sub>M<sub>2</sub>S and EM<sub>2</sub>C<sub>2</sub>S active. Varying the initial guesses for the k<sub>14</sub> and k<sub>16</sub> values in model 1c and 1d gave the same value for the fit 0.01 sec<sup>-1</sup>. Model 1d has higher error on a parameter value which indicates a bad fit.

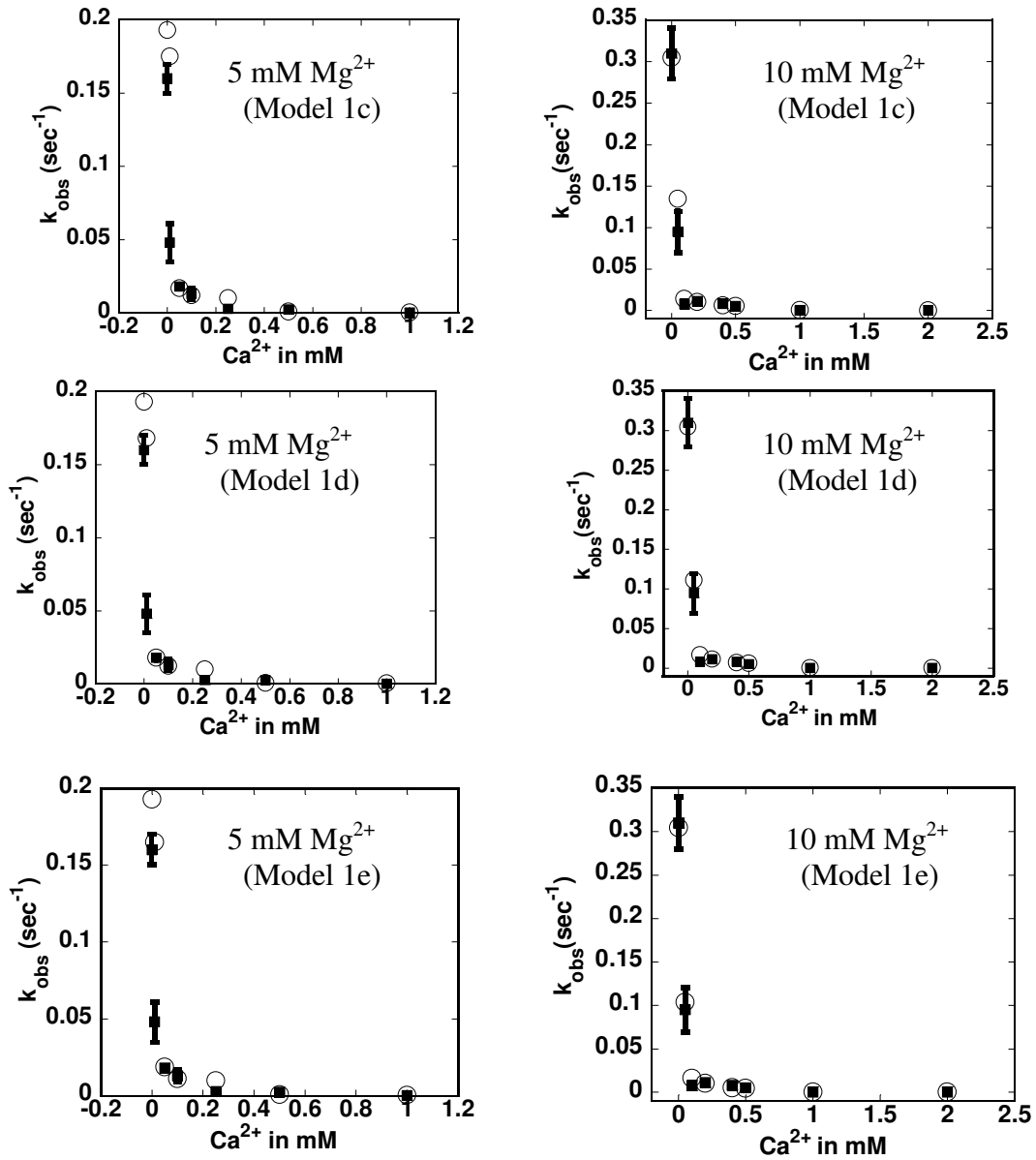


**Figure 3.8: Overlay plot of the experimental and fitted  $k_{obs}(\text{sec}^{-1})$ :** The  $k_{obs}(\text{sec}^{-1})$  of the experimental data at fixed  $\text{Mg}^{2+}$  concentrations of 5 mM and 10 mM with error bars are shown with black filled rectangles. The fitted values obtained from the output curves are shown with open circles for model 1c model 1d and model 1e as labeled.

Endonuclease V indicate the regulatory role of a metal site (Mones, et al., 2007; Feng, et al., 2006). Based on the parameter values shown in **Table 3.3** we can argue that the  $EC_2M_2S$  species activity is negligible which indicates towards a probable regulatory metal site in PvuII.

In model 1d where  $EM_2C_2S$  is not active, the rate constant for the activity of the  $EC_2M_2S$  species fits to  $0.013 \text{ sec}^{-1}$ , which is similar to that of the  $EM_2S$  species ( $k_{12}$ ). Also, the parameter  $K_{11}$  ( $EM_2C_2 + S$ ) fits to a value in micromolar range, with high errors, which is an unreasonable value for a DNA binding parameter. Based on model 1c, 1d, and 1e, it is seen that under the conditions used here, both mixed species are formed, and  $EC_2M_2S$  species has negligible cleavage activity. Model 1c and 1e shows similar fit and standard deviation, also both these models have  $EM_2C_2S$  species active. The bad fit of model 1d indicates that  $EC_2M_2S$  cannot be the more active mixed species and probably it is because in this species  $Ca^{2+}$  ions occupy the catalytic site.

#### **Concentration of species:**

Model 1e and the determined parameters can be used to examine the distribution of species at any time point or metal ion concentration. Simulation with fixed parameters at 10 seconds, 50 seconds, 120 seconds, and 600 seconds are shown in **Figure 3.9**. At no  $Ca^{2+}$  and low  $Ca^{2+}$  concentrations, we see more of  $E-Mg^{2+}$  species present at the 10 seconds time point. At the later time points, the inactive ( $EC_2S$  and  $EC_4S$ ) species and less active ( $EC_2M_2S$ ) species are more abundant. At high  $Ca^{2+}$  concentrations, we observe mixed species formed ( $EM_2C_2S$  and  $EC_2M_2S$ ) at all time points. The less active  $EC_2M_2S$  species are formed in abundance because of the equilibrium constant values and since these species are converted to product slowly they are present for a longer time.

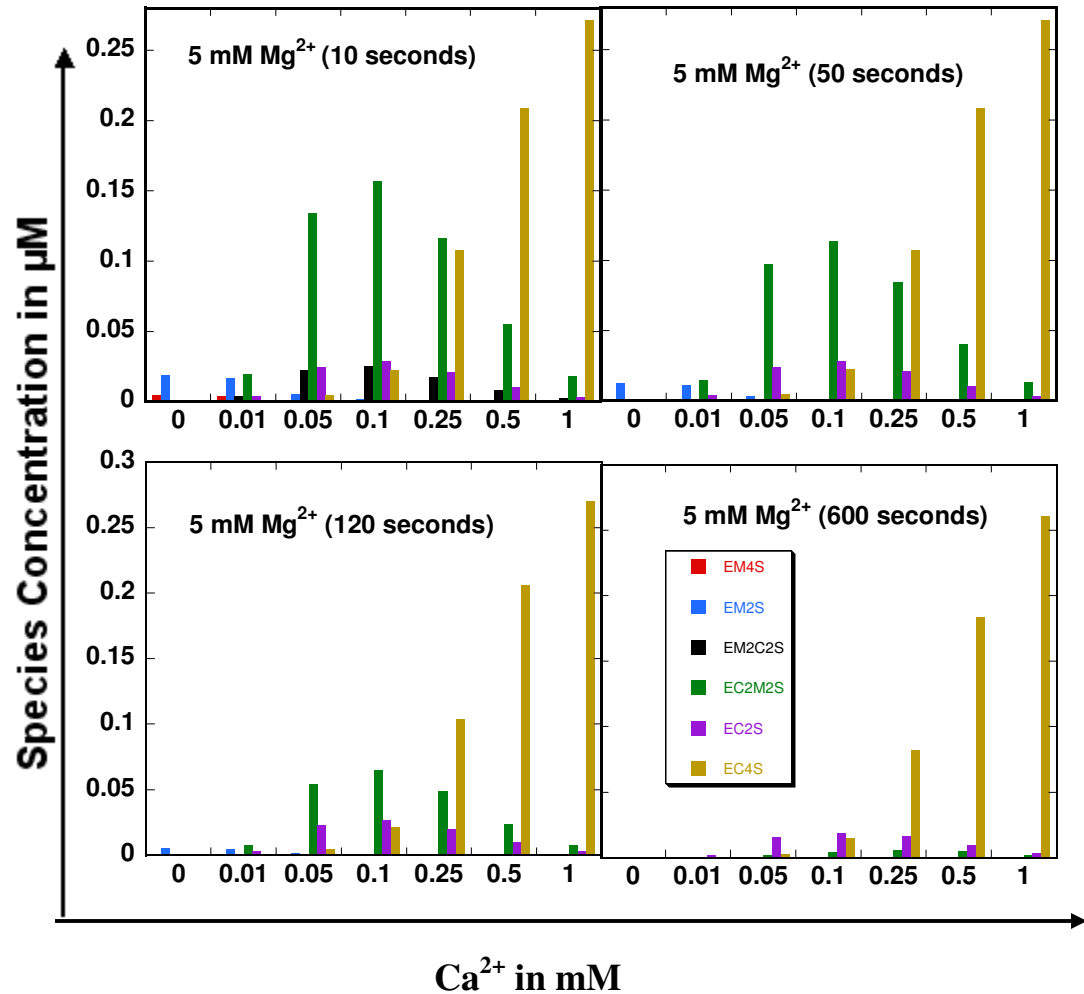


**Figure 3.9: Concentration of mixed species from the simulations using model 1e:** The simulations with 5 mM  $\text{Mg}^{2+}$  set is shown at varying  $\text{Ca}^{2+}$  concentrations. Four different time points shown here shows the abundance of these species early and late in the reaction. Symbol represents species concentration for  $\blacksquare$  EM<sub>4</sub>S,  $\blacksquare$  EM<sub>2</sub>S,  $\blacksquare$  EM<sub>2</sub>C<sub>2</sub>S,  $\blacksquare$  EC<sub>2</sub>M<sub>2</sub>S,  $\blacksquare$  EC<sub>2</sub>S, and  $\blacksquare$  EC<sub>4</sub>S respectively (as represented in one of the plots). We see that with 5 mM  $\text{Mg}^{2+}$  at all  $\text{Ca}^{2+}$  concentrations mixed species are formed. At high  $\text{Ca}^{2+}$  conditions and latter time points the inactive EC<sub>2</sub>S and EC<sub>4</sub>S species occupies the DNA substrate.

The EC<sub>2</sub>S and the EC<sub>4</sub>S species formed are inactive species and work as ‘DNA sink’, which explains why not all substrate contributes to product formation at higher Ca<sup>2+</sup> concentrations (data not shown).

### **Contributions to the product:**

Product contribution of each of the active species was calculated by multiplying the cleavage rate constant of each species by their concentration and dividing it by the overall product formed. These calculations were based on species concentration obtained from simulations and cleavage rate constant obtained from the fits. Product contribution of species using model 1e is shown in **Figure 3.10**. It is seen that EM<sub>4</sub>S species formed contributes maximum to the product formation early in the reaction at low Ca<sup>2+</sup> conditions. EM<sub>4</sub>S species have very fast cleavage rate (1.11 sec<sup>-1</sup>) and therefore all the species formed are converted to product very early in the reaction (10 seconds). At the latter time points, product formation is dominated by the mixed species. Mixed species contribute to the product formation at higher Ca<sup>2+</sup> concentrations. Also in all conditions, mixed species when formed contribute to the product formation at later time points. This explains why we do not see a fit to the experimental data with the models where the mixed species are not formed or active (model 1a and model 1b).

### **Mixed metal species active with inter-conversion:**

We tried models with the interconversion step to see if we increase the amount of active species formed whether we can better differentiate between the activity of mixed species. At the interconversion step, the enzyme-metal-DNA species binds another metal to form a more active species. **Scheme 3.4** shows models with mixed species active and interconversion step, model 2c where EM<sub>2</sub>C<sub>2</sub>S species is active, model 2d where EC<sub>2</sub>M<sub>2</sub>S

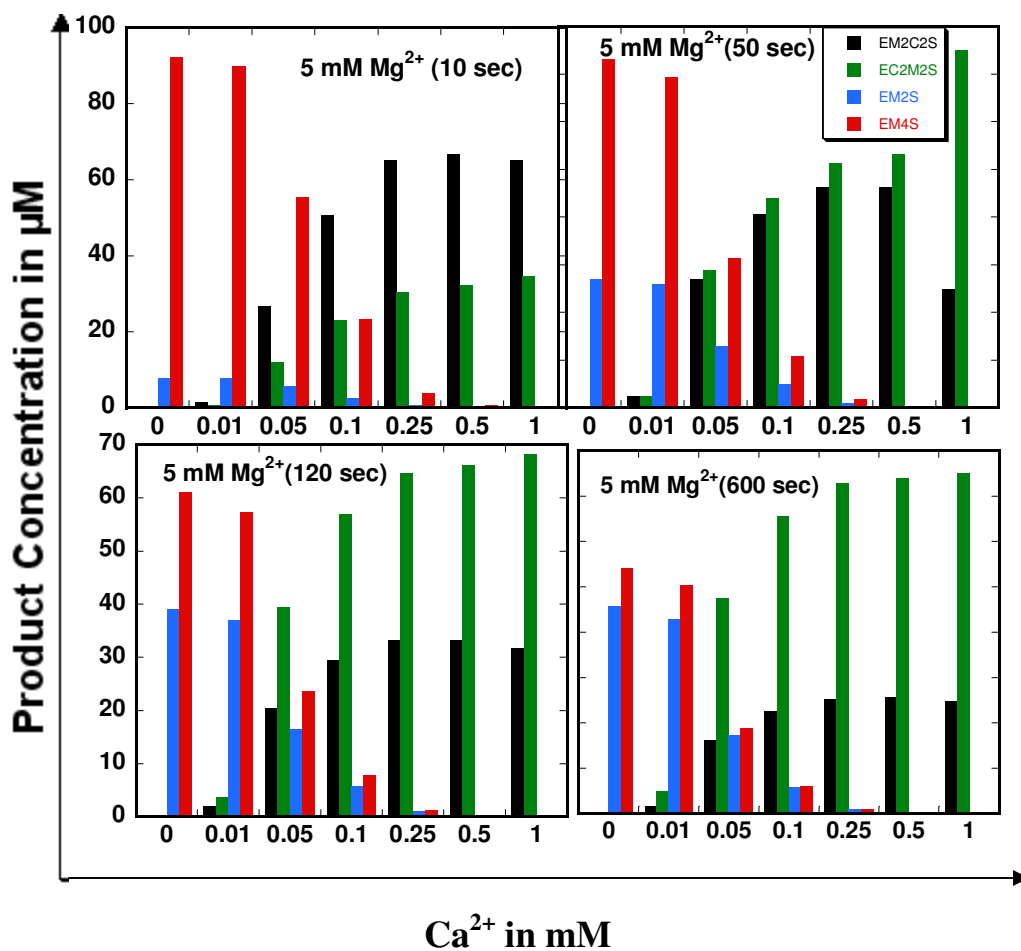
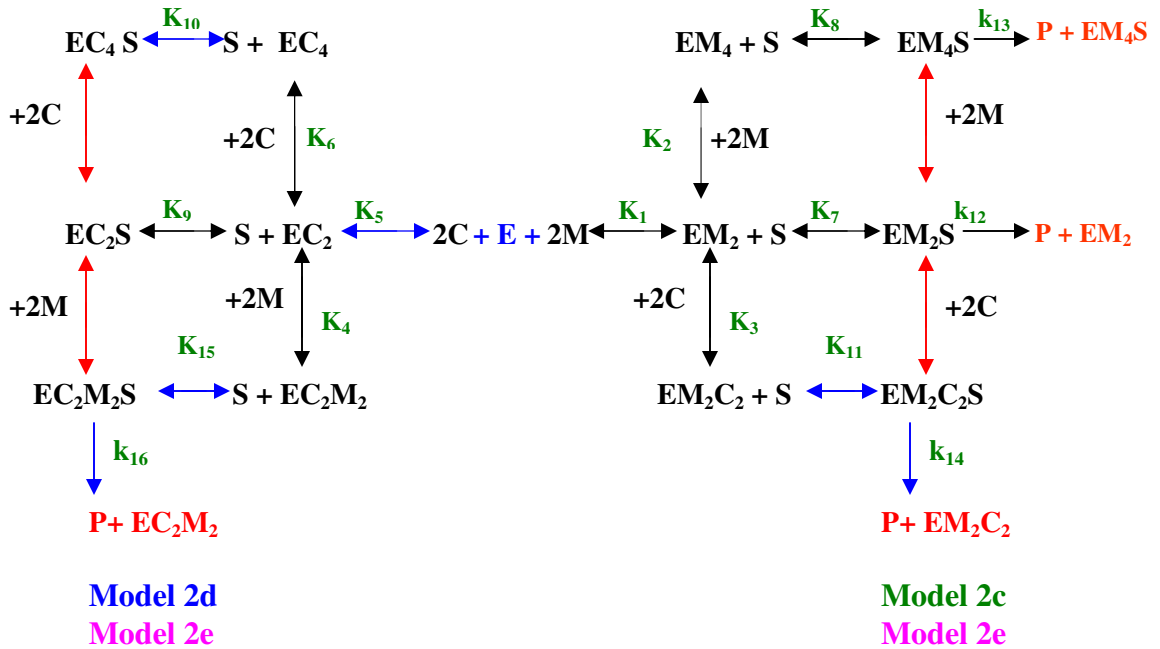


**Figure 3.10: Contribution of species to product from the simulations using model 1e:** The simulations with  $5 \text{ mM Mg}^{2+}$  set is shown at varying  $\text{Ca}^{2+}$  concentrations. Symbol represents contribution from  $\text{EM}_4\text{S}$  (red),  $\text{EM}_2\text{S}$  (blue),  $\text{EM}_2\text{C}_2\text{S}$  (black),  $\text{EC}_2\text{M}_2\text{S}$  (green), respectively (as represented in one of the plots). We see that at lower  $\text{Ca}^{2+}$  concentrations  $\text{EM}_4\text{S}$  contributes maximum to the product formation and at higher  $\text{Ca}^{2+}$  concentrations and latter time points the contribution to product is maximum from the mixed species. The time points shown here monitors the product contribution profile.



**Scheme 3.4: Models with mixed species active with interconversion:** E: homodimeric enzyme, S: Cognate 14 mer DNA duplex, M= Mg<sup>2+</sup> ion, C= Ca<sup>2+</sup> ion. The equilibrium step is represented by double arrows, and the cleavage step is represented by a single arrow. Equilibrium constant and the kinetic parameters are numbered and represented here in green. The cleavage products are shown in red. The arrows in blue indicate parameters which were varied in the trials. The interconversion step is represented by red arrows. Model 2c with the EM<sub>2</sub>C<sub>2</sub>S active, model 2d with EC<sub>2</sub>M<sub>2</sub>S active and model 2e, with both species active are labeled.



species is active, and model 2e where both the mixed species are active. All the models with interconversion step showed similar fit to the data as the models without the interconversion step (data not shown). The parameter numbers which were used for the models without inter conversion had to be modified within experimental error in order to get models with interconversion to converge. Modified parameters for this set of models are shown in **Table 3.4**. Model 2e where both the mixed species are formed and active is shown here in detail.

In these models, four extra steps are added, that is,  $EM_2S$  species binds two  $Ca^{2+}$ /two  $Mg^{2+}$  ions to form  $EM_2C_2S$  and  $EM_4S$  species, respectively, and  $EC_2S$  species binds two  $Mg^{2+}$ /two  $Ca^{2+}$  ions to form  $EC_2M_2S$  species and  $EC_4S$  species, respectively. The parameters used here for the interconversion steps are shown in **Table 3.5**. The initial values chosen for these interconversion parameters were from earlier fits and simulations. The parameter values for  $EM_2S + 2M$  was characterized in a earlier study to be 1.6 mM (Xie, et al., 2008). The mixed metal formation parameters ( $EM_2S + 2C$  and  $EC_2S + 2M$ ) were floated with an initial value of 1.29 mM. Parameter value for  $EC_4S$  formation ( $EC_2S + 2C$ ) was fixed as 400  $\mu M$  because from simulations it was seen that for a range of numbers from 200  $\mu M$ - 8 mM for this parameter the fits did not change. In these trials for  $EC_2S$  species binding two  $Ca^{2+}$  ions the parameter used ( $K_{18}$ ) shows stronger affinity for  $Ca^{2+}$  as compared to others ( $K_{17}$  and  $K_{19}$ ). **Figure 3.11** shows the plot of experimental and fitted  $k_{obs}(sec^{-1})$  vs the  $Ca^{2+}$  concentration for the datasets with 10 mM  $Mg^{2+}$  and varying  $Ca^{2+}$  for model 2e, which shows good fit. Parameters obtained, errors, and standard deviation from this fit are shown in **Table 3.5**.

These studies show all models with interconversion step have similar fit as the

**Table 3.4: List of parameters changed in the models with interconversion.**

Parameters	Values used	Source for the parameter values
$k_1$	$1.0 \times 10^{-4} \mu\text{M}^{-1} \text{sec}^{-1}$	$K_d = 3.16 \text{ mM}$ , changed from $4.6 \text{ mM}$ (Xie, et al., 2008)
$k_2$	$2.0 \times 10^{-4} \mu\text{M}^{-1} \text{sec}^{-1}$	$K_d = 2.23 \text{ mM}$ , changed from $3.16 \text{ mM}$ (Xie, et al., 2008)
$k_4$	$2 \times 10^{-4} \mu\text{M}^{-1} \text{sec}^{-1}$	Assumed to be the same as $k_2$ for $\text{EC}_2\text{M}_2$ $K_d = 2.23 \text{ mM}$ , changed from $3.16 \text{ mM}$
$k_7$	$0.1 \mu\text{M}^{-1} \text{sec}^{-1}$	$K_d = 10 \text{ nM}$ (Xie, et al., 2008) Changed from $27 \text{ nM}$
$k_{10}$	$50 \mu\text{M}^{-1} \text{sec}^{-1}$	$125 \text{ pM}$ as the initial value instead of $56 \text{ pM}$

The dissociation constant rate used for metal binding step was  $1000 \text{ sec}^{-1}$  (Xie, et al., 2008) and the dissociation constant rate used for the DNA binding step was  $0.001 \text{ sec}^{-1}$  (Conlan and Dupureur, 2002). All the other constants used were same as shown in Table 3.1.

**Table 3.5: Table shows the initial guess for the parameters in Model 2c, 2d and 2e.**

Parameters	Initial guess	Model 2e (% error)
$K_5$ (E+2C)	120 $\mu\text{M}$	42.6 $\mu\text{M}$ (14.2%)
$K_{10}$ (EC <sub>2</sub> +S)	20 pM	5.72 pM (11.7%)
<b><math>K_{17}</math></b> <b>(EM<sub>2</sub>S+ 2M)</b>	<b>1.6 mM</b>	12.6 mM (13.7%)
$K_{19}$ (EC <sub>2</sub> M <sub>2</sub> S+2M) (EM <sub>2</sub> C <sub>2</sub> S+2C)	<b>1.29 mM</b>	0.104 mM (238.3%)
Standard deviation		3.61e-8

In this model the parameters for the interconversion steps were floated. The bolded values are used as the initial guesses for the interconversion step (Xie and Dupureur, 2009). These values were floated in the later models; value for  $K_{18}$  was fixed to 400  $\mu\text{M}$  which was obtained from the simulations.

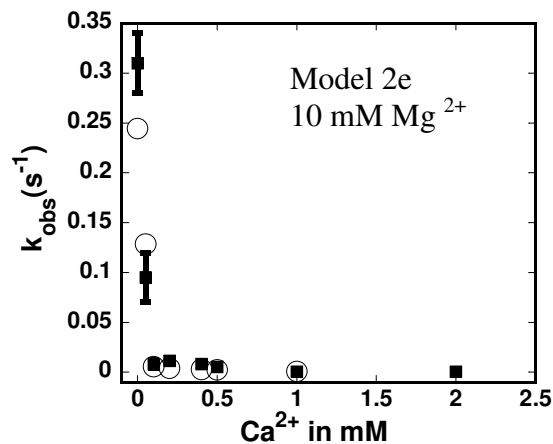
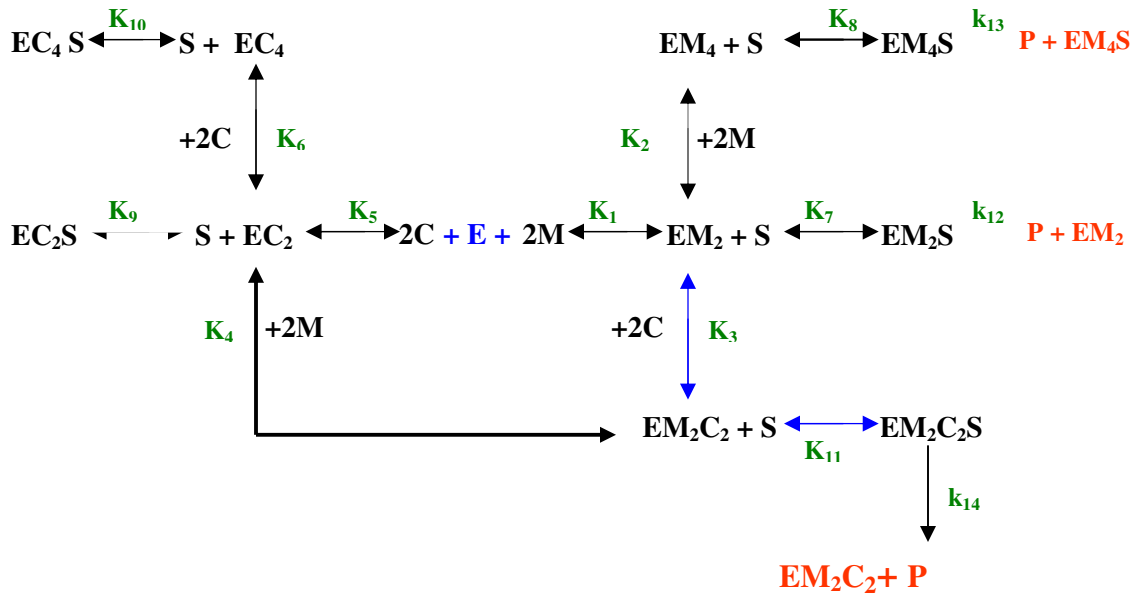


**Figure 3.11: Overlay plot of the experimental and fitted  $k_{\text{obs}}(\text{sec}^{-1})$  for models with interconversion step:** The  $k_{\text{obs}}(\text{sec}^{-1})$  of the experimental (black filled rectangles) at fixed  $\text{Mg}^{2+}$  concentration 10 mM with error bars and fitted values (open circles) for model 2e (both species are active). The parameters for the interconversion step were floated in these models. All the models fit very well to the experimental data. This trial could not distinguish whether one or both mixed species are active.

models without the interconversion step. However, it is difficult to make a direct comparison because in these models with inter conversion; some parameters used had to be changed from the numbers used in models without interconversion step. These numbers that were varied are within experimental error but they had to be varied to get the models with interconversion step to converge.

### **Ca<sup>2+</sup> and Mg<sup>2+</sup> metal ions at specific sites: Model with one mixed species formed.**

Metal site specificity is one of the reasons for one mixed species to form; each metal will bind at a particular site. In this model we made the assumption that the high affinity Ca<sup>2+</sup> site is the site B and under the mixed metal conditions there will only be EM<sub>2</sub>C<sub>2</sub> species formed. In model 1d and 1c, where either one of the mixed species was assumed to be active, we get the cleavage kinetics constant to be around 0.01 sec<sup>-1</sup> for both cases as shown in **Table 3.3**. For model 1e where both the species are active, we get a higher and a lower rate constant for the two mixed species. It is therefore possible that there is only one mixed species that is formed and active. Earlier studies show minimal or no positive cooperativity for metal binding at active site of PvuII (Xie and Dupureur, 2009). Based on the assumption that there are specific sites for the Ca<sup>2+</sup> and Mg<sup>2+</sup> at the active site of enzyme, we conducted a set of trials where only one type of mixed species (EM<sub>2</sub>C<sub>2</sub>S) is formed. This is a very broad assumption; here we consider that at all conditions, one site is specific for Ca<sup>2+</sup> and another for Mg<sup>2+</sup> in order for the mixed species to form. This assumption was made based on the high (0.08 sec<sup>-1</sup>) and the low (0.008 sec<sup>-1</sup>) rate constant value for the two mixed species (**Table 3.3**). While the fits were conducted using the model in **Scheme 3.5**, we expected to see two types of fits: one which underestimates the amount of product and other which overestimates the amount



**Scheme 3.5: Model with one mixed species formed  $EM_2C_2$ .** E: homodimeric enzyme, S: Cognate 14mer DNA duplex, M=  $Mg^{2+}$  ion, C=  $Ca^{2+}$  ion. The dissociation constant values are represented by double arrow and turnover step is represented by single arrow. The equilibrium constants and the kinetic parameters are numbered and represented here in green. The cleavage products are shown in red. The arrows in blue represent the parameters which are varied in the trials. From all the other models there will be more  $EM_2C_2$  formed in this case. Based on what number is chosen for  $K_{11}$  we can get different output for the fitted curves either underestimating the experimental data or overestimating it. But this model could not be converged without floating other parameters.

of product depending on what parameter values are chosen for the  $EM_2C_2 + S \rightleftharpoons EM_2C_2S$  step and  $EM_2C_2S \rightleftharpoons EM_2C_2 + P$  step. It was difficult to get this model to converge. A lot more parameters had to be floated for this model which makes it difficult to compare this model to all the others. The values used for constants in this model are those shown in **Table 3.4**. We observed a good enough fit to the experimental data with this model as shown in **Figure 3.12** only when a lot more parameters were floated and those parameters fitted to values with high errors (**Table 3.6**). Parameter values for  $K_4$  and  $K_{10}$  fitted to unreasonable numbers (bolded in **Table 3.6**). So this model where only one mixed species is formed does not explain the experimental data. From all these trials we can only say that under our conditions, both mixed species are formed, and one of these species should be active. The activity of mixed species formed is either similar to the one metal species  $EM_2S$  ( $0.01 \text{ sec}^{-1}$ ) or a value close to it since in all model fits the activity of mixed species ranged from  $0.008\text{-}0.08 \text{ sec}^{-1}$ . In our analysis we have never seen the mixed species formed to be as active as the  $EM_4S$  species ( $1.1 \text{ sec}^{-1}$ ). From the model analysis in order to explain the data obtained under mixed metal condition, mixed species should be formed and  $EM_2C_2S$  should be active in the models.

### **Conclusions:**

From our modeling attempts, we found that models with or without interconversion, where mixed species are not formed, the amount of product formed was underestimated. Models where mixed species were formed and active did fit to the experimental data irrespective of the interconversion step. The models with interconversion have more reaction steps and therefore more parameters and higher

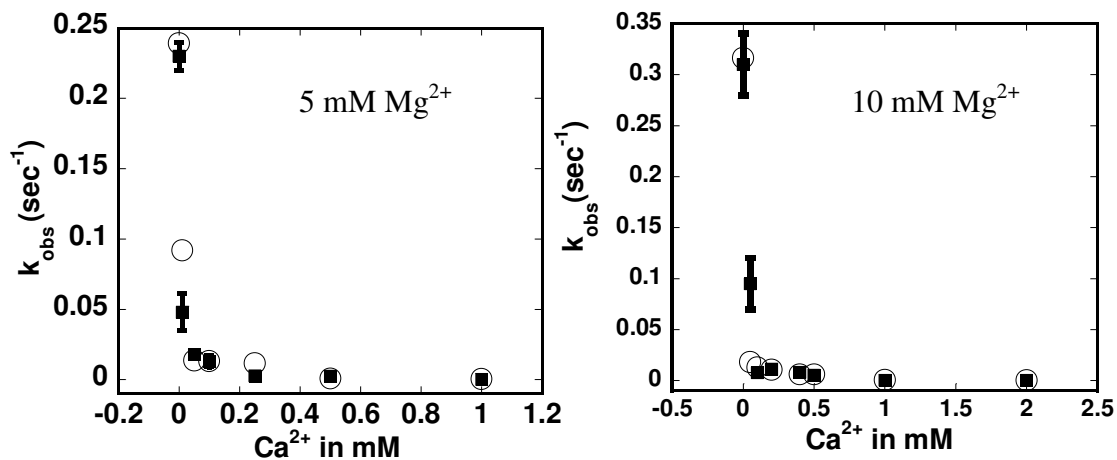


**Figure 3.12: Overlay plot for the experimental and fitted  $k_{\text{obs}}$  at  $\text{Ca}^{2+}$  concentrations in mM for model with only one mixed species (scheme 5):** The  $k_{\text{obs}}(\text{sec}^{-1})$  of the experimental at fixed  $\text{Mg}^{2+}$  concentration of 5 mM and 10 mM and varying concentration of  $\text{Ca}^{2+}$  with error bars is shown as black filled rectangles and fitted data curves from the fits are shown with open circles.



**Table 3.6: Table shows the initial guess and the fitted values for the model where one mixed species is formed as shown in scheme 5.**

Parameters (K <sub>d</sub> )	Initial guess	Model from scheme 5 (% error)
K <sub>3</sub> (EM2 + 2C)	270 μM	6.82 μM (26.2%)
K <sub>4</sub> (EC2 + 2M)	2.23 mM	<b>0.1M</b> <b>(135.1%)</b>
K <sub>5</sub> (E+2C)	70.7 μM	90.8 uM (32.1%)
K <sub>10</sub> (EC2+S)	20 pM	<b>50 μM</b> <b>(2403%)</b>
K <sub>11</sub> (EM2C2+ S)	3.3 nM	2.5 nM (24.7%)
k <sub>14</sub> (EM2C2S)	0.004 sec <sup>-1</sup>	0.015 sec <sup>-1</sup> (12.4%)

Parameters  $k_3$  and  $k_4$  had to be floated in order to get the model to converge.  $k_3$  and  $k_4$  were fixed at 1000 sec<sup>-1</sup> and used to derive the K<sub>d</sub> values shown here. Also for the DNA binding step the dissociation rate constants used was 0.001 sec<sup>-1</sup> to get the values of K<sub>10</sub> and K<sub>11</sub> from the association rate constants obtained from the fits. The bolded parameters are those that fit to unreasonable values.

errors. Inclusion of the interconversion step in different trials did not change the fit. The data collected here and the models used could not differentiate between the two mixed species. For models with and without interconversion step, we observe that when we have both species active, one species has a higher rate of cleavage than the other. When we remove the less active species from the models, there is no difference in the fit. When we remove the more active species from the model, the second species now fits to give a higher activity rate, and there is higher error on parameters which can indicate a bad fit of the model to the data. Based on this observation, we believe that there must be some other species other than the regular active species, EM<sub>2</sub> and EM<sub>4</sub>, formed under the mixed metal conditions which are active in order to explain the product formed.

Is there an in vivo purpose to mixed species formation? Mixed metal species might form so that they regulate some of the processes in the host system. The regulation of a process may occur because of inhibition or stimulation of activity observed depending on the type of mixed metal species formed. Such a situation is explained in the mixed metal experiments of EndonucleaseV. Evolution has made the nucleases choose Mg<sup>2+</sup> ions as the metal cofactor for cleavage activity (Pingoud, et al., 2005). One of the reasons explained is that small metal ions like Mg<sup>2+</sup> help stabilize the transition state species more efficiently than the larger ions (Bowen and Dupureur, 2003). A more quantitative analysis of the energetic contributions of metal ions on the transition state stabilization and the generation of a nucleophile would be required to model the mechanism for catalysis (Aqvist and Warshel, 1990; Pingoud, et al., 2005). In one such study using molecular dynamics, transition state stabilization energies were calculated in presence one or two metals at the active site for BamHI enzyme. From the calculations,

it was proposed that a metal ion at site A contributes more towards the phosphodiester cleavage and has to be occupied by catalytically active metal (Mones, et al., 2007). The activity of mixed species is not higher than the most active  $EM_4S$  species, and therefore we do not see any acceleration of enzymatic activity in PvuII under mixed metal conditions as opposed to many other enzymes. This mixed metal species might be formed in vivo because of the millimolar amounts of  $Mg^{2+}$  and  $Ca^{2+}$  ions present in the cell (Outten and O'Halloran, 2001). Whether or not they have role in the regulation of the enzymatic activity is an open question.

## **CHAPTER IV**

### **METAL EXCHANGE: TO STUDY THE METAL BINDING TO PvuII.**

#### **Introduction:**

Bound metal ions in many proteins are detected based on the indirect measurement because of the difficulty to observe these reactions. Alkali metals and alkaline earth metals are present in the living organisms in large excess and are used by many proteins and enzymes for its function (Nicholls, 1982). It is difficult to study metal binding and its role for alkaline earth metals because there is no convenient way to explore its physical and spectroscopic property (Cowan, 1991).

Luminescence spectroscopy has been used to study the environment of the bound metal ions because of the similarities of the lanthanide ions with  $\text{Ca}^{2+}$  ions (Burroughs and Horrocks, 1994). Lanthanides have similar ionic radii and coordination sites as  $\text{Ca}^{2+}$ . They also have luminescent properties which can be explored for metal binding (Walters and Johnson, 1990; Bruno, et al., 1992; Henzl, et al., 1992; Frey, et al., 1996). Many  $\text{Ca}^{2+}$  binding proteins are studied for their metal binding using lanthanide spectroscopy (Horrocks, 1993). The direct excitation titration of lanthanides and tyrosine sensitized luminescence are used to determine the stoichiometry and sequence of binding for metal ions (Burroughs and Horrocks, 1994).

Metal exchange reactions are studied to understand the relative association and dissociation rates of metal ion binding. Study of these metal ions reactions in small molecules are easier than in the macromolecules. Kinetic studies with exchange reactions under pseudo first order conditions can distinguish between the dissociative process where one metal ion leaves the site before another and associative process where

an intermediate with two metals are observed. Reactions which have associative mechanism will have a linear plot for rate constant vs concentration of attacking metal ions (Breen, et al., 1984). Calcium modulated proteins such as calmodulin, troponin C, and parvalbumin are examples of proteins that are studied for metal binding (Corson, et al., 1983; Breen, et al., 1984). Intrinsic dissociation rate constants ( $k_{\text{off}}$ ) of parvalbumin were calculated using stopped flow experiments on lanthanide exchange to compare the binding affinity of  $\text{Ca}^{2+}$  between the EF and CD sites of parvalbumin (Breen, et al., 1984). In this study depending on the type of lanthanide that occupied the sites there were differences in the measured dissociation and association rates. The occupancy of the free site was the measured fast step whereas the displacement of one metal with the other was the slower step (Breen, et al., 1984).

From lanthanide studies on PvuII, it is seen there is a strong affinity and a weak affinity site ( $2 \mu\text{M}$  and  $200 \mu\text{M}$ ) (Bowen, et al., 2004). This was different from the other metal ions that were studied like  $\text{Mg}^{2+}$ ,  $\text{Ca}^{2+}$ , and  $\text{Mn}^{2+}$ , where it was difficult to distinguish the affinity of the individual sites. Thus in this system, we can selectively fill a site with lanthanide (Bowen, et al., 2004).

In order to understand the role of each metal site on the enzymatic processes we studied the metal complexes formed in the presence of mixed metals where one of the metal binding sites is occupied with a lanthanide. **Figure 4.1** shows the model for our study where there are two metal sites and there are different metal ions binding. One metal site is filled with a lanthanide metal ( $\text{M}_B$ ), and changes in spectroscopic signal and enzymatic activity are measured with the addition of various second metal ions ( $\text{M}_A$ ).

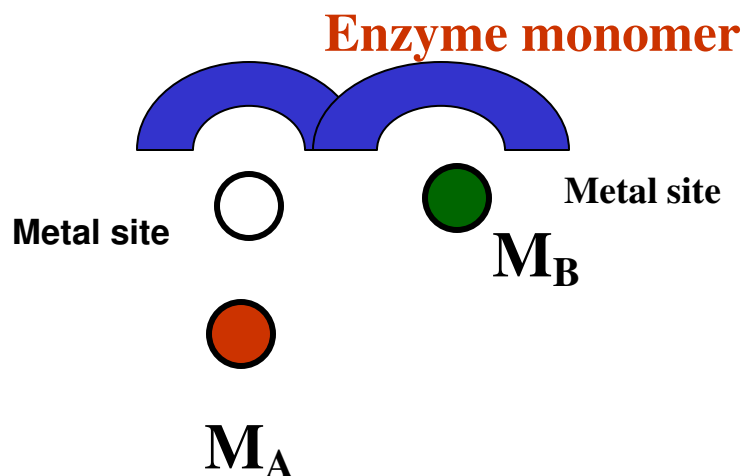


**Figure 4.1: Cartoon representation of a mixed metal enzyme complex.** The enzyme monomers of PvuII have two metal ions bound and residues Asp58, Glu68, and Lys70 and H<sub>2</sub>O molecules share the metal ligands.

Can mixed metal complexes be formed with a spectroscopically active lanthanide ion at one metal site of PvuII? Will they bind and cleave DNA? What is the difference in the rate of displacement of lanthanide from the active site by the alkaline earth metals? Can the details of this mixed metal study help us understand the role of each metal site and the association and dissociation rate for each metal at the active site?

From the earlier work it was seen that  $\text{Ca}^{2+}$  could displace the lanthanides bound at the active site of PvuII in an equilibrium experiment (Bowen, et al., 2004). The data is an equilibrium dissociation curve that can be fitted to obtain the equilibrium dissociation constant value for  $\text{Ca}^{2+}$  binding to PvuII. With this background information, we tried to form the mixed metal complexes with  $\text{Tb}^{3+}$  and study its enzymatic activity and the kinetics of lanthanide displacement using alkaline earth metals. We used competition experiments in order to detect the association and dissociation rate of various metal ions at the metal binding site of PvuII (Greenbaum, et al., 2001).

### **Methods:**

Enzyme, substrate and metal stocks were prepared as detailed in Chapter 2. Luminescence experiments used are also detailed in Chapter 2.

### **Cleavage kinetics:**

Single turnover experiments were performed with 10 nM enzyme and 2 nM DNA duplex. Reactions were performed with the mixed metals  $\text{Tb}^{3+}/\text{Mg}^{2+}$  and  $\text{Tb}^{3+}/\text{Mn}^{2+}$ . Reaction buffer has 10 mM Hepes, NaCl adjusted to a constant ionic strength and desired amount of metals. Buffer pH was adjusted to 7.0 at 37 °C. Ionic strength was fixed to a constant at 100 mM NaCl at 10 mM  $\text{MgCl}_2$ . DNA used was radiolabelled with  $^{32}\text{P}$  gamma ATP and for the reaction conditions; a small amount of radiolabelled DNA was

added to the cold DNA in order to observe the reaction. Reactions were quenched with stop dye (100mM EDTA and 10% glycerol) and analyzed as detailed in Chapter 2.

### **Fluorescence Anisotropy measurements:**

Fluorolog-3 (SPEX) machine equipped with the polarization assembly was used to measure the fluorescence intensities. HEX labeled oligonucleotide was used as the DNA substrate for the anisotropy measurements. Thermostated cell holder maintained the temperature at 25 °C and the DNA was excited at 540 nm and emission was observed at 556 nm. Anisotropy value was calculated using equation 1 below in triplicates.

$$A = (I_{\parallel} - I_{\perp}) / (I_{\parallel} + 2I_{\perp}) \quad (1)$$

The symbols in the equation represent I as the intensity of the respective polarizer orientation (parallel and perpendicular). Anisotropy is a measure of rate of tumbling of a molecule, therefore the rate of tumbling is faster for a small molecule and the anisotropy value is smaller. An increase in anisotropy values indicates a complex formation and thus can provide details about the binding (Conlan and Dupureur, 2002).

### **Results:**

#### **Competition titration for metals at the active site:**

Based on previous work at a low micromolar concentration of Tb<sup>3+</sup> (10 μM), we can specifically fill the high affinity metal binding site of PvuII (Bowen, et al., 2004). Low concentrations of protein (0.5 μM monomers) and lanthanides were used in these reactions to address the solubility issues of PvuII in presence of lanthanides. Luminescence of the bound Tb<sup>3+</sup> on PvuII was monitored to a constant signal before the addition of the second metal. The plot for these changes in the intensity of E-Tb<sup>3+</sup> complex at equilibrium (5 minutes incubation) in presence of different metals is shown in



**Figure 4.2.** This plot compares the luminescence signal for the  $\text{Tb}^{3+}$  bound complex of the enzyme with the addition of other metal ions at 5 minutes incubation time. The E- $\text{Tb}^{3+}$  complex is shown with the blue curve and with the addition of  $\text{Ca}^{2+}$ , there a decrease in the  $\text{Tb}^{3+}$  luminescence seen which is indicated by the green curve. This decrease in the luminescence indicates the displacement of  $\text{Tb}^{3+}$  from the active site of PvuII. The decrease in the  $\text{Tb}^{3+}$  luminescence was also seen with the addition of  $\text{Mn}^{2+}$  (orange curve in **Figure 4.2**). This decrease in the  $\text{Tb}^{3+}$  luminescence observed was greater with  $\text{Mn}^{2+}$  ions as compared to  $\text{Ca}^{2+}$  ions. The greater decrease in the luminescence signal with the addition of  $\text{Mn}^{2+}$  could be either because of the faster displacement of  $\text{Tb}^{3+}$  by  $\text{Mn}^{2+}$  ions than  $\text{Ca}^{2+}$  ions or a quenching of the  $\text{Tb}^{3+}$  signal by  $\text{Mn}^{2+}$  ions. With the smaller metal ion  $\text{Mg}^{2+}$ , there is an initial increase in the  $\text{Tb}^{3+}$  luminescence seen (red curve in **Figure 4.2**). This could be because  $\text{Mg}^{2+}$  binds at the second site and forms a mixed species with  $\text{Tb}^{3+}$ . This increase in the luminescence signal observed with  $\text{Mg}^{2+}$  was not an ionic strength effect because with the addition of KCl at the same ionic strength, there was no increase in intensity observed (data not shown). If we compare the ionic sizes (**Table 4.1**) of the metals used,  $\text{Mg}^{2+}$  ion is the smallest and can occupy the second metal site and effect the luminescence signal. It was seen that  $\text{Mg}^{2+}$  ions have similar affinity at the two metal sites of PvuII; and these sites are not coupled to each other and can be filled independently (Jose, et al., 1999; Xie and Dupureur, 2009). From these equilibrium studies, there are likely to be differences in the luminescence intensity of  $\text{Tb}^{3+}$  with the addition of  $\text{Ca}^{2+}$ ,  $\text{Mn}^{2+}$ , and  $\text{Mg}^{2+}$  ions. We analyzed the rate of displacement of  $\text{Tb}^{3+}$  by other metal ions ( $\text{Mn}^{2+}$ ,  $\text{Mg}^{2+}$ , and  $\text{Ca}^{2+}$ ) and mixed metal formation detailed in the later sections of this chapter.

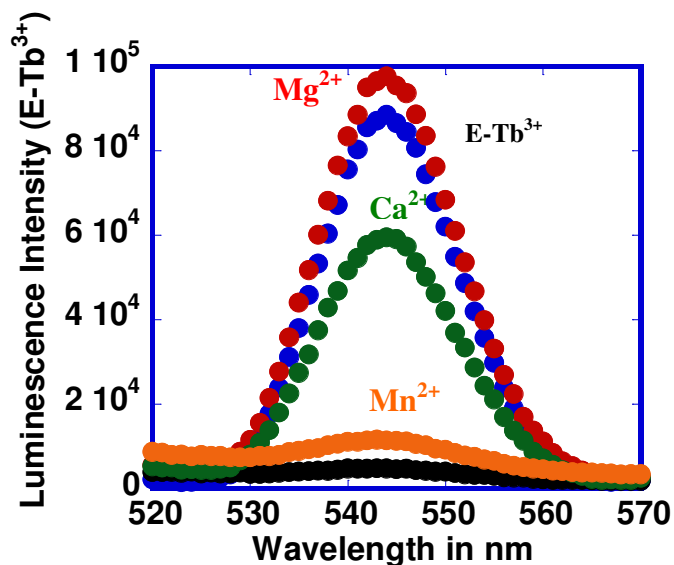


**Figure 4.2:** Luminescence intensity changes of E-Tb<sup>3+</sup> with metals, Mn<sup>2+</sup>, Ca<sup>2+</sup> and Mg<sup>2+</sup>: Changes in luminescence intensity was monitored for E-Tb complex (blue trace) formed, with 0.5  $\mu$ M PvuII monomers and 10  $\mu$ M Tb<sup>3+</sup> in a buffer 5 mM Hepes 400 mM NaCl pH 7.0 at 25 °C. When 10 mM Mg<sup>2+</sup> was added we see an increase in intensity (red trace). When 10 mM Ca<sup>2+</sup> was added we see a decrease in intensity (green trace) also with the addition of 10 mM Mn<sup>2+</sup> we see a decrease in intensity (orange trace). The black trace is for the buffer with Tb<sup>3+</sup>. Here we set the data at 5 minutes time frame. The decrease in the intensity of E-Tb complex observed is maximum with Mn<sup>2+</sup>.

**Table 4.1: Ionic radii of metal ions used in the study at various coordination.**

<b>Metals</b>	<b>Ionic radii (Å)</b>		
	<b>6</b>	<b>7</b>	<b>8</b>
<b>Mg<sup>2+</sup></b>	0.86	n/a	1.03
<b>Mn<sup>2+</sup></b>	0.97	1.04	1.10
<b>Tb<sup>3+</sup></b>	1.06	1.12	1.18
<b>Eu<sup>3+</sup></b>	1.09	1.15	1.21
<b>Ca<sup>2+</sup></b>	1.14	1.20	1.26
<b>Sr<sup>2+</sup></b>	1.32	1.35	1.40
<b>Ba<sup>2+</sup></b>	1.49	1.52	1.56

Notes: The values obtained from the reference, Shannon, 1976; Bowen and Dupureur, 2003.

**DNA binding and cleavage:**

From the equilibrium experiment using lanthanide ion and alkaline earth metals, we observed displacement of  $Tb^{3+}$  with  $Ca^{2+}$  and  $Mn^{2+}$  ions, whereas with  $Mg^{2+}$  there is mixed metal species formation. Will these mixed species formed with  $Mg^{2+}$  and  $Tb^{3+}$  bind DNA? Fluorescence anisotropy experiments with phosphoramidate DNA was performed to monitor the DNA binding of the enzyme in presence of mixed metals. Phosphoramidate DNA has modified phosphodiester backbone that has a nitrogen group instead of oxygen group at the 3'-phosphate bridging oxygen position (King, et al., 2004). An increase in anisotropy was observed under the mixed metal conditions used for PvuII, **Figure 4.3**. This increase in anisotropy, in presence of DNA, enzyme, and mixed metals  $Tb^{3+}$  and  $Mg^{2+}$  indicates that enzyme binds DNA in presence of mixed metals  $Tb^{3+}$  and  $Mg^{2+}$ .

DNA cleavage activity was measured in presence of  $Tb^{3+}$  and  $Mg^{2+}/Mn^{2+}$ . We preincubated the enzyme with  $Tb^{3+}$  for 10 minutes and then started the reaction using  $Mg^{2+}/Mg^{2+}$  ion and DNA. **Figure 4.4** shows the gel image for a reaction done at 10 mM  $Mg^{2+}$  with and without  $Tb^{3+}$ . Reactions without  $Tb^{3+}$  do show product formation, and therefore the reaction condition is not a reason for the absence of activity in presence of  $Tb^{3+}$ . We monitored these reactions at 5 mM, 10 mM, and 15 mM  $Mg^{2+}$  concentrations and did not see any product formation (data shown only for 10 mM  $Mg^{2+}$  in Figure 4). In the kinetic reactions where we pre-incubate the enzyme with  $Tb^{3+}$ , that is, when one of the metal binding sites of PvuII is filled with  $Tb^{3+}$ , DNA hydrolysis was not seen at varying  $Mg^{2+}$  concentrations. The inactivity of the enzyme could be due to the formation of a mixed metal species with  $Tb^{3+}$  and  $Mg^{2+}$  which binds DNA but does not support

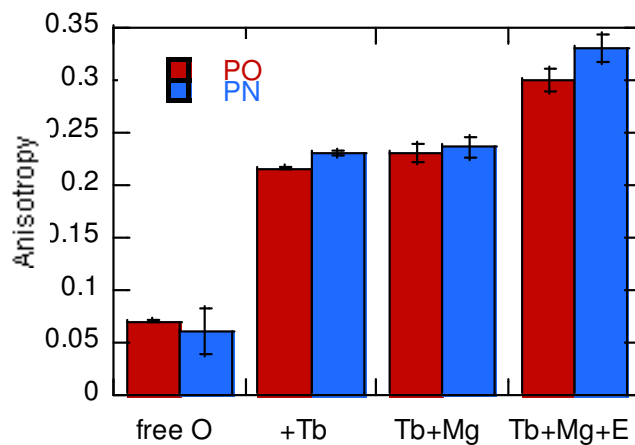


**Figure 4.3: DNA binding for the Mixed metal complexes:** Fluorescent labeled oligonucleotides (free O) with oxygen group (red bar) or nitrogen group (blue bar) at the 3' position was used for the anisotropy measurement. There is an increase in anisotropy seen for the E-DNA complex in presence of  $Tb^{2+}$  and  $Mg^{2+}$  (Dr. Dupureur's data).

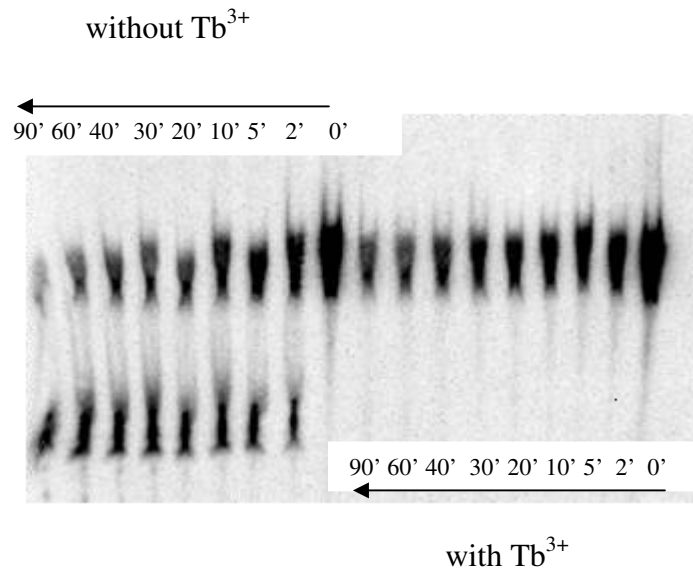


**Figure 4.4: Cleavage kinetics data of PvuII with Tb<sup>3+</sup> and Mg<sup>2+</sup> where Enzyme is preincubated with Tb<sup>3+</sup>:** 2 nM DNA and 10 nM PvuII dimers were used in the reaction at 10 mM Hepes, pH 7.0 and NaCl for constant ionic strength of 130 mM. Reactions were done at 37 °C. When the protein is incubated with Tb<sup>3+</sup> cleavage reactions is not seen at all even until 90 minutes. Under the same condition we see cleavage products when there is no Tb<sup>3+</sup>. Gel shows reactions conducted with 20 μM Tb<sup>3+</sup> and 10 mM Mg<sup>2+</sup>.

cleavage. The fact that with extended incubation no activity seen also suggests that there may not be an exchange between  $Mg^{2+}$  and  $Tb^{3+}$  because if  $EMg^{2+}Mg^{2+}$  species forms, it will hydrolyze the DNA. The data here indicate that the enzyme binds  $Tb^{3+}$  and  $Mg^{2+}$  ion cannot displace the lanthanide ion from the active site. When enzyme was not preincubated with  $Tb^{3+}$ , a distribution of metal species occurs and background DNA hydrolysis is seen, (**Figure 4.5**). This indicates the formation of  $EMg^{2+}Mg^{2+}$  and  $EMg^{2+}$  species under these conditions. After preincubation of enzyme and lanthanide,  $E-Tb^{3+}$  species is formed which could not be displaced by  $Mg^{2+}$ , and mixed metal complexes formed under these conditions are inactive.

We also looked at mixed metal complexes of  $Mn^{2+}$  and  $Tb^{3+}$ . In these reactions, there is a decrease in the rate of cleavage with  $Tb^{3+}$  as compared to that without  $Tb^{3+}$  (**Figure 4.6**). The difference in the rate is not very dramatic which could mean that the mixed species formed with  $Mn^{2+}$  and  $Tb^{3+}$  is active, or displacement of  $Tb^{3+}$  by  $Mn^{2+}$  occurs and the activity seen is from  $EMn^{2+}Mn^{2+}$  species.

In **Figure 4.6** we see the same overall trend of the activity with and without  $Tb^{3+}$ , which indicates towards the exchange of  $Tb^{3+}$  by  $Mn^{2+}$ . If there was mixed metal complex formation at higher  $Mn^{2+}$  concentration, there should have been more mixed species formed than lower  $Mn^{2+}$  and thus the overall trend of the activity should have been different.

#### **Kinetics of exchange of $Tb^{3+}$ from PvuII metal site:**

$Tb^{3+}$  luminescence spectroscopy shows that in presence of  $Ca^{2+}$  there is displacement of  $Tb^{3+}$ , which is monitored by a decrease in the  $Tb^{3+}$  luminescence. The decrease in the  $Tb^{3+}$  luminescence seen with  $Mn^{2+}$  was faster than  $Ca^{2+}$ . This could mean

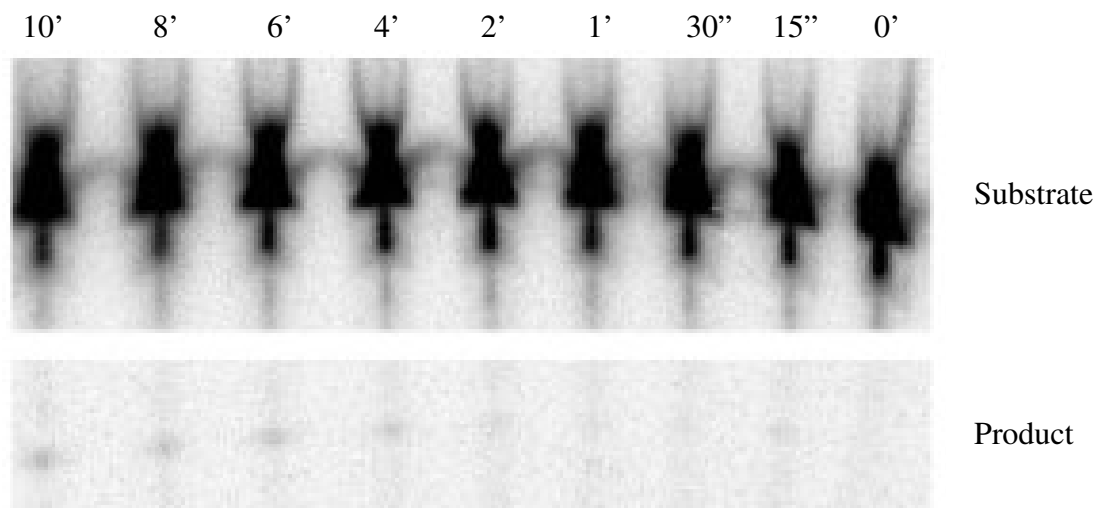


**Figure 4.5: Cleavage kinetics data of PvuII with  $Tb^{3+}$  and  $Mg^{2+}$  without preincubation of enzyme with  $Tb^{3+}$ :** 2 nM DNA and 10 nM PvuII dimers were used in the reaction at 10 mM HEPES, pH 7.0 and NaCl for constant ionic strength of 130 mM. Reactions were done at 37 °C. Gel shows reactions done with 20  $\mu$ M  $Tb^{3+}$  and 10 mM  $Mg^{2+}$ , hydrolysis activity is seen for the enzyme when both the metals are mixed together (F. Xie's work, adapted from the manuscript written by Dr. Dupureur).



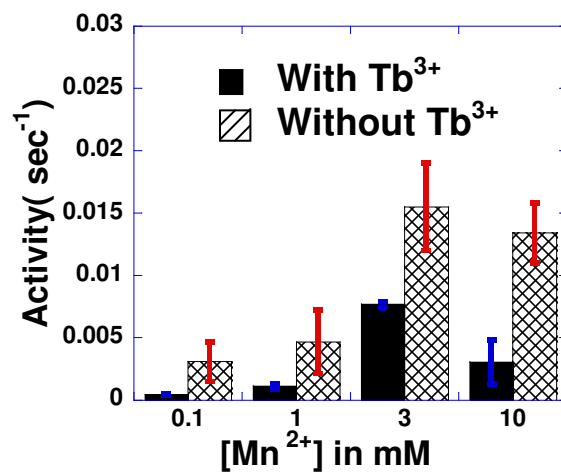


**Figure 4.6: Cleavage activity of PvuII in presence of Mn<sup>2+</sup> and Tb<sup>3+</sup>:** Cleavage activity is seen with and without Tb<sup>3+</sup>. 2 nM DNA and 10 nM PvuII dimers were used in the reaction at 10 mM HEPES, 100 mM NaCl pH 7.0 at 37 °C. At different concentrations there is activity of the enzyme with mixed metals Mn<sup>2+</sup> and Tb<sup>3+</sup>.

that the hydrolysis activity that we saw with  $\text{Mn}^{2+}$  and  $\text{Tb}^{3+}$  could mostly be due to  $\text{EMn}^{2+}\text{Mn}^{2+}$  species. With the smaller metal ion  $\text{Mg}^{2+}$  there is an initial increase in the  $\text{Tb}^{3+}$  luminescence seen. This could be because  $\text{Mg}^{2+}$  binds at the second site and forms a mixed species with  $\text{Tb}^{3+}$ . We obtained kinetic data for the each of these metals ( $\text{Mg}^{2+}$ ,  $\text{Mn}^{2+}$ , and  $\text{Ca}^{2+}$ ) to analyze for the relative dissociation rates. Data obtained is noisy and is limited to concentrations where the differences in intensity can be quantitated in real time. A set of data for the three different metals studied is shown in **Figure 4.7**, where we can see the clear difference between the exchange of these metals.

To check the reversibility of the reaction,  $\text{ETb}^{3+} + \text{Ca}^{2+} \rightleftharpoons \text{ECa}^{2+} + \text{Tb}^{3+}$ , we tried the reverse experiment where we form the  $\text{ECa}^{2+}$  complex and add  $\text{Tb}^{3+}$ . We see that as soon as  $\text{Tb}^{3+}$  is added to the  $\text{ECa}^{2+}$  complex, there is an increase in intensity seen which is stable (**Figure 4.8**). This can only be due to E- $\text{Tb}^{3+}$  complex formed. This reaction is indeed reversible under the conditions that we use and therefore the exchange process will have an association and dissociation rate constant. Both these forward and reverse rate of reaction will be a function of the association and dissociation rates for the metal ions.

We can conclude from these experiments that the size of metal ions plays an important role in its properties. Therefore  $\text{Mn}^{2+}$  and  $\text{Ca}^{2+}$  displace  $\text{Tb}^{3+}$  from the active site of PvuII, whereas  $\text{Mg}^{2+}$  does not. This displacement of  $\text{Tb}^{3+}$  is proven with the activity of the enzyme in presence of  $\text{Mn}^{2+}/\text{Tb}^{3+}$  metals. The time dependent kinetic profiles show that there are differences in the rate of displacement of the lanthanide ion from the active site by the three metal ions used here. Based on the half-life for the

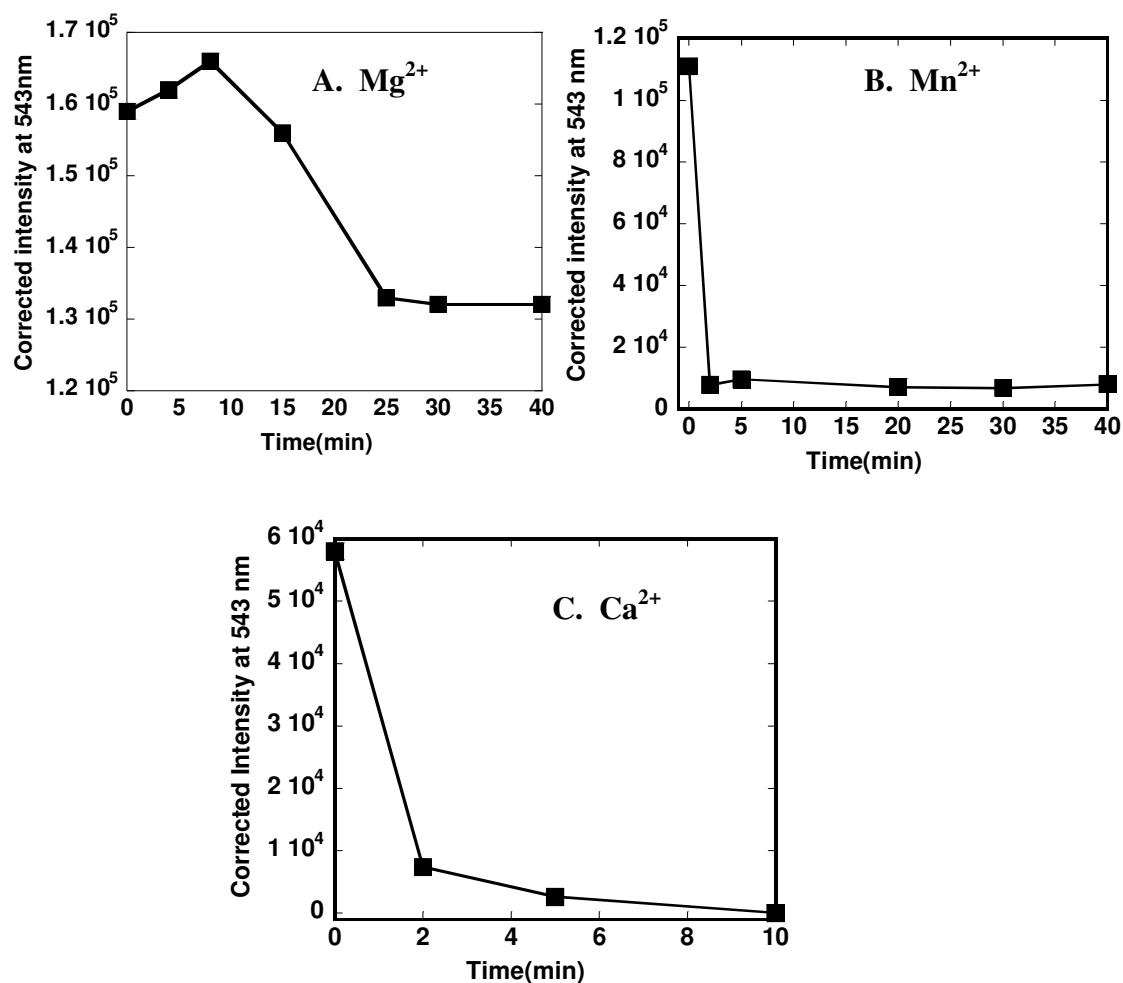


**Figure 4.7: Exchange kinetics data with three different metal ions:** A) Plot of corrected intensity vs time (min) for the competition of E-Tb<sup>3+</sup> complex with 10 mM Mg<sup>2+</sup>. B) Plot of corrected intensity vs time (min) for the competition of E-Tb<sup>3+</sup> complex with 10 mM Mn<sup>2+</sup>. C) Plot of corrected intensity vs time (min) for the competition of E-Tb<sup>3+</sup> complex with 10 mM Ca<sup>2+</sup>. Conditions: 0.5 μM enzyme monomers in 5 mM Hepes pH 7.0 and constant ionic strength of 130 mM with Puratronic NaCl and 10 μM Tb<sup>3+</sup>. Line is not a fit and is shown here to guide the eye for the trend.

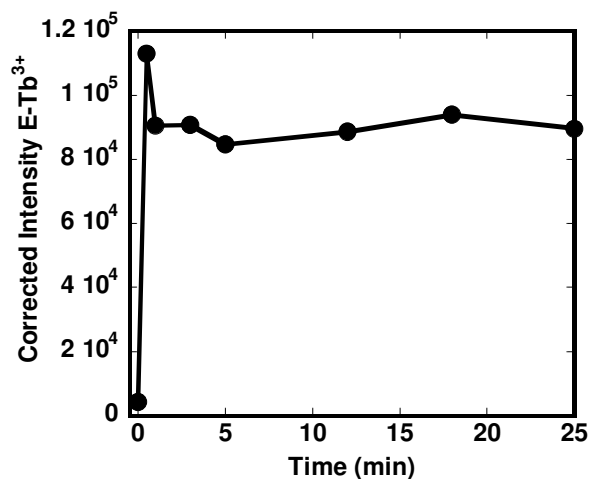


**Figure 4.8:** Exchange kinetics to check reversibility of step  $\text{ETb}^{3+} + \text{Ca}^{2+} \rightleftharpoons \text{ECa}^{2+} + \text{Tb}^{3+}$ . Plot of corrected intensity vs time (min), for the formation of  $\text{E-Tb}^{3+}$  complex on addition of  $\text{Tb}^{3+}$  to the  $\text{ECa}^{2+}$  complex. Reaction condition was  $0.5 \mu\text{M}$  enzyme monomers,  $10 \text{ mM Ca}^{2+}$  incubated for 20 minutes in  $5 \text{ mM Hepes pH } 7.0$  buffer with constant ionic strength of  $130 \text{ mM}$  using puratronic  $\text{NaCl}$ .  $5 \mu\text{M}$  of  $\text{Tb}^{3+}$  was added to check the formation of  $\text{E-Tb}^{3+}$  complex.

displacement reaction we propose that the relative rates of displacement of lanthanide by these metals is  $Mn^{2+} > Ca^{2+} > Mg^{2+}$  (**Figure 4.7**).

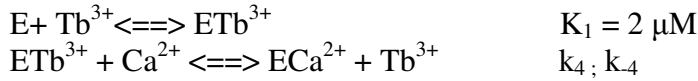
#### **Preliminary analysis of data:**

We tried to quantitate the exchange data for the relative association and dissociation rates for these metals. Initial analysis was with model shown in **Scheme 4.1** which details the filling of a site with  $Tb^{3+}$  and the exchange step in presence of  $Ca^{2+}$ . This model will account for all the free species and the single metal species ( $ETb^{3+}$  and  $E Ca^{2+}$ ). The two metal ion species are not included in this initial analysis. In presence of enzyme and two metal ions there are three possible two metal species the  $ETb^{3+}Tb^{3+}$ , the  $E Ca^{2+}Ca^{2+}$  and the  $E Ca^{2+}Tb^{3+}$ . From our experimental conditions we can rule out the  $ETb^{3+}Tb^{3+}$  species and also under these conditions  $ETb^{3+}Ca^{2+}$  does not form. Therefore this model does not account for the  $E Ca^{2+}Ca^{2+}$  species alone.

For the model in **Scheme 4.1**, we derived the differential equation as shown below which relates the concentration of  $ETb^{3+}$  species to the forward and the reverse rates of

$$\left[ ETb^{3+} \right] = e^{-\left[ k_{forward} [Ca^{2+}] - k_{reverse} K_d^{Tb^{3+}} [Ca^{2+}] / K_d^{Ca^{2+}} [Tb^{3+}] \right] t}$$

the exchange step. The equation was used to fit the data using the program Scientist to estimate the forward and the reverse rates of the exchange step. Using this scheme, the forward rate observed was  $0.8 M^{-1}sec^{-1}$ , which is a very slow association rate for metal ion displacement (**Figure 4.9**) (Breen, et al., 1984). Another limitation with this model was that we do not consider the  $E Ca^{2+}Ca^{2+}$  species formed. Therefore this model could not be used to explain the exchange process that we observe because we cannot eliminate the

**Scheme 4.1: Model for the exchange reaction using  $Tb^{3+}$  and  $Ca^{2+}$ :****Scheme 4.2: Model for the exchange reaction using  $Tb^{3+}$  and  $Ca^{2+}$  in Dynafit program:**

**Notes:** The equilibrium constants,  $K_1$ ,  $K_2$ , and  $K_3$  are known, and the association rate constant values are calculated from the dissociation rate constant values from previous studies (Conlan and Dupureur, 2002; Xie, et al., 2008). Scheme 2 has two more added steps as compared to Scheme 1.  $k_4$  is the forward rate and  $k_{-4}$  is the reverse rate for the exchange step.

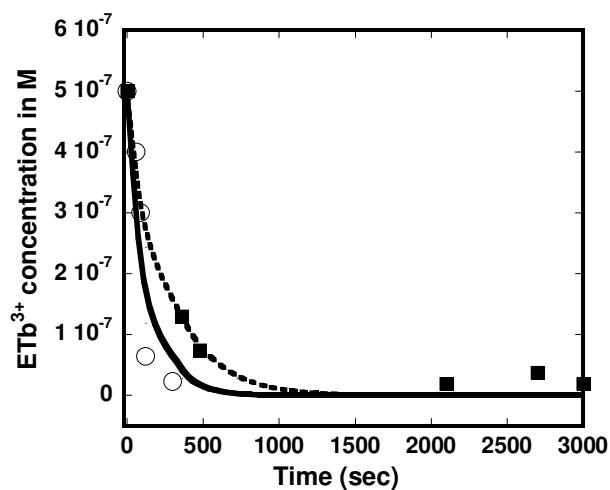


**Figure 4.9 :** Experimental data ( $\text{Ca}^{2+}$  and  $\text{Tb}^{3+}$ ) fit with model from Scheme 4.1:

Experimental data with 10 mM  $\text{Ca}^{2+}$  are shown with open circles, and the simulated curve from the model fit for the same is a solid line. The experimental data for 5 mM  $\text{Ca}^{2+}$  is shown in filled squares and simulated curve from the model fit for the same is in dashed line. The dissociation constant for the formation of  $\text{ETb}^{3+}$  used is 2  $\mu\text{M}$ . The values obtained from the model fits are  $k_{\text{forward}} = 0.8 \text{ M}^{-1}\text{sec}^{-1}$  and  $k_{\text{reverse}} = 0.01 \text{ sec}^{-1}$ .

filling of  $\text{Ca}^{2+}$  at the second site and therefore the  $\text{EC}_2$  formation. Another model shown in **Scheme 4.2** was analyzed for the forward and reverse rate of the exchange step which includes all the possible species. The data from the competition experiments was used to fit to the model using program Dynafit. The limitation of this analysis is the amount of data available. From the earlier work done in the lab, the dissociation constant values  $K_1$  (Bowen, et al., 2004),  $K_2$  and  $K_3$  (Jose, et al., 2002) are known. From this, educated guesses were made for the dissociation rate, and association rates were calculated. All the data sets fits to this model reasonably well and the parameters floated have low errors (**Figure 4.10**). The floated association rate for the step fits to  $k_4 = 0.5 \text{ M}^{-1} \text{ sec}^{-1}$  and the dissociation rate  $k_{-4} = 0.001 \text{ sec}^{-1}$ . The equilibrium constant calculated for the  $K_4$  step from the fitted association and dissociation rate is 2.23 mM. The association rate here represents association rate of calcium by displacing terbium. The values obtained for the association rate is  $0.5 \text{ M}^{-1} \text{ sec}^{-1}$  and that for the dissociation rate as  $0.001 \text{ sec}^{-1}$  which is slow for the metal binding step.

### **Conclusion:**

A question that has received attention in many enzymes and proteins is if there are multiple metal binding sites whether or not all metal sites have to be occupied in order for the protein/enzyme to function. The protein calmodulin has been investigated for whether it is necessary to fill all four sites of calmodulin in order to activate it (Tsai, et al., 1987). Many proteins/enzymes are studied in order to understand the role of each metal site in various processes. Indirect measurement of the metal association and dissociation rate were also characterized in such studies in order to understand the metal binding at the active site. In our study, under mixed metal condition using  $\text{Mg}^{2+}$  and  $\text{Tb}^{3+}$



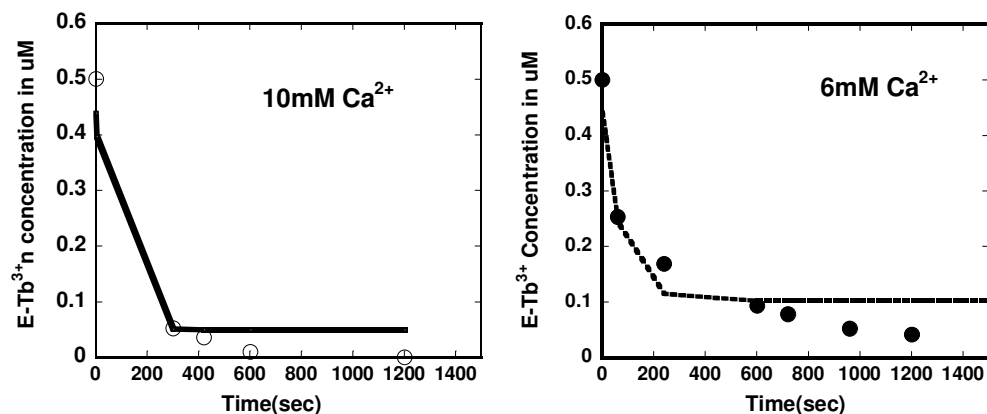


**Figure 4.10 :** Experimental data ( $\text{Ca}^{2+}$  and  $\text{Tb}^{3+}$ ) fit with model from Scheme 4.2:

Experimental data with 10 mM  $\text{Ca}^{2+}$  are shown with open circles, and the simulated curve from the model fit for the same is a solid line. The experimental data for 6 mM  $\text{Ca}^{2+}$  is shown in filled circles and simulated curve from the model fit for the same is in dashed line. The dissociation constants used for  $\text{ECa}^{2+}\text{Ca}^{2+}$  formation was 2 mM, 2  $\mu\text{M}$  for the  $\text{ETb}^{3+}$  formation, and 120  $\mu\text{M}$  for the formation of  $\text{ECa}^{2+}$ . The model fits for the exchange step,  $\text{ETb}^{3+} + \text{Ca}^{2+} \rightleftharpoons \text{ECa}^{2+} + \text{Tb}^{3+}$ , association and dissociation rate constant and the calculated equilibrium constants obtained is 2.23 mM.

ions did not show any cleavage activity. Also we observed the displacement of  $Tb^{3+}$  ions from the active site with the addition of  $Mn^{2+}$  and  $Ca^{2+}$  which is confirmed by the cleavage activity. The exchange kinetics data for the displacement of  $Tb^{3+}$  ions from the active site with the addition of other metal ions were analyzed for the association and dissociation rates for the metals. This analysis is limited because of the limited data which could be collected. Solubility issues limit the conditions at which data can be collected, and the spectroscopic silence of the metal ions like  $Ca^{2+}$  and  $Mg^{2+}$  limits the type of species that could be observed. From the preliminary analysis using  $Ca^{2+}$  data parameters for the exchange step was obtained. This analysis will be complete and we can have more confidence on the parameters obtained only if the model used could be analyzed for datasets with other metals. So far we do not have data sets with other metal ions in order to do this analysis. With  $Mg^{2+}$  ion we could not get data at different concentrations without the noisy background, whereas for the  $Mn^{2+}$  ions the data obtained was very fast. Metal ions like  $Ba^{2+}$  and  $Sr^{2+}$  ions will be tried in order to collect more data for the global analysis. Also, these trials in another protein will help us clarify some of the values for the parameters associated with the exchange reactions, obtained from our preliminary analysis.

**References:**

- Andersson, T., T. Drakenberg, et al. (1981). "Calcium binding to porcine pancreatic phospholipase A2 studied by  $^{43}\text{Ca}$  NMR." *FEBS Lett* **123**(1): 115-7.
- Aqvist, J. and A. J. Warshel (1990). "Free energy relationships in metalloenzyme-catalyzed reactions. Calculations of the effects of metal ion substitutions in Staphylococcal nuclease." *Journal of American Chemical Society* **112**: 2860-2868.
- Balendiran, K., J. Bonventre, et al. (1994). "Expression, purification, and crystallization of restriction endonuclease PvuII with DNA containing its recognition site." *Proteins* **19**(1): 77-9.
- Barshop, B. A., R. F. Wrenn, et al. (1983). "Analysis of numerical methods for computer simulation of kinetic processes: development of KINSIM-A flexible, Portable system." *Analytical Biochemistry* **130**: 134-145.
- Bauer, W. (1978). *Annual Review of Biophysics and Bioengineering* **7**: 287-313.
- Beernink, P. T., B. W. Segelke, et al. (2001). "Two divalent metal ions in the active site of a new crystal form of human apurinic/aprimidinic endonuclease, Ape1: implications for the catalytic mechanism." *J Mol Biol* **307**(4): 1023-34.
- Beese, L. S. and T. A. Steitz (1991). "Structural basis for the 3'-5' exonuclease activity of Escherichia coli DNA polymerase I: a two metal ion mechanism." *Embo J* **10**(1): 25-33.
- Berezin, B. D., S. V. Rumyantseva, et al. (2004). "Kinetics of metal exchange between cadmium Mesoporphyrin and Zinc and Cobalt salts in organic solvents." **30**(4): 291-295.
- Biver, T., R. Friani, et al. (2008). "Mechanism of Indium(III) exchange between NTA and Transferrin: A Kinetic Approach." *Journal of Physical Chemistry* **112**: 12168-12173.
- Black, C. B. and J. A. Cowan (1997). "Inert chromium and cobalt complexes as probes of magnesium-dependent enzymes. Evaluation of the mechanistic role of the essential metal cofactor in Escherichia coli exonuclease III." *Eur J Biochem* **243**(3): 684-9.
- Bowen, L. M. and C. M. Dupureur (2003). "Investigation of restriction enzyme cofactor requirements: a relationship between metal ion properties and sequence specificity." *Biochemistry* **42**(43): 12643-53.
- Bowen, L. M., G. Muller, et al. (2004). "Lanthanide spectroscopic studies of the dinuclear and Mg(II)-dependent PvuII restriction endonuclease." *Biochemistry* **43**(48): 15286-95.
- Brautigam, C., K. Aschheim, et al. (1999). "Structural elucidation of the binding and inhibitory properties of lanthanide(III) ions at the 3'-5' exonucleolytic active site of the Klenow fragment." *Chemistry and Biology* **6**: 901-908.
- Breen, P. J., J. A. Kenneth, et al. (1984). "Stopped flow kinetic studies of metal ion dissociation or exchange in a tryptophan containing Parvalbumin." *Biochemistry* **24**: 4997-5004.
- Bruno, J., W. D. J. Horrocks, et al. (1992). "Europium(III) luminescence and tyrosine to terbium(III) energy transfer studies of invertebrate(octopus) calmodulin." *Biochemistry* **31**(7016-7026): 31.

- Burroughs, S. E. and W. D. J. Horrocks (1994). "Characterization of the lanthanide Ion-binding properties of calcineurin-B using laser induced luminescence spectroscopy." Biochemistry **33**: 10428-10436.
- Conlan, L. H. and C. M. Dupureur (2002). "Dissecting the metal ion dependence of DNA binding by PvuII endonuclease." Biochemistry **41**(4): 1335-42.
- Conlan, L. H. and C. M. Dupureur (2002). "Multiple metal ions drive DNA association by PvuII endonuclease." Biochemistry **41**(50): 14848-55.
- Corson, D. C., T. C. Williams, et al. (1983). "Calcium Binding Proteins: Optical Stopped-Flow and Proton Nuclear Magnetic Resonance Studies of the Binding of the Lanthanide Series of Metal Ions Parvalbumin." Biochemistry **22**: 5882-5889.
- Cowan, J. A. (1991). "Coordination Chemistry of Mg<sup>2+</sup> and 5s rRNA (Escherichia coli): Binding parameters, ligand symmetry and Implications of activity." Journal of american chemical society **113**: 675-676.
- Cuatrecasas, P., S. Fuchs, et al. (1967). "Catalytic properties and specificity of the extracellular nuclease of Staphylococcus aureus." J Biol Chem **242**(7): 1541-7.
- Diamond, T. L. and F. D. Bushman (2006). "Role of metal ions in catalysis by HIV integrase analyzed using a quantitative PCR disintegration assay." Nucleic Acids Res **34**(21): 6116-25.
- Doan, L., B. Handa, et al. (1999). "Metal ion catalysis of RNA cleavage by the influenza virus endonuclease." Biochemistry **38**(17): 5612-9.
- Drakenberg, T., T. Andersson, et al. (1984). "Calcium ion binding to pancreatic phospholipase A2 and its zymogen: a <sup>43</sup>Ca NMR study." Biochemistry **23**(11): 2387-92.
- Dupureur, C. M. (2008). "Roles of metal ions in nucleases." Curr Opin Chem Biol **12**(2): 250-5.
- Dupureur, C. M. and L. H. Conlan (2000). "A catalytically deficient active site variant of PvuII endonuclease binds Mg(II) ions." Biochemistry **39**(35): 10921-7.
- Etzkorn, C. and N. C. Horton (2004). "Mechanistic insights from the structures of HincII bound to cognate DNA cleaved from addition of Mg<sup>2+</sup> and Mn<sup>2+</sup>." J Mol Biol **343**(4): 833-49.
- Feng, H., L. Dong, et al. (2006). "Catalytic mechanism of endonuclease v: a catalytic and regulatory two-metal model." Biochemistry **45**(34): 10251-9.
- Fersht, A. (1999). "Structure and mechanism in protein Science." W.H. Freeman and Co., NY, NY: 1-631.
- Fierke, C. A. and G. G. Hammes (1995). "Transition kinetic approaches to enzyme mechanisms." Methods Enzymol. **249**: 3-37.
- Forsen, S., A. Andersson, et al. (1983). "Calcium binding proteins."
- Frankel, A. D., J. M. Berg, et al. (1987). "Metal dependent folding of a single zinc finger from transcription factor IIIA." Proc Natl Acad Sci U S A **84**: 4841-4845.
- Frey, M. W., S. T. Frey, et al. (1996). "Elucidation of the metal binding properties of the Klenow fragment of echerichia coli polymerase I and bacteriophage T4 DNA polymerase by lanthanide (III) luminescence spectroscopy." **3**(5): 393-403.
- Gifford, J. L., M. P. Walsh, et al. (2007). "Structures and metal-ion-binding properties of the Ca<sup>2+</sup>-binding helix-loop-helix EF-hand motifs." Biochem J **405**(2): 199-221.

- Greenbaum, N. L., C. Mundoma, et al. (2001). "Probing of metal binding domains of RNA Hairpin loops by laser induced lanthanide(III) luminescence." Biochemistry **40**: 1124-1134.
- Grigorescu, A., M. Horvath, et al. (2004). "The integration of recognition and cleavage: X-ray structures of the pre-transition state complex, post reactive complex and the DNA-free endonuclease." In: Restriction Endonucleases: 137-177.
- Groll, D. H., A. Jeltsch, et al. (1997). "Does the restriction endonuclease EcoRV employ a two metal ion mechanism for DNA cleavage?" Biochemistry **36**(38): 11389-11401.
- Haraguchi, K. and H. Frieser (1983). "Kinetics and Mechanism of the metal exchange reaction of the Bis(8-mercaptoquinolato)nickel(II) chelate with copper(II) ion by an Exchange-Extraction method." Inorganic Chemistry **22**: 653-655.
- Harris, W. R., Z. Wang, et al. (2003). "Kinetics of Metal Ion Exchange between Citric Acid and Serum Transferrin." Inorganic Chemistry **42**: 5880-5889.
- Hayes, R. L. and K. F. Hubner (1983). "Metal ions in Biological system." **16**.
- Henzl, M. T., C. L. Trevino, et al. (1992). "Evidence that deprotonation of serine-55 is responsible for the pH dependence of the parvalbumin  $\text{Eu}^{3+}$  7F<sub>0</sub> → 5D<sub>0</sub> spectrum." FEBS Lett **314**(2): 130-134.
- Horton, J. R. and X. Cheng (2000). "PvuII endonuclease contains two calcium ions in active sites." J Mol Biol **300**(5): 1049-56.
- Horton, N. C. and J. J. Perona (2004). "DNA cleavage by EcoRV endonuclease: two metal ions in three metal ion binding sites." Biochemistry **43**(22): 6841-57.
- Jack, W. E., L. Greenough, et al. (1991). "Overexpression, purification and crystallization of BamHI endonuclease." Nucleic Acids Res **19**(8): 1825-9.
- Jose, T. J., L. H. Conlan, et al. (1999). "Quantitative evaluation of metal ion binding to PvuII restriction endonuclease." J Biol Inorg Chem **4**(6): 814-23.
- Junop, M. S. and D. B. Haniford (1996). "Multiple roles for divalent metal ions in DNA transposition: distinct stages of Tn10 transposition have different Mg<sup>2+</sup> requirements." Embo J **15**(10): 2547-55.
- King, J. B., L. M. Bowen, et al. (2004). "Binding and conformational analysis of phosphoramidate-restriction enzyme interactions." Biochemistry **43**(26): 8551-9.
- Kostrewa, D. and F. K. Winkler (1995). "Mg<sup>2+</sup> binding to the active site of EcoRV endonuclease: a crystallographic study of complexes with substrate and product DNA at 2 Å resolution." Biochemistry **34**(2): 683-96.
- Kuzmic, P. (1996). "Program DYNAFIT for the analysis of enzyme kinetic data: application to HIV proteinase." Anal Biochem **237**(2): 260-73.
- Kuzmic, P., A. G. Peranteau, et al. (1996). "Mechanical effects on the kinetics of the HIV proteinase deactivation." Biochem Biophys Res Commun **221**(2): 313-7.
- Lee, M. E. and T. Nowak (1992). "Metal ion specificity at the catalytic site of yeast enolase." Biochemistry **31**(7): 2172-80.
- Lippard, S.J. and Berg, J.M. (1994). Principles of Bioinorganic Chemistry. Mill Valey, California, University Science Books.
- Lott, W. B., B. W. Pontius, et al. (1998). "A two-metal ion mechanism operates in the hammerhead ribozyme-mediated cleavage of an RNA substrate." Proc Natl Acad Sci U S A **95**(2): 542-7.

- Lukas, C. M., R. Kucera, et al. (2000). "Understanding the immutability of restriction enzymes: crystal structure of BglII and its DNA substrate at 1.5 Å resolution." Nat Struct Biol **7**: 134-150.
- Martell, A. E. and R. M. Smith (1989). "Critical stability constants." Plenum, New York.
- Martin, R. B. (1984). "Metal ions in Biological systems." Sigel, H., Ed, Marcel Dekker, New York **17**: 32-49.
- Moeller, T. (1963). "The chemistry of the lanthanides." Reinhold, New York.
- Mones, L., P. Kulhanek, et al. (2007). "Probing the two-metal ion mechanism in the restriction endonuclease BamHI." Biochemistry **46**(50): 14514-23.
- Mones, L., I. Simon, et al. (2007). "Metal-binding sites at the active site of restriction endonuclease BamHI can conform to a one-ion mechanism." Biol Chem **388**(1): 73-8.
- Nastri, H. G., P. D. Evans, et al. (1997). "Catalytic and DNA binding properties of PvuII restriction endonuclease mutants." J Biol Chem **272**(41): 25761-7.
- Newman, M., K. Lunnen, et al. (1998). "Crystal structure of restriction endonuclease BglII bound to its interrupted DNA recognition sequence." Embo J **14**: 5466-5476.
- Nowotny, M., S. A. Gaidamakov, et al. (2005). "Crystal structures of RNase H bound to an RNA/DNA hybrid: substrate specificity and metal-dependent catalysis." Cell **121**(7): 1005-16.
- Outten, C. E. and T. V. O'Halloran (2001). "Femtomolar sensitivity of metalloregulatory proteins controlling zinc homeostasis." Science **292**(5526): 2488-92.
- Pace, C.N., Vajdos, F., Fee, L., Grimsley, G. and Gray, T. (1995). "How to measure and predict the molar absorption coefficient of a protein." Protein Sci **4**:2411-23.
- Pakdaman, R., F. B. Abdallah, et al. (1999). "Transferrin, is a Mixed Chelate-Protein Ternary Complex Involved in the Mechanism of Iron Uptake by Serum-transferrin in Vitro?" Journal of Molecular Biology **293**: 1273-1284.
- Papadakos, G.A. (2008). "The effect of active site mutations on the homodimeric behavior of the PvuII restriction endonuclease." Dissertation thesis.
- Pennella, M. A. and D. P. Giedroc (2005). "Structural determinants of metal selectivity in prokaryotic metal-responsive transcriptional regulators." Biomaterials **18**(4): 413-28.
- Pingoud, A., M. Fuxreiter, et al. (2005). "Type II restriction endonucleases: structure and mechanism." Cell Mol Life Sci **62**(6): 685-707.
- Pingoud, A. and A. Jeltsch (2001). "Structure and function of type II restriction endonucleases." Nucleic Acids Res **29**(18): 3705-27.
- Pingoud, V., A. Sudina, et al. (2005). "Specificity changes in the evolution of type II restriction endonucleases: a biochemical and bioinformatic analysis of restriction enzymes that recognize unrelated sequences." J Biol Chem **280**(6): 4289-98.
- Shan, S., A. V. Kravchuk, et al. (2001). "Defining the catalytic metal ion interactions in the Tetrahymena ribozyme reaction." Biochemistry **40**(17): 5161-71.
- Soundar, S., M. O'Hagan, et al. (2006). "Identification of Mn<sup>2+</sup>-binding aspartates from alpha, beta, and gamma subunits of human NAD-dependent isocitrate dehydrogenase." J Biol Chem **281**(30): 21073-81.
- Spyridaki, A. C., T. Matzen, et al. (2003). "Structural and Biochemical characterization of a new Mg<sup>(2+)</sup> binding site near Tyr94 in the restriction endonuclease PvuII." Biol Chem **331**(2): 395-406.

- Stahley, M. R., P. L. Adams, et al. (2007). "Structural metals in the group I intron: a ribozyme with a multiple metal ion core." J Mol Biol **372**(1): 89-102.
- Steitz, T. A. and J. A. Steitz (1993). "A general two-metal-ion mechanism for catalytic RNA." Proc Natl Acad Sci U S A **90**(14): 6498-502.
- Sun, H., H. Li, et al. (1999). "Human serum transferrin cobalt complex: Stability and cellular uptake of cobalt." Chem reviews **99**.
- Suzuki, T., S. Hirofusa, et al. (1994). "Kinetics of the Metal exchange reaction of a Cu(II)-Poly(vinyl Alcohol) complex with Zn(II)-Ethylenediamine-N,N,N',N'-tetraacetic Acid in aqueous solution." Journal of Inorganic and organometallic Polymers **4**(3): 251-257.
- Tock, M. R. and D. Dryden (2005). "The biology of restriction and anti restriction." **8**: 466-472.
- Tsai, M. D., T. Drakenberg, et al. (1987). "Is the binding of Magnesium(II) to calmodulin significant? An Investigation by magnesium-25 Nuclear Magnetic Resonance." Biochemistry **26**: 3635-3643.
- Viadiu, H. and A. K. Aggarwal (1998). "The role of metals in catalysis by the restriction endonuclease BamHI." Nat Struct Biol **5**(10): 910-6.
- Vipond, I. B., G. S. Baldwin, et al. (1995). "Divalent metal ions at the active sites of the EcoRV and EcoRI restriction endonucleases." Biochemistry **34**(2): 697-704.
- Vipond, I. B. and S. E. Halford (1995). "Specific DNA recognition by EcoRV restriction endonuclease induced by calcium ions." Biochemistry **34**(4): 1113-9.
- Walters, J. D. and J. D. Johnson (1990). "Terbium as luminescent probe of metal binding sites in Protein kinase C." Journal of biological chemistry **265**(8): 4223-4226.
- Xie, F. and C. M. Dupureur (2009). "Kinetic analysis of product release and metal ions in a metallonuclease." Arch Biochem Biophys **483**(1): 1-9.
- Xie, F., S. H. Qureshi, et al. (2008). "One- and two-metal ion catalysis: global single-turnover kinetic analysis of the PvuII endonuclease mechanism." Biochemistry **47**(47): 12540-50.
- Zhang, D., I. M. Kovach, et al. (2008). "Locating the rate-determining step(s) for three-step hydrolase-catalyzed reactions with DYNAFIT." Biochim Biophys Acta **1784**(5): 827-33.

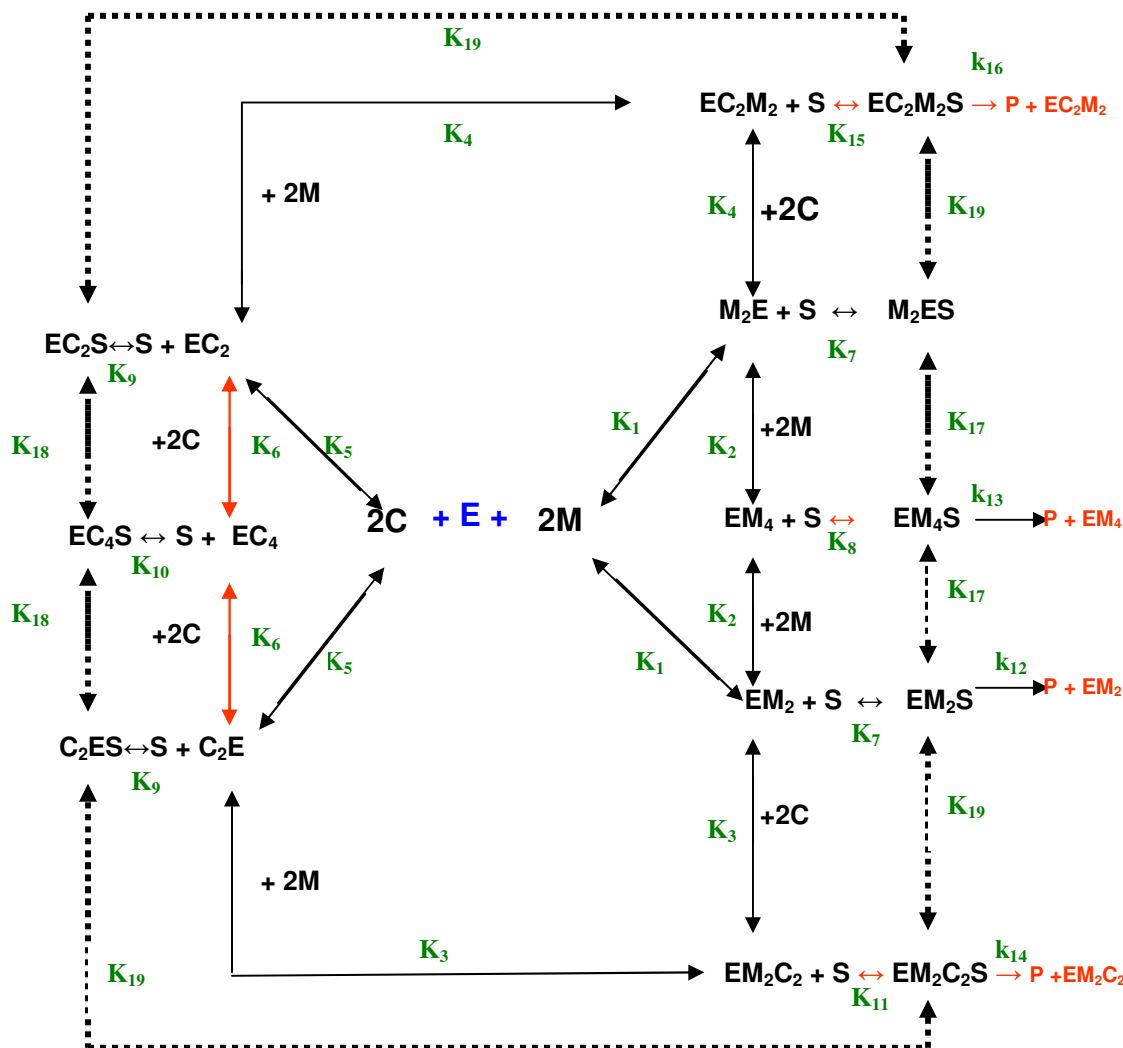
## APPENDIX

### Models using specific sites for metal binding.

PvuII binds to two metal ions and therefore we can specify the metal binding sites as site A and site B. Either of the site can be filled by a particular metal first followed by the other under mixed metal condition. For  $\text{Ca}^{2+}$  ion binding there is a higher affinity site that was previously studied (Jose, et al., 1999). It is not known whether this high affinity site is site A or site B. In our models we also tried site specific models where we represented site A species as  $\text{EM}_2/\text{EC}_2$  and the site B species as  $\text{M}_2\text{E}/\text{C}_2\text{E}$  species. These models as shown in **Scheme A1**, with and without interconversion step, did fit the experimental data when one or both mixed species are active. Parameters used for this set of trials are shown in **Table 3.4**.  $\text{EM}_2$  and  $\text{M}_2\text{E}$  formation were given the same parameter values. These species are differentiated only at the cleavage step where  $\text{EM}_2\text{S}$  species is active and  $\text{M}_2\text{ES}$  species is inactive. In our initial trials, we only used models with  $\text{EM}_2/\text{M}_2\text{E}$  species. The species  $\text{EM}_2$ ,  $\text{M}_2\text{E}$ ,  $\text{EC}_2$ , and  $\text{C}_2\text{E}$  cannot be distinguished experimentally and therefore all these parameters used were estimated. There are no experimental or calculated parameter values for the  $\text{M}_2\text{E}$  and  $\text{C}_2\text{E}$  species that are used in these model trials to specify the sites. Addition of these species to the models increases the number of unknown parameters in these models and therefore provides less confidence on the ability of these models to explain the experimental data.

An overlay plot at 10 mM  $\text{Mg}^{2+}$  and varying  $\text{Ca}^{2+}$  concentration for this model with or without interconversion step is shown in **Figure A1**. A lot more parameters had to be floated in order to get these set of models to converge. These models might have





**Scheme A1: Model with the site specific species  $M_2E$  and  $C_2E$ :** Here a model with the site specific species is shown. The dotted line represents the interconversion step. The model trials performed for this model did not include all steps since it was difficult for models to converge. Species shown in red are at the product step.  $M_2E$  species formed are assumed to be inactive in order to specify sites.

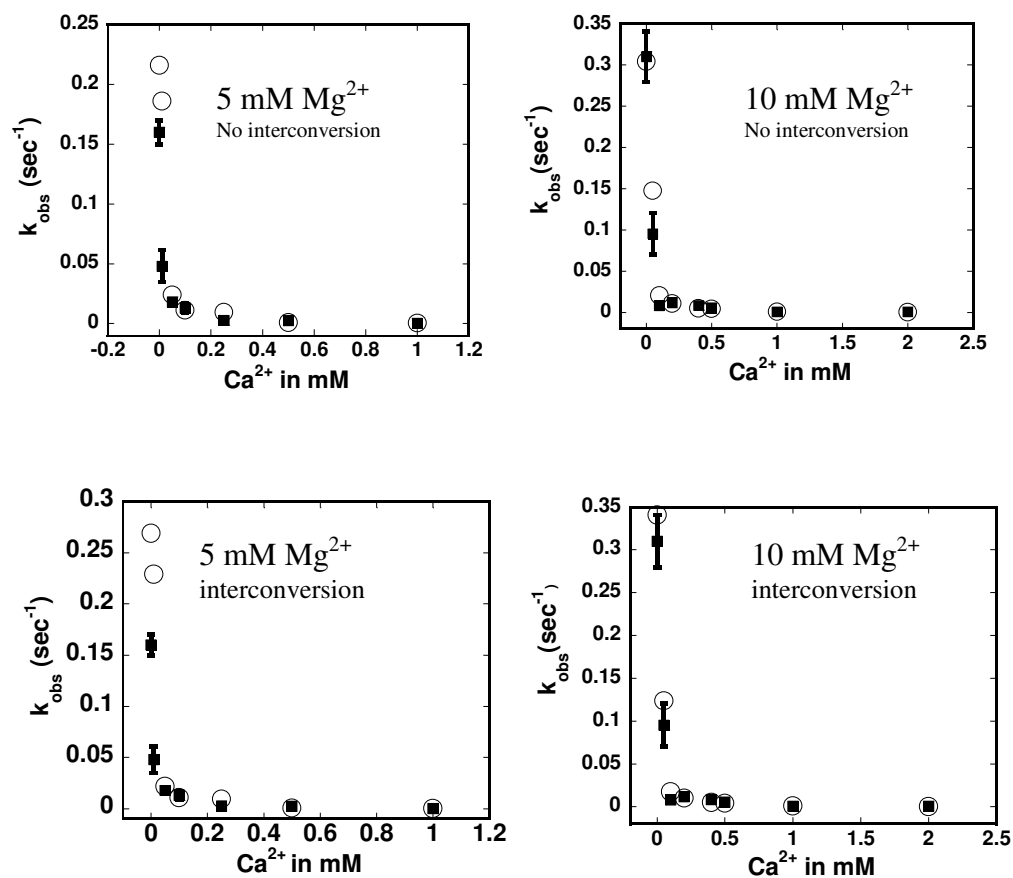


**Figure A1: Model with site specific species  $\text{EM}_2$  and  $\text{M}_2\text{E}$ :** The  $k_{\text{obs}}(\text{sec}^{-1})$  of the experimental data at fixed  $\text{Mg}^{2+}$  concentration of 5 mM and 10 mM and varying concentrations of  $\text{Ca}^{2+}$  with error bars is shown as black rectangles and fitted data curves from the fits are shown with open circles. The top panels are for models without interconversion and bottom panels for the models with interconversion.  $\text{C}_2\text{E}$  steps are not included in these model trials.

helped us distinguish between what types of mixed species are formed and whether all the mixed species formed are active. We could not continue with our analysis of these types of models because there were many steps added in this model, which made it difficult to analyze them.

### **Simulations for mixed species parameter that effects the model fit.**

In most of the models with mixed species shown in Chapter 3, there are 6 parameters that were floated. For models with mixed species formed and active, the output for these parameter values were similar to each other and with smaller errors. We also tried to vary fewer parameters in order to see which of these parameters effects model fit the most. In one such trial, we floated only the  $K_5$  and  $K_{10}$  parameters, and the model output (model 1e) is similar to that obtained from the fit where we floated more parameters (**Figure A2**). Other parameters were fixed to values obtained from the earlier fits.

This leads to a question about how much we know about these numbers and to what range can these numbers be varied? In **Scheme 3.3**, where we have all the mixed species formed, we do not have information about parameters  $K_3$ ,  $K_4$ ,  $K_{11}$ ,  $K_{15}$ ,  $k_{14}$  and  $k_{16}$ . Based on the  $Ca^{2+}$  and  $Mg^{2+}$  species studied for the metal binding and DNA binding of PvuII, we can guess for these parameters which has mixed metal species. We can surely restrict the numbers so that they are at a certain range for example, the parameters  $K_{11}$  and  $K_{15}$  represents DNA binding values of mixed species which can be varied in nanomolar to picomolar range for a nuclease such as PvuII. Parameter  $K_3$  is the  $Ca^{2+}$  binding at the second site when there is one  $Mg^{2+}$  ion at the active site. We guessed this parameter value to be in micromolar range because of the indicative tighter  $Ca^{2+}$  site from

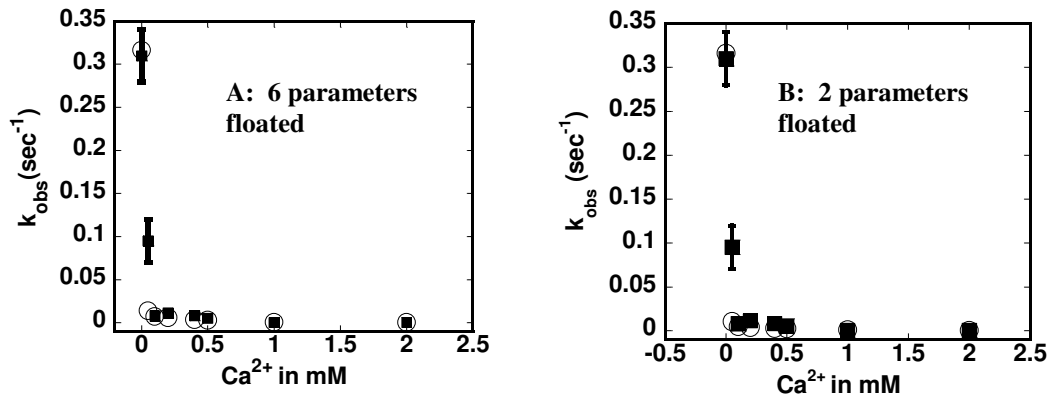


**Figure A2: Fits using Model 1e with different set of parameters floated.** In panel **A** for the fit using model 1e there were 6 parameters that were floated ( $k_5$ ,  $k_{10}$ ,  $k_{11}$ ,  $k_{15}$ ,  $k_{14}$ , and  $k_{16}$ ). In panel **B** for the fit to model 1e only  $k_5$  and  $k_{10}$  were floated. The association rate constants for the steps were floated with the fixed number for the dissociation rate constant as described in table1. The floated value of the association rate constant gives varying numbers for the Dissociation constants ( $K_d$ ) of each of these steps. We see similar fits for these two cases, so we conclude that all the model fits depends mostly on parameters  $K_5$  and  $K_{10}$ .

our datasets. From the model fits, the parameter value obtained for  $K_3$  is 270  $\mu\text{M}$ . We also tried varying this number in the models in order to see effect of this parameter on the model. The fit would converge only when this parameter ( $K_3$ ) could be varied in the micromolar range in our simulations (data not shown).

The parameter  $K_4$ , which is the  $\text{Mg}^{2+}$  binding at the second site when there is one  $\text{Ca}^{2+}$  ion at the active site, could not be varied very much. From the model fits, the parameter value that we used was 3.16 mM, which is consistent with the second  $\text{Mg}^{2+}$  binding step for single metal species (Xie, et al., 2008). In simulations parameter  $K_4$  could only be varied in low mM range, which did not change the amount of product formed. As shown in **Figure A3**, the progress curve output from a simulation using model 1e, are similar for  $K_4$  values from 1 mM-3 mM range. The experimental data obtained for the 10 mM  $\text{Mg}^{2+}$ , 100  $\mu\text{M}$   $\text{Ca}^{2+}$  overlays well with the simulated curves using  $K_4$  values ranging 1-3 mM. Simulations for  $K_{11}$  and  $K_{15}$  showed that there is not a big difference in the fits when this set of parameters is varied from  $\mu\text{M}$  to pM range; these parameters were always floated during the model fits. From our model trials, we learned that a fit to the experimental data depends on the amount of active mixed species and parameter  $K_5$  and  $K_{10}$ . Models are dependent on these parameters and therefore on the amount of  $\text{EC}_2$  and the  $\text{EC}_4\text{S}$  formed. Our analysis shows that the models used here mostly depend on parameters  $K_5$  and  $K_{10}$  which were determined experimentally (Jose, et al., 1999; Bowen and Dupureur, 2003). All the numbers for the mixed metal steps can be varied and the range of numbers that we can get from our models can be judged on the basis of metal and DNA binding parameters of single metal species. These

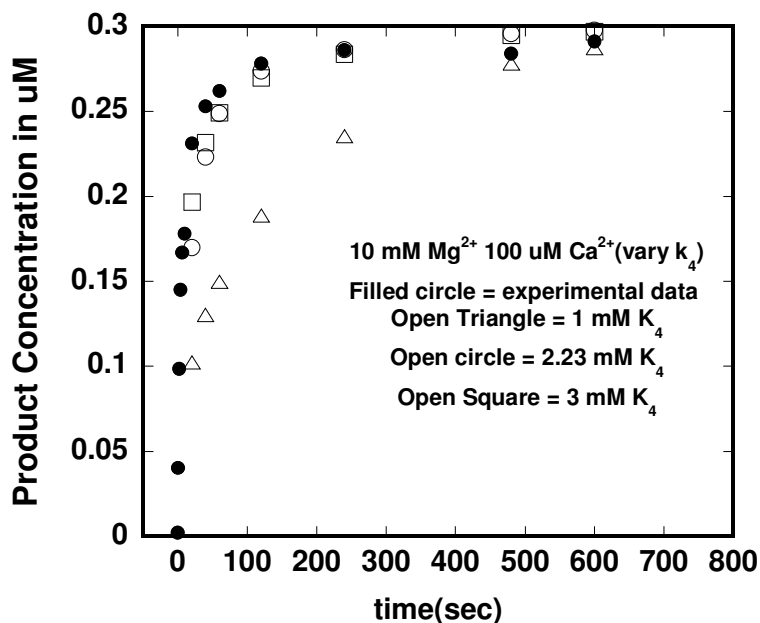


**Figure A3: Progress curve output from the simulation of parameter value  $K_4$  ( $EC_2M_2$  formation):** An initial guess for these numbers were made based on the values that are known for single metal ion binding. For the  $EC_2M_2$  formation we used a value 3.1 mM same as that for the  $EM_4$  formation (Xie, et al., 2008). This parameter represents the binding of second  $Mg^{2+}$  ion in presence of one metal ion either  $Ca^{2+}/Mg^{2+}$ . The experimental data obtained for the 10 mM  $Mg^{2+}$ , 100  $\mu M$   $Ca^{2+}$  overlays very well with the simulated curves using  $K_4$  values at 2 and 3 mM respectively.

simulations helped to get confidence on the initial guesses for the parameters which are floated.

### **Mixed metal experiments at higher $Mg^{2+}$ concentration.**

At higher  $Mg^{2+}$  concentrations, 15 mM  $Mg^{2+}$ , there was a decrease in the rate of product formation that was observed under single turnover conditions. This inhibition of cleavage rate at higher  $Mg^{2+}$  could be due to electrostatic effects or because of substrate inhibition. We tried a set of conditions for cleavage kinetics where we used 15 mM  $Mg^{2+}$  and 50  $\mu M$   $Ca^{2+}$  and monitored the rate of cleavage of DNA by PvuII. The idea behind this experiment was to form more of the mixed metal species at these conditions and therefore possibly observe a cleavage rate that is higher than the rate with 10 mM  $Mg^{2+}$  alone. As shown in **Figure A4** at 15 mM  $Mg^{2+}$ , 50  $\mu M$   $Ca^{2+}$  condition (red bar), there is an increase in the rate of product formation as compared to the 15 mM  $Mg^{2+}$  alone (black bar). We observed an increase in the rate of product formed under these conditions as compared to that of the 10 mM  $Mg^{2+}$  and 50  $\mu M$   $Ca^{2+}$  but lower than the 10 mM  $Mg^{2+}$  alone. This means at conditions of 15 mM  $Mg^{2+}$  and 50  $\mu M$   $Ca^{2+}$ , we form more active species than at 10 mM  $Mg^{2+}$  and 50  $\mu M$   $Ca^{2+}$  set but not more than that at 10 mM  $Mg^{2+}$  alone. **Figure A4** compares the data with and without 50  $\mu M$   $Ca^{2+}$  at different  $Mg^{2+}$  concentrations. All the experimental data without  $Ca^{2+}$  were collected earlier (Xie, et al., 2008). In this plot we see that there is a steady increase in the rate of cleavage with increasing  $Mg^{2+}$  concentration in presence of  $Ca^{2+}$ . There can be two possibilities for this process to occur: one is that the inhibitory effects are neutralized with the addition of  $Ca^{2+}$ , and second is that there are more mixed species formed under these conditions. In the absence of  $Ca^{2+}$ , we see a decrease in the rate of cleavage at 15 mM  $Mg^{2+}$ .

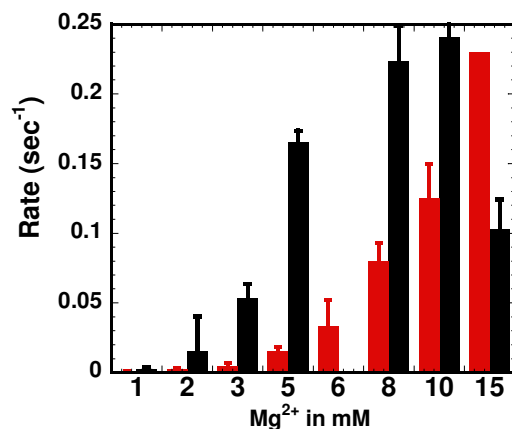


**Figure A4:** The rate of cleavage ( $\text{sec}^{-1}$ ) vs  $\text{Mg}^{2+}$  concentration in mM at different  $\text{Mg}^{2+}$  concentrations. The activity of enzyme at different  $\text{Mg}^{2+}$  concentrations with and without  $50 \mu\text{M Ca}^{2+}$ . The data here shows that the increase in activity in presence of  $\text{Ca}^{2+}$  occurs only in presence of increasing  $\text{Mg}^{2+}$  concentrations under the single turnover conditions used for the reactions. Experimental data without  $\text{Ca}^{2+}$  were collected earlier (Xie, et al., 2008). The red bar show data with  $\text{Ca}^{2+}$  concentration, and black bar indicates that only  $\text{Mg}^{2+}$  is present.



An overlay plot of the experimental and the fitted curve from the model 1e, for 15 mM  $Mg^{2+}$  and 15 mM  $Mg^{2+}/ 50 \mu M Ca^{2+}$  conditions is shown in **Figure A5**. The model used here (model 1e) fits the datasets in presence of  $Ca^{2+}$  (**Figure A5 A**) but overestimates the data sets with the  $Mg^{2+}$  alone (**Figure A5 B**). If we understood the decrease in activity of enzyme at higher  $Mg^{2+}$  and add those parameters into the model this dataset at higher  $Mg^{2+}$  concentration could have detailed more about mixed species formation and its activity.

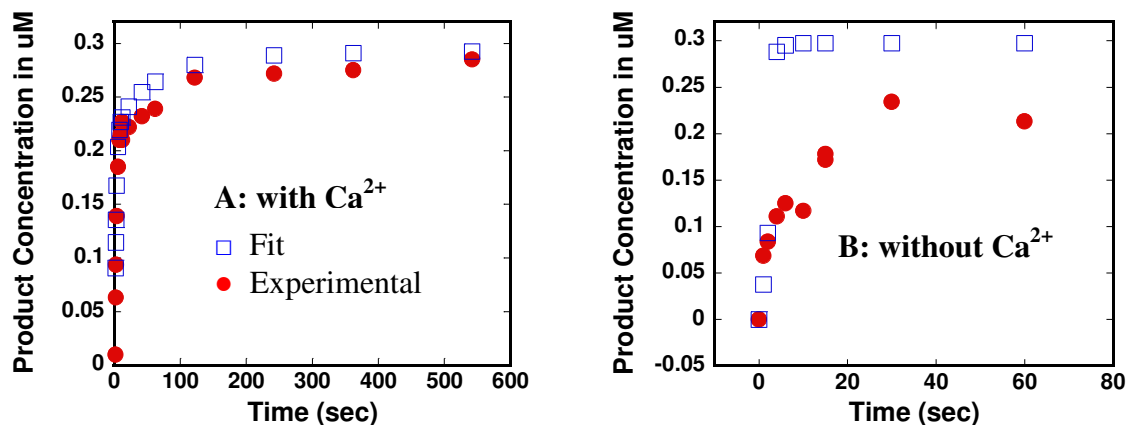


**Figure A5: Fit with model 1e at higher  $\text{Mg}^{2+}$  concentrations with and without  $\text{Ca}^{2+}$ :**

**A:** An overlay plot of the fitted and experimental data at 15 mM  $\text{Mg}^{2+}$  and 50  $\mu\text{M}$   $\text{Ca}^{2+}$  using model 1e where both the mixed species are formed and active. **B:** An overlay plot of the fitted and experimental data at 15 mM  $\text{Mg}^{2+}$  alone using model 1e. The symbols represent  $\bullet$  experimental points and  $\square$  fitted points. The data here shows that the model does explain the amount of product in presence of  $\text{Ca}^{2+}$ . The model cannot explain for the decrease in activity seen at high  $\text{Mg}^{2+}$  concentrations.

## Vita

Charulata B. Prasannan was born on January 22, 1980 in Varkala, Kerala, India to Mr. B. Prasannan and Smt. M.C. Sarasija. Charulata B. Prasannan received her Bachelor's degree in chemistry from St.Xavier's College affiliated to the University of Mumbai, India. She finished her Master's degree from Institute of Science, University of Mumbai in physical chemistry. Before pursuing the graduate studies she taught chemistry for the undergraduate classes at the University of Mumbai and did biochemical research with Dr. Rohit Mittal at Tata Institute of Fundamental Research. In fall of 2004 she joined University of Missouri-Saint louis graduate program at the Department of Chemistry and Biochemistry and received M.S degree in 2006.

### Permanent Address

Charulata Prasannan  
Krishna Nivas  
Near Railway Station  
P.O Chiraiyinkil  
Thiruvananthapuram (dist)  
Kerala, India, 695304.